NASA CR-
147484

AMPS DEFINITION STUDY

ON

OPTICAL BAND IMAGER AND PHOTOMETER SYSTEM

(OBIPS)

Prepared by

T. N. Davis
C. S. Deehr
T. J. Hallinan
E. M. Wescott

Geophysical Institute
University of Alaska
Fairbanks, Alaska 99701

September, 1975

Final Report on NASA Contract NAS 9-14645
with Lyndon B. Johnson Space Center, Houston, Texas.

Principal Investigator: T. Neil Davis
Phone: (907)-479-7393

NOTICE

The approach in this study is to emphasize the capabilities readily achievable with existing technology. Consequently, we make heavy use of available data from manufacturers of imaging devices, these data being selected to represent generic types of imagers. It should not be inferred that we are recommending a particular manufacturer or a particular image tube. Rather, our purpose is to provide a broad outline of the desirable characteristics for imagers within the context of demonstrated feasibility.

The Human Comedy

By STAN DRYER

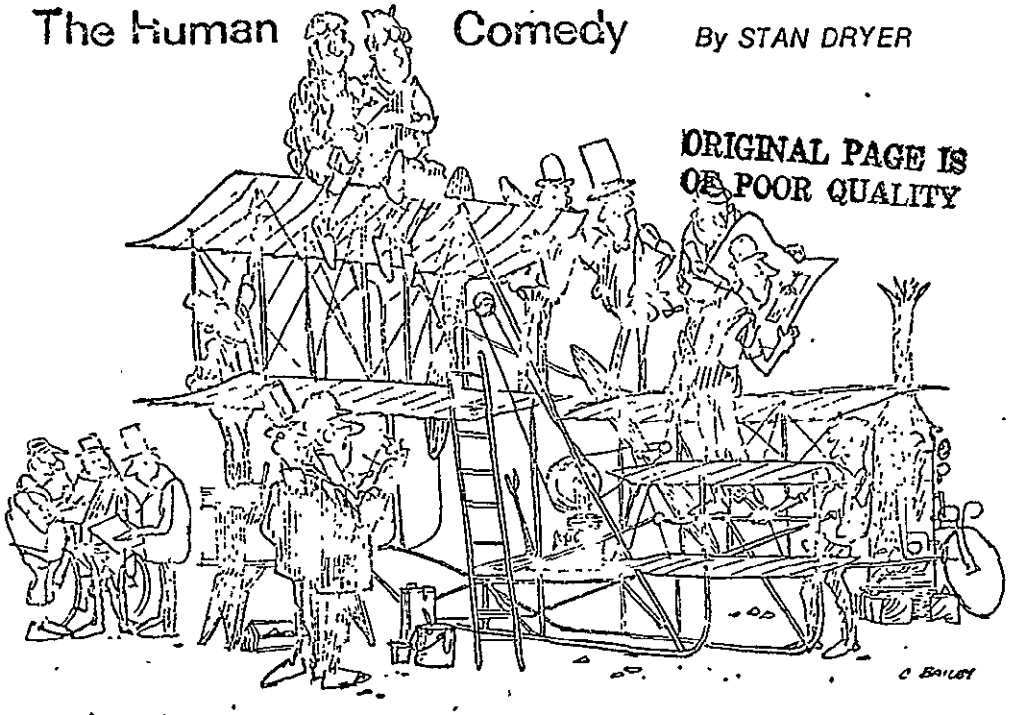

A feasible flying machine

After four years of experimenting in their spare time, two bicycle repairmen named Orville and Wilbur Wright flew the first powered airplane in 1903. Their cash outlay was about $1,000.

What would have happened if the Wright Brothers had built their airplane under a modern, government-financed, research-and-development contract? The record might read as follows.

To: J. L. Flailer, Vice President in Charge of Research, Mammoth Bicycle Corp.
From: Orville Wright, Manager, Kitty Hawk Test Station

Little progress was made on the flying machine this week. Wilbur was at the Symposium on Flying Machine Progress, and I was tied up in paper work. Monday I completed employee-evaluation reports. Tuesday I checked procurement vouchers. Wednesday I signed security-clearance forms. Thursday and Friday were used up in meetings.

I am worried about your plan to double the size of the test station. Although I realize that under our Army contract this could double our profits, I cannot see that it will speed things up. I favor leveling off the work force to a technical staff of about 100 with a support staff of not over 700.

The men you have been sending for interviews seem to be overly concerned with what you call the "systems approach." I think you should stop running that ad in the bicycle trade journals which shows a hand holding the earth like a baseball and says, "The flying machine is an integrated system." The machine we are working on will have four wings, a motor, two propellers and some control surfaces. All we want to do is make it fly. I do not need any more bright young men who talk about ops, analysis and systems configurations. However, if you can spare Joe, the mechanic in the motor pool, send him down.

The union problems seem to be settled. We're agreed that members of the electricians', mechanics', chambenders', carpenters' and seamstresses' unions will all be on the launch team.

To: Orville Wright
From: J. L. Flailer

Regarding your report of November 3, I am worried at your insistence on directing work toward production of equipment. Frankly, I would be happier to see more concept-oriented work. Remember that our contract calls for a feasibility study and does not specify hardware development. From the standpoint of obtaining future study contracts, a good report in the hands of the right people in Washington is worth far more than the production of hardware.

In regard to our expansion plans, I have retained the Coordinated Research Institute to assist this effort. Their teams of research-methodology consultants will visit the facility this week.

To: J. L. Flailer
From: Orville Wright

Wilbur returned Monday and was angry when he found one wing had been put on the flying machine upside down. Our staff psychologist was upset when Wilbur chewed out the engineer in charge. He feels that Wilbur has "disrupted the stability of the command structure" by taking direct action at two levels below his own in the hierarchy. Nonetheless, the engineer got the wing on right side up in one day.

Your research-methodology people say they have "delineated a satisfactory dynamic organizational phaseover philosophy." My general feeling is that expansion is a mistake and I strongly object to their recommendation that Wilbur and myself be separated in the management structure.

To: Orville Wright
From: J. L. Flailer

I have read the C.R.I. report. As it points out, a management partnership of brothers may fail due to latent sibling rivalry. I am therefore moving ahead with its recommendations to break the facility into East Coast and West Coast divisions, with each of you heading one division.

Our biannual report on flying-machine feasibility is due in two weeks. Your last biannual report was very terse, and this should make up for that deficiency. I suggest a minimum of four pounds of single-spaced typed material.

To: J. L. Flailer
From: Orville Wright

As you have probably read in the newspapers, about 50 people picketed the front gate yesterday. Gus Hanks, our public-relations specialist, informed me that these were two sets of protest marchers who had gathered in response to a rumor that we were about to test a flying machine. A scuffle broke out between the group carrying the Flying Machines Are a Threat to World Peace signs and the group carrying the World Peace Through U.S. Air Power signs. We had to call the police to restore order.

The irony is that there was no possibility of any test flight. Although the body and wings of the flying machine have been completed, no engine has yet been provided. The propulsion-systems analyst you hired just completed a massive report titled, *Power Plant Selection for Heavier-than-Air Flying Machines*. I hoped it might contain at least the specifications for an engine, but it seems to be only a proposal for a two-year feasibility study.

To: Orville Wright
From: J. L. Flailer

Newspaper accounts of the episode at the test facility have produced some extremely bad publicity for the company. I have had calls from stockholders who are disturbed about potential effects on our bicycle sales, and have assured them that an announcement will be made that no testing of flying machines is currently planned. I trust you will issue the necessary press release.

I read the report of Ed McGurty, the propulsion-systems analyst whom you criticized, and I find it a well-written exposition of the problems inherent in the selection of a power plant for a flying machine. A two-year study of this area does not seem to me to be at all out of order. I must emphasize again that our contractual task is the *study of the feasibility of heavier-than-air flying machines*. Let me remind you that the biannual progress report is due in my hands next week.

TWX REPORT TO: J. L. FLAILER
FROM: ORVILLE WRIGHT
HEAVIER-THAN-AIR FLYING MACHINE A REALITY. WILBUR AND I MADE FOUR FLIGHTS TODAY. AVERAGE SPEED 31 MILES AN HOUR. LONGEST FLIGHT 59 SECONDS

To: J. L. Flailer
From: Orville Wright

As you may find my telegram somewhat unbelievable, I want to fill you in on the details. Last Friday, when Wilbur returned from committee meetings, we discussed the engine problem, and he suggested we might use the engine from one of the guards' motor scooters.

Saturday morning we went to the deserted facility, removed the engine from a scooter, bent some mounting brackets and installed it in the flying machine. We had two of the security guards help us move the machine out to the south parking lot. I climbed aboard and Wilbur started the engine. After a run of about 100 feet, the machine became airborne. The first flight lasted 12 seconds. As we became more adept, the flights became longer, with the longest lasting 59 seconds. On the final flight a rough landing damaged one wing and forced abandonment of the tests. I think you will agree that these flights prove the feasibility of a heavier-than-air flying machine.

In place of a biannual report, I am enclosing:

1. A two-page description of our test flights.
2. Two photographs taken by one of the security guards of the flying machine in the air.
3. Complete plans of the flying machine.

To: Orville Wright and Wilbur Wright
From: J. L. Flailer

I regret to inform you that as of this date you have been terminated as employees of the corporation. The reasons for this decision are as follows:

1. You conducted tests of the flying machine after specific orders from me not to do so.
2. Your substitute report is inadequate in size and concept.
3. The Zootscoop model 4G-78 motor-scooter engine you specify as the power plant is not manufactured by the Mammoth Bicycle Corp., which *does* manufacture a line of low-horsepower engines for its motor bicycles. Company policy requires that in-house equipment be used whenever possible in systems developed by the company.
4. Government property was removed from the test site without approval, and was damaged.
5. Guards took photos without authorization.

I regret that this decision is necessary, particularly in view of your long service with our firm. Please feel free to utilize our personnel office for assistance in obtaining new positions. □

Illustration by Colin Bailey

FROM SATURDAY EVENING POST ??
DATE UNKNOWN

AMPS DEFINITION STUDY ON OPTICAL BAND IMAGER AND PHOTOMETER SYSTEM

(University of Alaska)

SUMMARY AND MAIN CONCLUSIONS

- The objectives of this study are to define the characteristics of a modular optical diagnostic system (OBIPS) for AMPS, to provide input to Phase B studies and to give information useful for experiment planning and design of other instrumentation.

- The system described consists of visual and UV-band imagers and visual and UV-band photometers; of these the imagers are most important because of their ability to measure intensity as a function of two spatial dimensions and time with high resolution.

- The various subsystems of OBIPS are in themselves modular with modules having a high degree of interchangeability for versatility, economy and redundancy.

- Imager subsystems using the 40 man SIT (Silicon Intensifier Target) tube are described. The SIT appears to the best imager now available for use on AMPS. New state-of-the-art developments hopefully will provide better devices, but the interface characteristics are unlikely to change much; any changes are likely to reduce rather than increase requirements on interfacing.

- OBIPS Subsystems can be placed on a common steerable mount or be separated and placed at various locations on the spacecraft or even on auxillary spacecraft. Chapter 6 of this report gives somewhat-detailed engineering

specifications for OBIPS, but many of the specifications are estimates and subject to change.

- A serious problem to optical observation on AMPS missions is stray light. The main sources are direct sunshine, direct earthshine and moonshine reflecting off spacecraft components. These sources scatter light into lens and windows to give background levels that can prevent observation of active experiments or other targets.

- To minimize the stray light problem, light shields can be built that provide rejection of stray light by a factor $\geq 10^9$.

- Satisfactory light shields are so large that they effectively preclude the use of optical systems with lens greater than 15 cm (6 in.) in diameter.

- Unless light shields meeting the requirements defined in this study are used, active experiments requiring optical support can be performed only when the spacecraft is in darkness.

- The requirement for experiments only in darkness is highly restrictive. Unless missions are carefully planned, little mission time will be available; at best approximately 40% of any given orbit.

- According to present design, optical observation can be made only in the hemisphere above the x-y plane of the spacecraft. Booms or other obstructions reduce the view direction possibilities. The obstruction problem is especially severe if observations are to be made

with the spacecraft exposed to sunshine or earthshine.

- Chapter 8 of this study includes a brief review of active experiments using gas releases, electron accelerators and explosive barium ion ejections.

- In the planning and conduct of active experiments it is most practical and convenient to utilize the concepts of volume emission (in photons/cm^3 sec at a particular wavelength or wavelength increment) and apparent emission rate (in rayleighs; 1R = an apparent emission rate of 10^6 photons/cm^2 sec over 4π steradians). Methods of converting from other units are given.

- Once the emission source to be observed and the background are specified in rayleighs, it is relatively easy to follow procedures given here to calculate the response of a specified optical instrument so as to determine the viability of a particular experiment concept.

- The response of state-of-the-act imagers to light sources of given brightness as specified by industry standards disagrees with our laboratory tests and emperical experience by a factor of 25; our results indicate the lower sensitivity. Pending needed investigation of the cause of the discrepancy, we adopt the lesser emperical sensitivity.

- We conclude that state-of-the-art imagers permit useful end-on observation of artifical auroras created by electron beams of minimum power 0.02 kw and observation from the side of artifical auroras generated by electron

beams of minimum power 1 kw, as long as the angle subtended by the artificial aurora is equal to or greater than a resolution element of the detector. The angular resolution of the imagers is equal to the field of view divided by 200 to 300.

- The report terminates with a brief outline of the steps required to calculate the feasibility of an active experiment.

- There is need to extend the calculations to particular experiment configurations using electron and ion accelerators, barium ion injections and gas releases.

TABLE OF CONTENTS

AMPS DEFINITION STUDY ON OPTICAL BAND IMAGER AND PHOTOMETER SYSTEM

1. INTRODUCTION

1.1 PRIMARY STUDY OBJECTIVES

1. To define characteristics of an optical diagnostic system suitable for flight on the first AMPS mission and which, on future missions, can be expanded with modular subsystems to form a core instrument for observation of weak, transient or small-scale phenomena occurring naturally or generated by active experiments such as particle accelerators, shaped-charge barium releases, chemical ejections or perturbation phenomena created by active experiments.

2. To provide input to the Phase B studies on the requirements of the Optical Band Imager and Photometer System (OBIPS) upon the spacecraft, mission planning, crew activities and other interfaces.

3. To prepare for other design activities a statement of the OBIPS capability stressing factors that will influence the power levels and duty cycles, etc., of active experiments expected to produce phenomena observable by the OBIPS or similar devices.

4. Review briefly results and conduct of past experiments that bear on design of active experiments for AMPS missions and provide other information useful to AMPS experiment designers.

1.2 APPROACH

The approach used in this study is to examine the problems with a heavy reliance on experience gained in the use of a variety of optical devices for the observation of active experiment phenomena from

ground-based and aircraft platforms and also input from previous Shuttle studies and satellite experiment planning efforts. The work is the effort of approximately eight of the staff of the Geophysical Institute. Major contributions were made by Dr. C. S. Deehr, Dr. E. M. Wescott and Mr. T. J. Hallinan. Other contributors include Dr. G. J. Romick, Dr. G. G. Sivjee, Mr. H. M. Stenbaek-Nielsen and Mr. B. S. Delana. Miss Judith Holland was responsible for various aspects of the report preparation, including typing.

1.3 THE IMPORTANCE OF OPTICAL DIAGNOSTICS TO AMPS

Basically, there are three diagnostics for active experiments and the background environment: 1) fields and waves diagnostics; 2) particle phase space diagnostics and 3) optical emission diagnostics. In essence, both the particle and the fields and waves diagnostic techniques require *in situ* measurement. Largely because of this requirement the AMPS program is having to give much attention to the complex and expensive deployment of tethered or free-flying secondary observing platforms. There is concern that the Shuttle environment may preclude many particle and wave measurements on board. On the other hand, the optical diagnostics are remote sensing techniques and therefore permit observation from Spacelab and also from other platforms including ground, aircraft, balloons and secondary satellites.

In general, all three diagnostic methods will be required for most active experiments contemplated for AMPS. But, with few exceptions, the active and tracer experiments conducted so far have relied very heavily or entirely upon optical diagnostics as the main source of observational

data. Quite obviously the same will be true for AMPS experiments, especially during early missions when it is unlikely that all of the desired diagnostics can be flown.

Consequently, it is particularly critical to the scientific success of early AMPS missions that we 1) foster the development of an effective, practical and versatile core optical diagnostic system, 2) ensure that the system has adequate attention to its requirements from Phase B and other planning and design efforts, and 3) bring to the attention of experiment planners the inherent limitations of this diagnostic system as an aid to planning scientifically successful active experiments.

2. OPTICAL INSTRUMENT TYPES

The three basic types of optical instruments potentially useful for AMPS missions are 1) spatial scanning photometers, 2) wavelength scanning spectrophotometers and 3) imagers. Table 2.1 shows the essential characteristics of these types (present state of the art).

TABLE 2.1

BASIC OPTICAL INSTRUMENTATION RESOLUTION

	Type of Instrument		
Parameter	Spatial Scanning	Wavelength Scanning	Imaging
Wavelength Resolution	1-10 Å	0.01 Å to 10 Å	20 Å
Spatial Resolution	Worse than 0.2^{o}	0.2^{o} to 10^{o}	Better than 0.2^{o}
Temporal Resolution	1 sec	10 sec to 10 min	0.017 sec
Measures	$I = I(x,t)$	$I = I(\lambda,t)$	$I = I(x,y,t)$

Spatially scanning photometers basically consist of some form of optics that defines the field of view, filtering to restrict the wavelength of the admitted light and a detector of photons. A particular instrument might consist of any combination selected from the lists shown in Table 2.2.

TABLE 2.2

COMPONENTS OF SPATIAL SCANNING PHOTOMETERS

Light Gathering Optics	Filtering	Detector
1. Mirror Systems	1. Broad-band	1. Vacuum Photodiode
2. Collimator System	2. Interference	2. Gas-filled phototubes
3. Thick Lens System	3. Bi-refringent	3. Photomultiplier
		4. Photoconductive solid-state detector
		5. Photovoltaic solid-state detector

Table 2.3 shows some of the naturally-occurring emissions in the upper atmosphere that are suitable for spatial scanning observations on AMPS missions. Active experiments, in some cases, will alter the intensity of certain of these same emissions.

There also are several types of wavelength scanners; these share certain characteristics with spatial scanners, i.e., light gathering systems and photon detection elements, but they additionally incorporate some means to permit wavelength scanning. Types of wavelength scanners and some of their potential uses are shown in Table 2.4.

Imaging systems fall into two main categories, image-intensifiers (see Fig. 2.1) and television camera tubes employing raster scanning (see Fig. 2.2).

TABLE 2.3

EMISSIONS SUITABLE FOR SPATIAL SCANNING OBSERVATIONS

WAVELENGTH	EMITTER	INTENSITY (IBC III AURORA)	BANDWIDTH	FIELD	CONTROL	PURPOSE
4250 A 4268 A	N_2^+ 1 Neg (0,1)	10 kR 5 kR	5 A 5 A	½° ½°	None	The ratio of these emissions is proportional to the rotational temperature which is indicative of the altitude of the main emitting region and hence the energy of the precipitated particles.
4278 or 3914 4709 and 4652	N_2^+ 1 Neg "	100 R-10 kR "	15 A 15 A	½°		Investigate distribution of enhancement of higher vibrational levels.
6300 5577	OI OI	1-20 kR 100 kR	10 A 10 A	½° ½°		Ratio with N_2^+ 1 N to indicate altitude of main auroral emission
4850 4880	HS HS	100 R 75 R	5 A 5 A	1° 1°		Observe spatial distribution of change in doppler profile of hydrogen emission due to proton precipitation.
1216 1304 1200 1400 ~	La(H) OI NI N_2 LBH	1 kR 10 kR 5 kR 4 kR	Variable	5°		Series of emissions used for mapping the extent of electron and proton emission around the entire oval even when the activity is so high that the dayside oval moves into the twilight region.
8446 7774 4368 7990	OI OI OI OI	10 kR 5 kR 1 kR	5-10 A	< 5°		Determine spatial extent of OI emissions. Evaluate possible excitation mechanisms.
4135-90	OII	10 kR				Document extent of emissions associated with proton aurora
584	HeI		100 A			Map spatial extent of various emissions
303	HeII		100 A			
5000	NII	1 kR	5 A			
4414	OII	1 kR	7 A			
430	OII		100 A			
672	NII					

TABLE
2.4

SOME PROPOSED WAVELENGTH SCANNING OPTICAL INSTRUMENTS AND EXPERIMENTS

INSTRUMENT	WAVELENGTH	EMITTER	INTENSITY IBC III AURORA	RESOLUTION Δλ	Δt	Δθ	PURPOSE
15 cm aperture Fabry-Perot Interferometer	6300 A, 7319 A 5577 A, 3728 A 4414 A	OI,OII	1 kR - 10 kR	0.01 A,	< 1 min,	< 5°	Line profiles of metastable atomic lines are obtained in various directions from the Shuttle. Changes in the shape of the doppler profile are interpreted in terms of the neutral and ionized wind components (> 50 m/sec).
Field Widened Michelson Interferometer	5577 A	OI	1 kR - 100 kR		< 1 sec	5°	Changes in the fringes of the Michelson pattern are used to record rapid temperature variations and hence altitude variations of the emitting region.
Ultraviolet Spectrometer or Spectrograph	200-500 A	HeI, HeII		10 A		10°	Explore far UV spectrum by directing spectrograph towards various emitting regions and evaluation read out of electronically intensified detector.
Ultraviolet (1150-1700 A) High Speed Scanning Spectrometer	1640 A	HeII	50 R	10 A	5 sec	5°	Determine spatial extent of emissions and compare multiplet intensities.
	1216	La	1 to 4 kR				
	1200	NI	8 kR				
	1301-04-06	OI	20 kR				
	1356	OI	1 kR				
	1400	N_2 LBH	1 kR				
UV Spectrometer (con't) (2100-3400 A)	2150 A	NOγ	1 kR	10 A	5 sec	5°	Map location of NO enhancements
	2800	N_2 VK	1 kR				Compare with I (5577 A) OI ('S)
	2972	OI ('S)	6 kR				
	3159, 3371	N_2 (2 Pos)	13 kR				
Visible Scanning Spectrometer	4861	Hβ					
	4278	N_2^+ 1st Neg	16 kR	4 A	5 sec	5°	Map regions of differing vibrational distribution associated with proton aurora
	4236		2 kR				
	5577 4368 6300 3947 7744 8446	OI	500 R	5 A	< 20 sec	5°	OI excitation problem + Compare with UV and O_2^+
	3466	NI	5 kR				Lifetime and correlation with other emissions
	5199		1 kR				
	5199						
	5999	O_2^+	12 kR	10 A	10 Sec	10°	Determine extent of O_2^+ emissions
	6013	N_2 1P	5 kR				Map region of differing vibrational distribution associated with electron aurora
		N_2 1P (6,3) (5,2) (4,1)	25 kR				
Michelson Interferometer	9.3μ	O_3	mH	50 A	1 min	10°	Determines spatial extent of possible enhancement
	Numerous	OH	10 kR				
	1.27μ 1.58	O_2 $^1\Delta g$	~ 100 kR				
	10880 A	HeI	10 kR				
	Numerous	OI	weak				Determine existence of infrared counterparts of known visible OI lines. Establish intensities of bands not seen from ground absorbed in lower atmosphere).
	1.129μ						
	1.317μ						
		N_2^+ Meinel	1-20 kR				
		N_2 1P					
	> 2μ			5 cm^{-1}	1 min	10°	Explore infrared spectrum of aurora bevond 2μ. Evaluate thermal radiation of atmosphere.

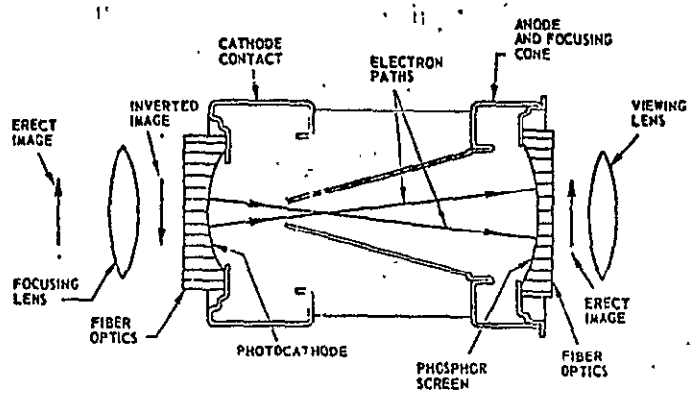

1 *Schematic diagram of an electrostatic-type image tube.*

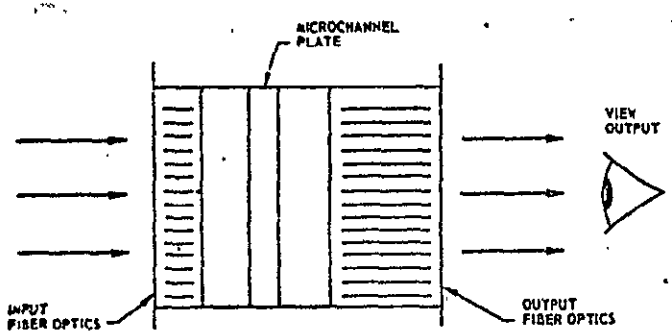

2 *Schematic diagram of proximity focus image tube of the "wafer" design utilizing an MCP to increase gain.*

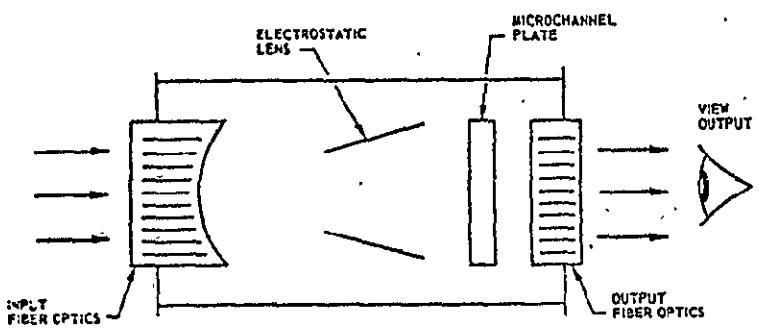

3 *Schematic diagram of electrostatic-focus type image tube utilizing an MCP to increase gain.*

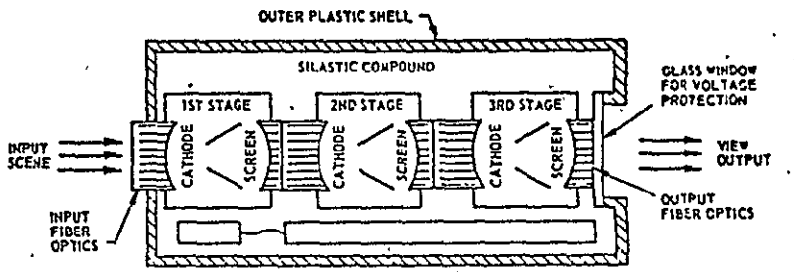

4 *Schematic diagram of typical three-stage electrostatically focused image tube.*

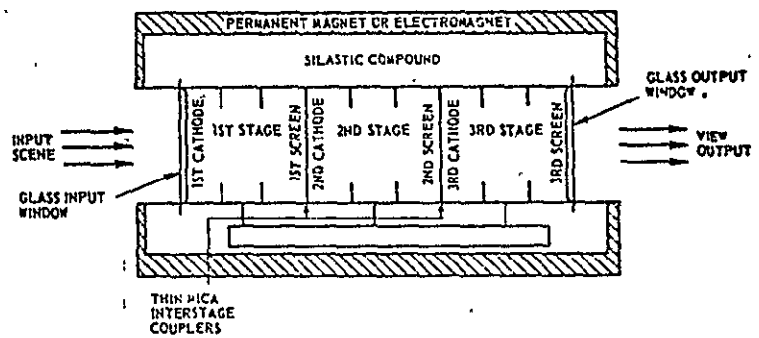

5 *Schematic diagram of typical three-stage magnetically focused image tube.*

FIG. 2.1 Image Intensifiers

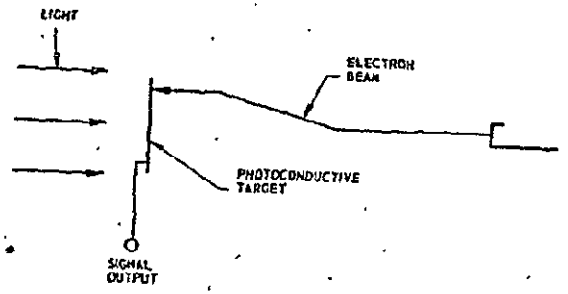

1 *Schematic representation of vidicon camera tube.*

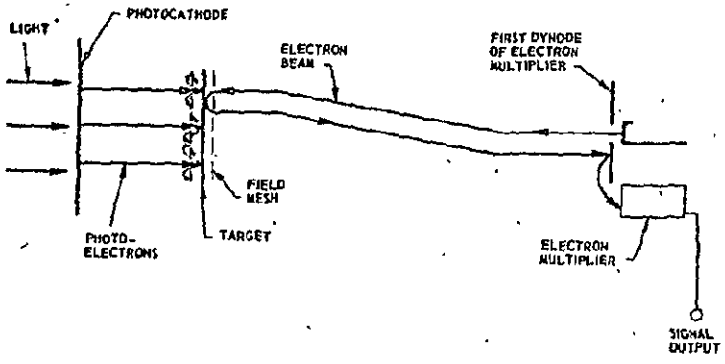

2 *Schematic representation of image orthicon camera tube.*

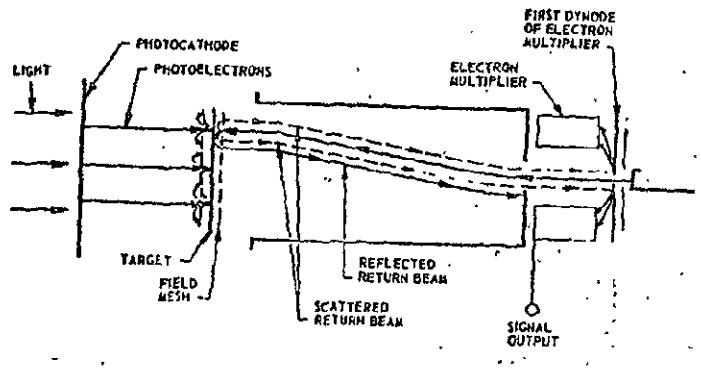

3 *Schematic representation of image isocon camera tube.*

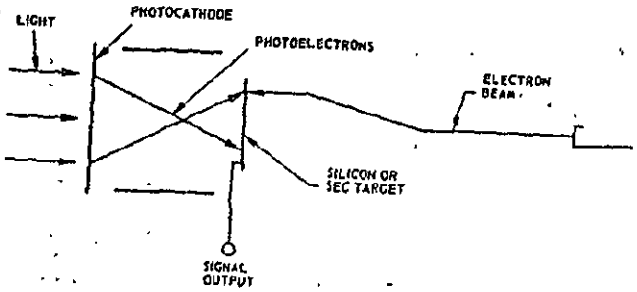

4 *Schematic representation of SIT and SEC camera tube.*

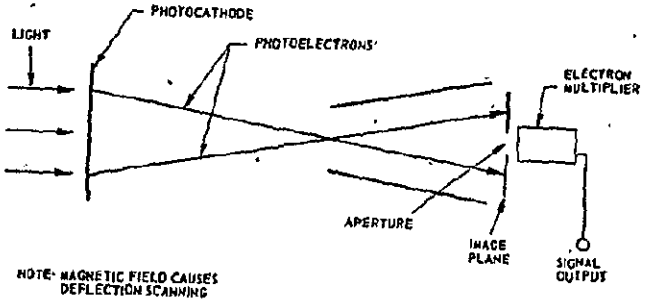

5 *Schematic representation of image dissector camera tube.*

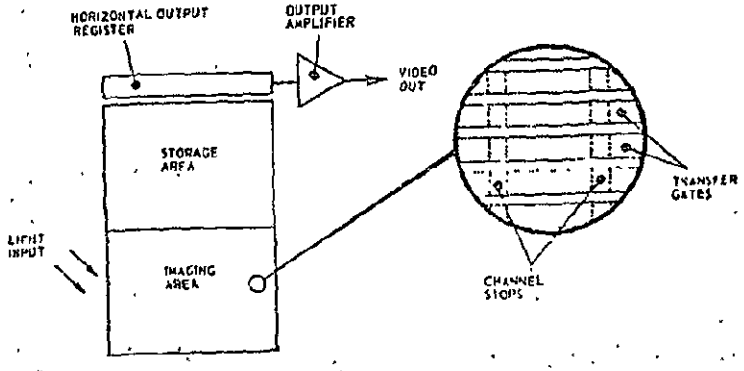

6 *Schematic representation of CCD (Charge-Coupled Device), a solid-state imager.*

FIG. 2.2 Television Tube Types

3. SELECTION CRITERIA FOR CORE OPTICAL DIAGNOSTICS

Factors entering into instrument selection are:

A. Wavelength resolution

B. Spatial resolution

C. Temporal resolution

D. Sensitivity

E. Dynamic range

F. Calibration capability

G. Stability

H. Versatility

I. Dependability

J. Interference Dependence

K. Size

L. Weight

M. Cost

N. Power consumption

O. Crew requirement

P. Data handling requirement

Q. Control requirement

R. Ruggedness

4. RATIONALE FOR SELECTION OF PARTICULAR CORE INSTRUMENTS

4.1 SELECTION OF INSTRUMENT TYPES

If only one optical diagnostic instrument could be flown on a particular AMPS mission, the entries in Table 2.1 immediately dictate that this instrument would be an imager. An imager's high spatial and temporal resolution combined with its ability to measure intensity as a function of two spatial dimensions clearly make it the leading choice. Emperical verification of the correctness of this choice comes from review of the scientific results from past active experiments involving electron accelerators, high-speed ion jets and emissive tracer elements.

The ideal imaging system provides a measure of the absolute intensity of optical emissions from each point in a scene with temporal and spatial resolutions adequate to describe all relevant details. For many purposes, existing low-light level imaging cameras employing conventional scanning formats approximate this ideal. However, there are substantial problems in the area of intensity calibration which arise mainly from four causes;

1) In many cases the physically relevant quantity is the photon density at a particular wavelength. Yet the inherent sensitivity and field of view necessarily employed often preclude the use of narrow-band interference filters on the imaging camera; in consequence the imager output frequently represents a complex composite of many wavelengths.

2) The dynamic range of the most sensitive imagers is usually less than two decades for any single setting of controls. Therefore, during the course of any particular experiment, it likely is necessary to alter the settings, and hence the calibration.

3) Imaging cameras utilize separate schemes for detecting the

diffuse background and the contrast within a scene. Consequently, absolute calibration can require two different intensity scale factors and an additive background factor.

4) The detector signal is inherently analog. Therefore amplifier drifts can be significantly detrimental to establishing calibration scale factors.

With the possible exception of the first, the above problems represent technical difficulties rather than inherent limitations. It may be feasible to develop a fully calibrated low-light-level imager for the early AMPS missions. For various reasons we suspect that this will not be done, and it seems wisest to plan for calibration through the use of one or more photometer subsystems that can be bore-sited with the imager subsystems. It is feasible to arrange the photometer subsystem outputs to be handled independently or to be merged into the video outputs of the imager subsystems. A proper match of photometer and imager subsystems can provide a powerful optical diagnostic sufficiently versatile to qualify as an essential core instrument for all AMPS missions.

A minimal optical diagnostic system should include an imaging subsystem for the visible-near IR band and one for the UV band. It should include a photometer subsystem for each of these two wavelength regions.

4.2 SELECTION OF INSTRUMENTS WITHIN A TYPE

The related questions of size and weight are always important in space applications. In this case, the camera lens size is particularly important since it determines the size of the sunshade. In order to

understand the trade-offs, we will consider, in Table 4.1, three detector sizes with the same lens diameter and the same field of view. Each is to view a 1.7 kR barium cloud in the 4554 emission. The required focal lengths, the resultant f numbers and the expected limiting resolution are shown in Table 4.1.

TABLE 4.1

COMPARISON OF DETECTOR SIZES

Photocathode diameter (mm)	16	25	40
Lens diameter (mm)	18.75	18.75	18.75
FOV (Degrees)	12 x 16	12 x 16	12 x 16
Focal length (mm)	42	66.63	105
f number	2.24	3.6	5.6
Photocathode current ($\mu a/cm^2$)	6.2×10^{-7}	2.6×10^{-7}	1.0×10^{-7}
*Horizontal resolution (TV lines)	260	280	280

*Based on RCA curves for SIT tubes with 16, 25, and 40 mm photocathodes.

The general conclusion is that the lens diameter and FOV determine the resolution--not the photocathode diameter. (The differences in resolution shown in Table 4.1 are within measurement error, including the errors in both resolution and intensity measurements.) The scattered light from the lens surface produces an intensity at the photocathode which is dependent on focal length in the same manner as is the light from the observed scene. Hence the expected contrast is independent of the lens size.

5. GENERAL DESCRIPTION OF PROPOSED CORE DIAGNOSTICS SYSTEM (OBIPS - OPTICAL BAND IMAGER AND PHOTOMETER SYSTEM)

For various reasons, largely discussed in later sections, the light gathering and detecting elements of the OBIPS must be mounted outside the pressurized portions of the spacecraft. These elements can be pallet mounted, mounted elsewhere, or perhaps be portable such that their positions can be changed with the manipulator arms. Control functions and power supplies will be inside the Spacelab or Shuttle. A simplified conceptual diagram of the OBIPS is given in Fig. 5.1.

A schematic diagram of a Type P (photometer) subsystem is given in Fig. 5.2 and that for the Type I (imager) subsystem appears in Fig. 5.3.

Similarly, the control, power supply and data handling components located in a crew-accessible area are shown in Fig. 5.4.

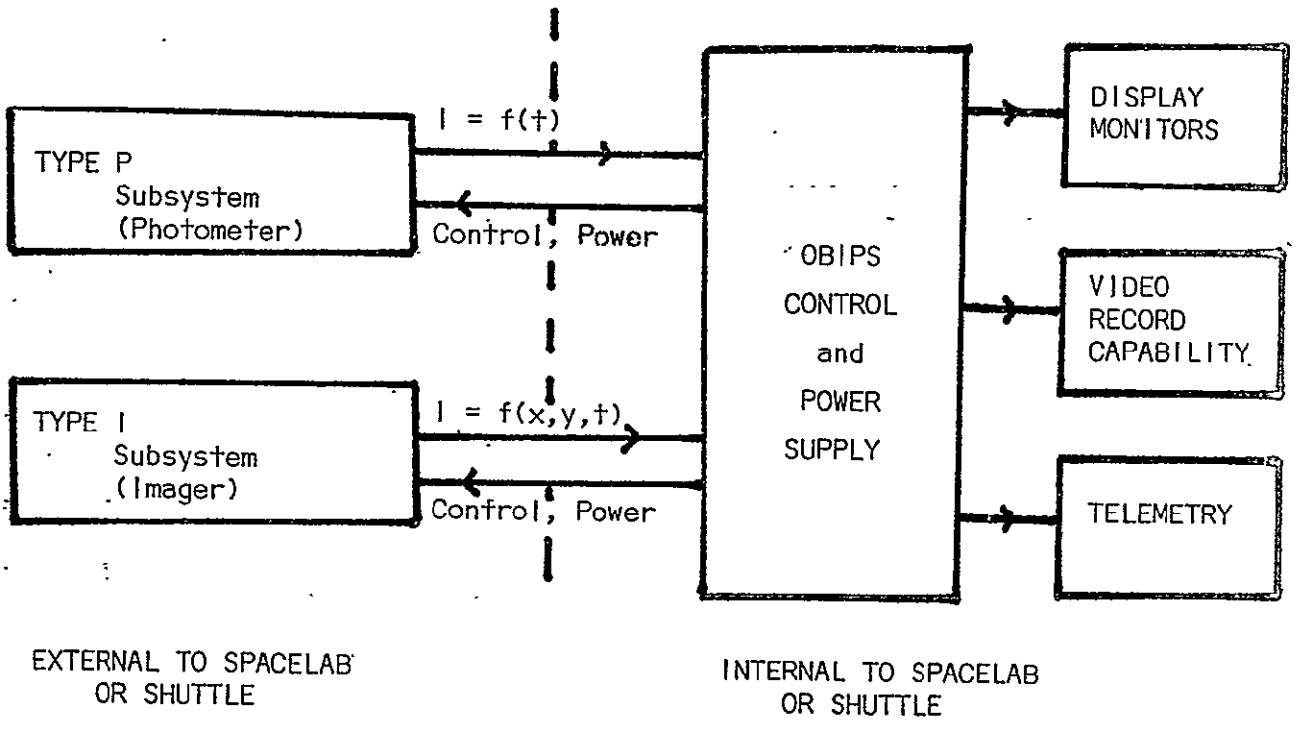
TYPE P
Subsystem
(Photometer)
I = f(t)
Control, Power
TYPE I
Subsystem
(Imager)
I = f(x,y,t)
Control, Power
OBIPS
CONTROL
and
POWER
SUPPLY
DISPLAY
MONITORS
VIDEO
RECORD
CAPABILITY
TELEMETRY
EXTERNAL TO SPACELAB
OR SHUTTLE
INTERNAL TO SPACELAB
OR SHUTTLE

FIG. 5.1

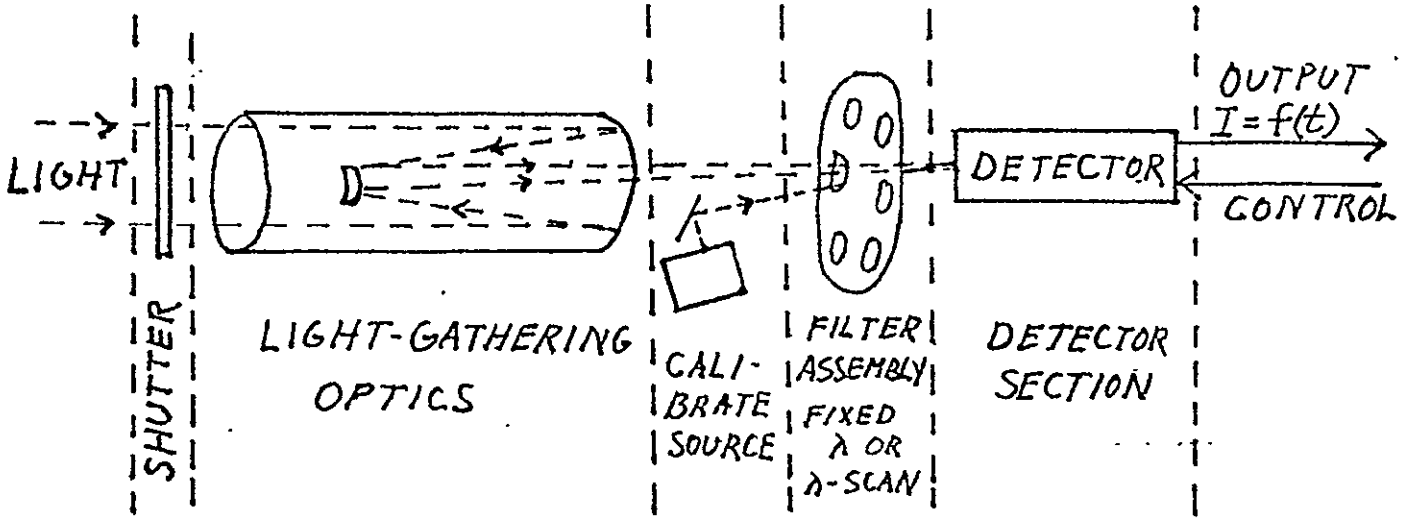

FIG. 5.2 TYPE P SUBSYSTEM

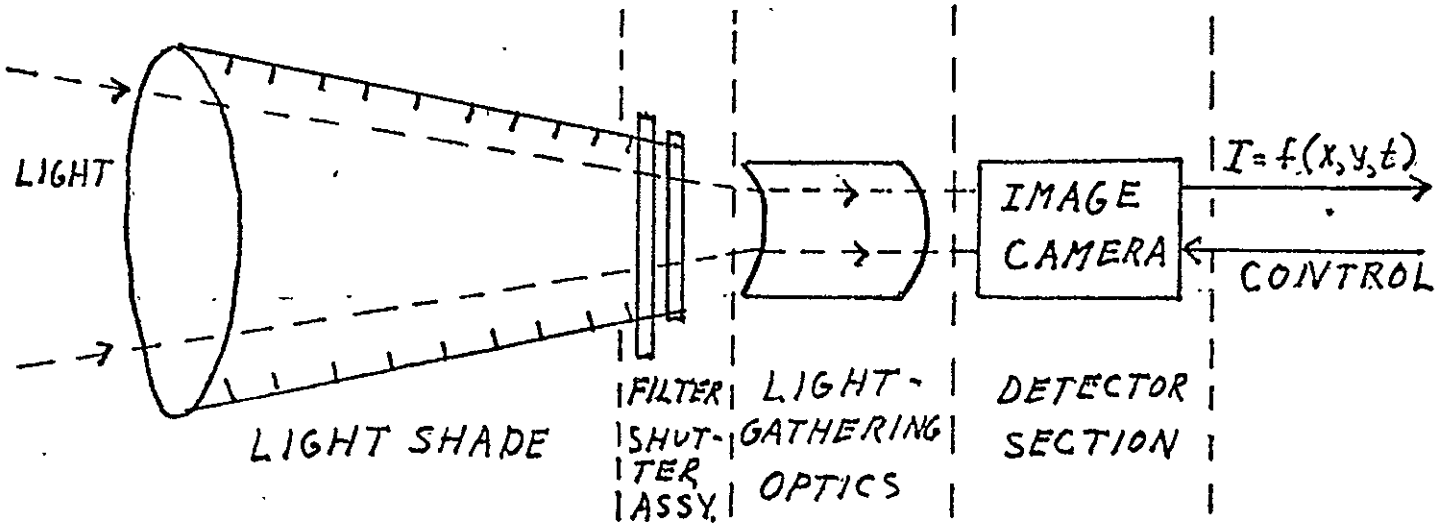

FIG. 5.3 TYPE I SUBSYSTEM

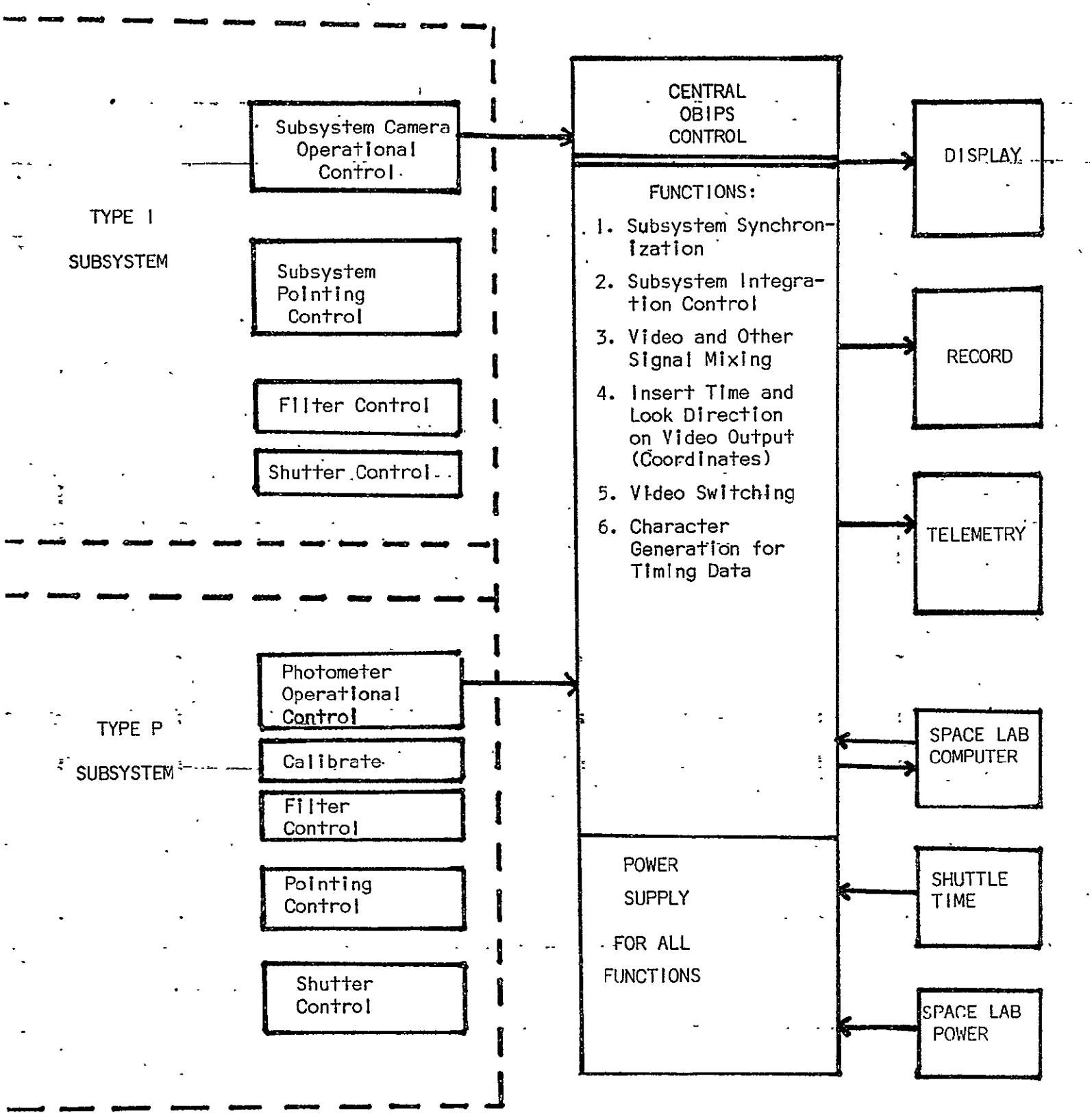
TYPE I
SUBSYSTEM
Subsystem Camera Operational Control
Subsystem Pointing Control
Filter Control
Shutter Control
TYPE P
SUBSYSTEM
Photometer Operational Control
Calibrate
Filter Control
Pointing Control
Shutter Control
CENTRAL OBIPS CONTROL
FUNCTIONS:
1. Subsystem Synchronization
2. Subsystem Integration Control
3. Video and Other Signal Mixing
4. Insert Time and Look Direction on Video Output (Coordinates)
5. Video Switching
6. Character Generation for Timing Data
POWER SUPPLY FOR ALL FUNCTIONS
DISPLAY
RECORD
TELEMETRY
SPACE LAB COMPUTER
SHUTTLE TIME
SPACE LAB POWER

FIG. 5.4

6. ENGINEERING DESCRIPTION OF OBIPS

6.1 GENERAL

With improvement in imaging technology, there will be some change in the specific characteristics of OBIPS subsystems, however, it is unlikely that there will soon be significant changes that will affect the OBIPS interface characteristics in ways to increase support requirements. Technological improvements should do just the opposite--reduce volume, weight, power requirements and lessen control requirements. Readers must realize that it is beyond this study effort to precisely define many engineering characteristics.

6.2 TYPICAL SYBSYSTEM COMPLEMENT

The most minimal subsystem complement should consist of one visible-near IR imager and a photometer subsystem operating in the same spectral region. A more rational complement for a minimal OBIPS system will include also an imager and a photometer to operate in the ultraviolet UV. The discussion here assumes that a minimal mission complement will contain four subsystems as follows:

1. Subsystem 1 Visible-near IR imager
2. Subsystem 2 Ultraviolet spectrum imager
3. Subsystem 3 Visible-near IR photometer
4. Subsystem 4 Ultraviolet photometer

6.3 SUBSYSTEM NO. 1, VISIBLE-NEAR IR IMAGER

6.3.1 General Characteristics

The central component of subsystem No. 1 will be, or be equivalent

to, a Silicon Intensifier Target (SIT) imaging system with a 40 mm diameter photocathode (S25) and interlaced target scan at 525 lines per frame. The light gathering system and the internal characteristics will permit imaging in the spectral region 4000 Å to 9000 Å. The camera will produce 200 TV line resolution with a photocathode current of 7×10^{-8} $\mu a/cm^2$ (faceplate illumination of 4×10^{-7} fc (footcandle)) and 400 TV lines at 2.2×10^{-4} $\mu a/cm^2$ (1.3×10^{-6} fc). It should produce useful images with scenes corresponding to as much as 0.1 fc faceplate illumination, i.e., it will have a dynamic range of 10^6 and it should physically survive exposure to 200 fc faceplate illumination, the illumination that will result from viewing the sunlit earth.

The camera will be fitted with a lens having controlled f stops and having a field of view of approximately 16^o. There will be a mechanism to permit, by manually-activated command, insertion of one of a selection of interference or broad-band filters. A shutter, actuated by manual command, will be necessary to protect the optics from too-bright light sources and from deposition of near-spacecraft pollutants. A sizable light shield surrounding and projecting beyond the lens will be necessary if the subsystem is to operate during portions of the orbit when the spacecraft is exposed to sunlight or earthshine.

For convenience we identify the various modules of the subsystem as follows, and carry the same scheme through the discussion of other subsystems.

Subsystem No. 1 - Visual-near IR Band Imager

1.1 Basic Camera Module

1.2 Light Gathering Optics (Lens) Module

1.3 Filter, Shutter, Calibrate Module

1.4 Light Shield Module

1.5 Control and Power Supply (in Spacelab) Module

6.3.2 Engineering Characteristics of Module 1.1 (Basic Camera)

6.3.2.0 General Description: 40 mm SIT or equivalent

6.3.2.1 Weight

11 kg or less.

6.3.2.2 Stored and Operating Dimensions

22 cm x 18 cm x 52 cm.

6.3.2.3 Power Requirement

10 watts continuous at 28 vdc during operation; standby if any TBD (supplied from Module 1.5).

6.3.2.4 Output Signal Characteristics

Video, 4 MHz bandpass (to Module 1.5).

6.3.2.5 Data Acquisition Duty Cycle

Variable depending upon general usefulness; minimum 10 min to major portions of orbits.

6.3.2.6 RFI, Magnetic Interference

Module does not generate significant RFI or magnetic fields, it is mildly susceptible to RFI below 4 Mhz, maximum allowable magnetic field in vicinity of camera 10^{-4} webers/m^2 (1 gauss).

6.3.2.7 Temperature Range

Allowed range $+5^{\circ}$ C to $+35^{\circ}$ C.

6.3.2.8 Shock and Vibration

TBD.

6.3.2.9 Spectral Response

3000 Å to 8800 Å, S25 photocathode, maximum response at 4000 Å.

6.3.2.10 Resolution and Sensitivity

100 TV lines at 7×10^{-8} $\mu a/cm^2$ photocathode current (4×10^{-7} fc).

400 TV lines at 2×10^{-7} $\mu a/cm^2$ photocathode current (1.3×10^{-6} fc).

6.3.2.11 Data Collection Rate

(1) Primary mode: conventional TV roster at 60 fields per sec;

(2) integration mode: one complete raster scan in 1/30 sec at intervals set by controls: 0.1, 0.5, 1.0 and 2.0 sec.

6.3.2.12 Control Requirements

1. Gain

   10 positions

2. Beam Current

   Continuous over range

3. Integration Mode

   5 positions

6.3.2.13 Housekeeping Data Requirement

Temperature, accuracy 1° C.

6.3.2.14 Dynamic Range

2×10^{-6} ft. lamberts to 200 ft. lamberts scene brightness through gain changes and aperture changes within module.

6.3.2.15 Pre-launch Support

Simple operational tests with test equipment to be furnished.

6.3.2.16 Design Life

Five years with between-mission servicing.

6.3.2.17 Module Location

On steerable pallet mounted platform or detachable for placement as desired with manipulator arm.

6.3.3 Engineering Characteristics of Module 1.2 (Light Gathering Optics)

6.3.3.0 General Description

105 mm Delft f0.7 with aperture control to pinhole or equivalent.

6.3.3.1 Weight

12 kg.

6.3.3.2 Stored and Operating Dimensions

18 cm x 18 cm x 18 cm.

6.3.3.3 Power Requirement

Intermittent - 10 watts at 28 vdc to change aperture on manual command.

6.3.3.4 Output Characteristics

Optical image in wavelength range 3900 Å to 9000 Å focused 3.5 mm behind rear faceplate.

6.3.3.5 Data Acquisition Duty Cycle

Same as 6.3.2.5.

6.3.3.6 RFI, Magnetic Interference

Not susceptible to either; possible minor generation of RF noise during aperture changes.

6.3.3.7 Temperature Range

Allowed range -10° C to $+35^{\circ}$ C.

6.3.3.8 Shock and Vibration

TBD.

6.3.3.9 Spectral Response

T 0.8 within range 3900 Å to 9000 Å.

6.3.3.10 Resolution and Transmittance

60 line pairs/mm, T 0.8.

6.3.3.11 Data Collection Rate

N/A

6.3.3.12 Control Requirements

Aperture control on manual command, 9 positions.

6.3.3.13 Housekeeping Data Requirement

None.

6.3.3.14 Dynamic Range

N/A

6.3.3.15 Pre-launch Support

Same as 6.3.2.15.

6.3.3.16 Design Life

Ten years.

6.3.3.17 Module Location

Rigidly attached to front of Module 1.1.

6.3.4 Engineering Characteristics of Module 1.3 (Filter, Shutter, Calibrate Module

6.3.4.0 General Description

The detailed design of this module is not available, so dimensions, weights, etc., are estimates. It is necessary to have a shutter to protect optical surfaces from pollutants at non-observing times and

also shuttering to protect against excessive light. Two different shutters might be involved. The light protection shutter could be either in Module 1.3 or perhaps in 1.2 and it probably should be automatically controlled by a light-sensing device to avoid catastrophic loss of Module 1.1 through human error. Selectable filters need to be included to permit observation either unfiltered or through narrow- or broad-band filters to isolate particular emissions or to reduce background emission. A mission involving barium releases will require a barium ion filter (4554 Å), and it is likely that a broad-band red filter and perhaps one or more narrow-band filters at prominent auroral wavelengths will be desired on most missions. The simplest means of intensity calibration is by means of an infinity-focused light source permanently in the field of view. This object can be small enough to have little effect on the light-gathering power. The source intensity might be switch controllable to permit its use essentially as a time-dependent gray scale.

6.3.4.1 Weight

Estimate 5 kg.

6.3.4.2 Stored and Operating Dimensions

Estimate 15 cm x 25 cm x 40 cm (15 cm thickness along optical path).

6.3.4.3 Power Requirement

Intermittent filter switching 2 watts at 28 vdc; intermittent calibrate power < 1 watts at 28 vdc; intermittent shutter operation 2 watts at 28 vdc. Perhaps require heater circuit to maintain filter temperature < 2 watts at 28 vdc.

6.3.4.4 Output Characteristics

Broad-band light of known intensity from calibration source passed through whatever filter inserted in optical path.

6.3.4.5 Data Acquisition Duty Cycle

See 6.3.2.5.

6.3.4.6 RFI Magnetic Interference

Not susceptible, possible generation of minor RFI during switching operations.

6.3.4.7 Temperature Range

Generally 0^{o} C to $+35^{o}$ C except that narrow band filters shift frequency with temperature at a rate of approximately 0.2 Å per ^{o}C. Therefore temperature control circuit to hold temperature within $+ 5^{o}$ may be necessary.

6.3.4.8 Shock and Vibration

TBD.

6.3.4.9 Spectral Response

N/A

6.3.4.10 Resolution and Sensitivity

N/A

6.3.4.11 Data Collection Rate

See 6.3.2.11.

6.3.4.12 Control Requirements

1. Filter change 5 positions.
2. Shutter control 2 positions.
3. Calibrate control 10 positions.

6.3.4.13 Housekeeping Data Requirement

1. Temperature, accuracy 1^{o} C.

2. Filter Position Indicator 5 positions.

3. Calibrate source intensity 10 positions.

6.3.4.14 Dynamic Range

N/A

6.3.4.15 Pre-Launch Support

Simple operational tests.

6.3.4.16 Design Life

Overall module 10 years with filter and calibrate source replacement between missions as required.

6.3.4.17 Module Location

Attached to front of Module 1.2.

6.3.5 Engineering Characteristics of Module 1.4 (Light Shield Module)

6.3.5.0 General Description

Sunshine, earthshine or light from these sources reflecting from the spacecraft present a serious problem to optical observation. As discussed in Chapter 7, a means to reduce this source of interference is the inclusion of a light shield. An example of an effective light shield for a light gathering system of diameter 6 inches (15 cm) is shown in Fig. 6.1. The light shield in the operating configuration is 80 inches (2.03 m) long and 38.5 inches (0.98 m) in diameter. The module can be built such that it fits in a confined volume 40 cm x 40 cm x 25 cm in the stowed position and can then be expanded to full size by gas pressure or other means prior to use.

6.3.5.1 Weight

Approximatly 10 kg.

6.3.5.2 Dimensions

Stored 25 x 40 x 40 cm.

Operating 1.0 x 1.0 x 2 m.

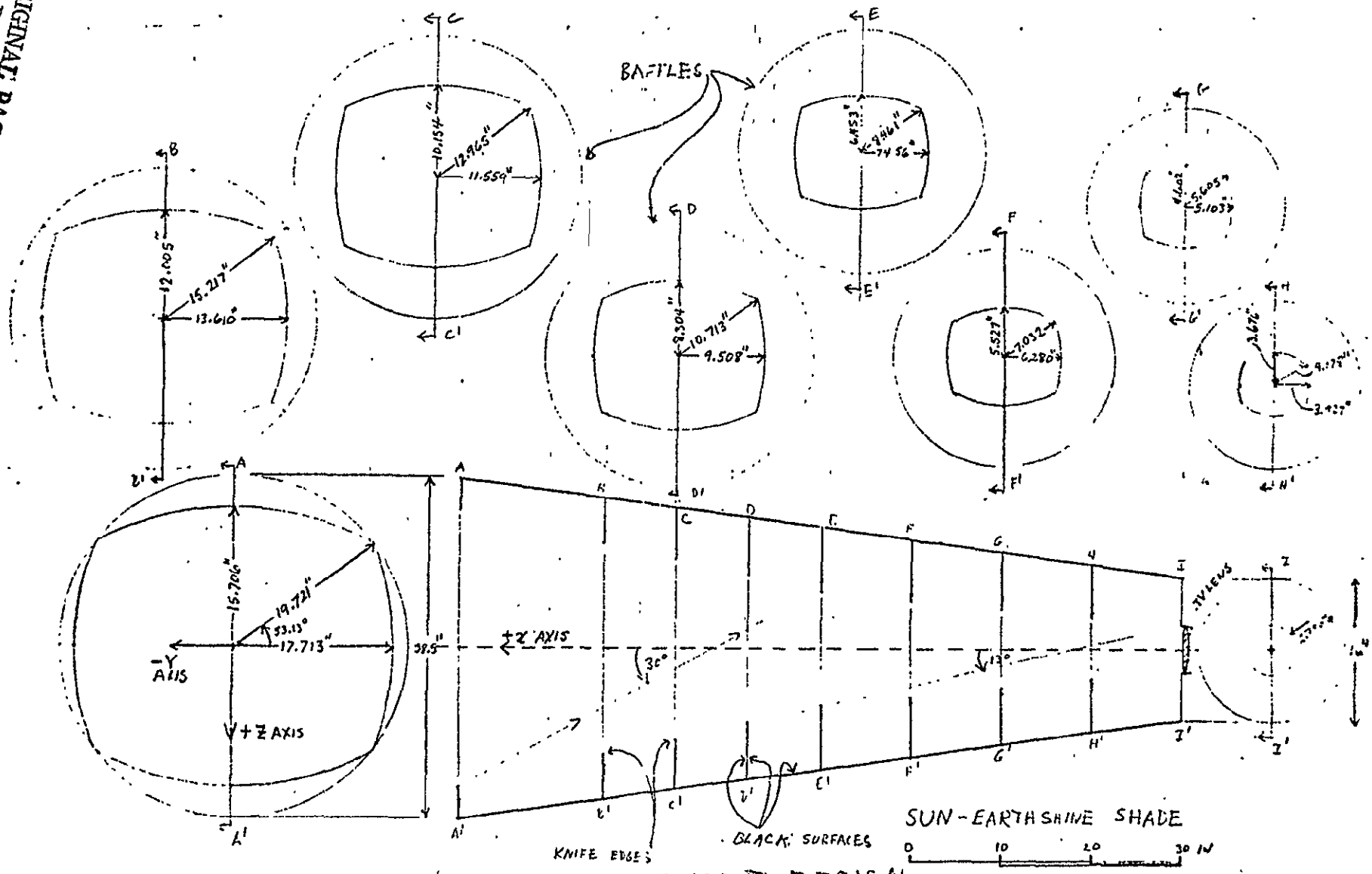

FIG 6.1 SAMPLE SUNSHADE DESIGN

U OF ALASKA
E WESCOTT

6.3.5.3 Power Requirement

None, except possibly for deployment purposes TBD.

6.3.5.4 Output Signal Characteristics

10^6 or better light rejection 15^o off pointing axis.

6.3.5.5 Data Acquisition Duty Cycle

See 6.3.2.5.

6.3.5.6 RFI, Magnetic Interference

Not susceptible, non-producing except possibly during deployment.

6.3.5.7 Temperature Range

Ambient Space Environment allowed.

6.3.5.8 Shock and Vibration

Stowed position minimum 30 g shock, 5 g vibration to 5 Hz.

6.3.5.9 Spectral Response

Designed for use in visual band.

6.3.5.10 Resolution and Sensitivity

N/A

6.3.5.11 Data Collection Rate

N/A

6.3.5.12 Control Requirements

If deployed by EVA, none; if deployed from cabin need deployment control. If flown in erected position, none.

6.3.5.13 Housekeeping Data Requirement

None.

6.3.5.14 Dynamic Range

See Section 7 for optical characteristics, otherwise N/A.

6.3.5.15 Pre-Launch Support

None.

6.3.5.16 Design Life

Could be ejected at end of each mission or could be designed for repeated use over several years.

6.3.5.17 Module Location

Attached to front of Module 1.3.

6.3.6 Engineering Characteristics of Module 1.5 (Control and Power Supply Module, Including Inter-modular Cabling)

6.3.6.0 General Description

The Control and Power Supply Module will provide approximately 7 voltages to Module 1.1 and contain various controls for subsystem 1. These include 1) gain control, 2) focusing control, 3) pedestal control, 4) beam control, 5) aperture control (with switch position allowing automatic aperture control), 6) high-voltage on-off control and 7) Module 1.1 on-off control. By definition we include within Module 1.5 the cabling required to interconnect the control and power supply components of Module 1.5 with the other modules of subsystem 1.

6.3.6.1 Weight

Estimate main module 5 kg.

Estimate cabling 5 kg.

6.3.6.2 Stored and Operating Dimensions

Main module - 20 x 20 x 25 cm.

Cabling - 3 cm diameter by 10-15 cm.

6.3.6.3 Power Requirement

12 watts continuous at 28 vdc during operation, standby, if any TBD.

6.3.6.4 Output Signal Characteristics

Video, 4 MHz bandpass (to contral OBIPS Control Module).

6.3.6.5 Data Acquisition Duty Cycle

See 6.3.2.5.

6.3.6.6 RFI, Magnetic Interference

See 6.3.2.6.

6.3.6.7 Temperature Range

Main module $+5^{o}$ C to $+30^{o}$ C.

Cabling, space environment.

6.3.6.8 Shock and Vibration

TBD

6.3.6.9 Spectral Response

See 6.3.2.9.

6.3.6.10 Resolution and Sensitivity

See 6.3.2.10.

6.3.6.11 Data Collection Rate

See 6.3.2.11.

6.3.6.12 Control Requirements

Manual control only by crew.

6.3.6.13 Housekeeping Data Requirement

None, except manually accessible test points.

6.3.6.14 Dynamic Range

See 6.3.2.14.

6.3.6.15 Pre-Launch Support

See 6.3.2.15.

6.3.6.16 Design Life

10 years.

6.3.6.17 Module Location

Panel mounted within Spacelab or Shuttle Cabin, cabling from that point to Module 1.1.

6.4 SYSTEM NO. 2, ULTRAVIOLET IMAGER

6.4.1 General Description

System No. 2 is an imaging system which is sensitive in the far ultraviolet region of the spectrum and which is specifically blind to emissions in the visible and infrared (solar blind). Except for the spectral response, the requirements are similar to those for system No. 1 (visible imaging system). Where possible, the two systems should employ identical components. Primary differences will be in the detector, optics, and sunshade. The system should produce 200 TV lines resolution with a photocathode current density of 7×10^{-8} $\mu a/cm^2$ and 400 TV lines with a current density of 2.2×10^{-7} $\mu a/cm^2$. (Photocurrent densities are used here instead of foot candles since they are easily related to incident radiation through the spectral responsitivity curves).

The camera will be fitted with a reflecting type optical system having a field of view of approximately 16^{o}. The optical design will include aperture control and provision will be made to insert filters in flight either to isolate or to block specified optical wavelengths. A manually-actuated cover will be necessary to protect the optics from deposition of near-spacecraft pollutants. A filter which blocks visible and infrared light will be used within or in front of the optics to prevent the thermal damage which could result from the focusing of sunlight. No sunshade will be necessary.

The various modules are identified in accordance with the scheme used in 6.3.1.

6.4.2 Engineering Characteristics of Module 2.1 (Basic UV Camera)

6.4.2.0 General Description

40 mm SIT with UV/visible image converter or equivalent system.

6.4.2.1 Weight.

11 kg.

6.4.2.2 Stored and Operating Dimensions

22 cm x 18 cm x 52 cm.

6.4.2.3 Power Requirement

12 watts continuous at 28 vdc during operation; standby, if any, TBD (supplied from Module 2.5).

6.4.2.4 Output Signal Characteristics

Video, 4 MHz bandpass (to Module 2.5).

6.4.2.5 Data Acquisition Duty Cycle

Variable depending upon general usefulness; 10 minutes to major portions of orbits.

6.4.2.6 RFI, Magnetic Interference

Module does not generate significant RFI or magnetic fields; it is mildly susceptible to RFI below 700 kHz.

6.4.2.7 Temperature Range

Allowed range $+5^{\circ}$ C to $+35^{\circ}$ C.

6.4.2.8 Shock and Vibration

TBD.

6.4.2.9 Spectral Response

1200 Å to 1800 Å.

6.4.2.10 Resolution and Sensitivity

Limiting resolution of 200 to 400 TV lines when incident radiation is sufficient to produce a photocathode current density between 7 x 10^{-8} $\mu a/cm^2$ and 2 x 10^{-7} $\mu a/cm^2$.

6.4.2.11 Data Collection Rate

(1) Primary mode: conventional TV raster at 60 fields per sec; (2) integration mode, one complete raster scan in 1/30 second at intervals set by controls: 0.1, 0.5, 1.0, 2.0 sec.

6.4.2.12 Control Requirements

1. Gain 10 positions
2. Beam Current continuous
3. Integration Mode 5 positions

6.4.2.13 Housekeeping Data Requirement

Temperature accuracy 1^{o} C.

6.4.2.14 Dynamic Range

10^{9} with gain control and aperture control.

6.4.2.15 Pre-launch Support

Simple operational tests with test equipment to be furnished.

6.4.2.16 Design Life

Five years with between-mission servicing.

6.4.2.17 Module Location

On steerable pallet mounted platform or detachable for placement as desired with manipulator arm.

6.4.3 Engineering Characteristics of Module 2.2 (Light Gathering Optics)

6.4.3.0 General Description

Schmidt-Cassegrain telescope which transmits in far UV with a field of view of approximately 16°. The effective aperture will be adjustable from a very small aperture to approximately f1.5. The mirrors will be coated with a 250 Å thick layer of MgF_2 to obtain high reflectance ($\sim$ 80%) in the far UV. The system will also include an MgF_2 Schmidt corrector plate of 1.75 mm thickness.

6.4.3.1 Weight

TBD, probably less than 10 kg.

6.4.3.2 Stored and Operating Dimensions

TBD, probably 20 cm diameter by 50 cm long maximum.

6.4.3.3 Power Requirement

Intermittent < 1 watt at 28 vdc to change aperture.

6.4.3.4 Output Characteristics

6.4.3.5 Data Acquisition Duty Cycle

Same as 6.4.2.5.

6.4.3.6 RFI, Magnetic Interference

Not susceptible to either; possible minor generation of RF noise during aperture changes.

6.4.3.7 Temperature Range

Allowed range $+5^{\circ}$ C to $+35^{\circ}$ C.

6.4.3.8 Shock and Vibration

6.4.3.9 Spectral Response

Transmits over range 1100 Å to 1800 Å.

6.4.3.10 Resolution and Transmittance

In the range 1100 Å to 1800 Å the optical system should have an effective T number of 2.5. The resolution should exceed 25 lines per mm.

6.4.3.11 Data Collection Rate

N/A

6.4.3.12 Control Requirements

Aperture control on command, 9 positions.

6.4.3.13 Housekeeping Data Requirement

None.

6.4.3.14 Dynamic Range

N/A

6.4.3.15 Pre-launch Support

Same as 6.4.2.15.

6.4.3.16 Design Life

Five years.

6.4.3.17 Module Location

Rigidly attached to front of Module 2.1.

6.4.4 Engineering Characteristics of Module 2.3 (Filter, Shutter, Calibrate Module)

6.4.4.0 General Description

Same as 6.3.4.0 except that different filters would be used.

6.4.4.1 Weight

Estimated 5 kg.

6.4.4.2 Stored and Operating Dimensions

Estimated 15 cm x 25 cm x 40 cm (15 cm along optical path).

6.4.4.3 Power Requirement

Intermittent - TBD.

6.4.4.4 Output Signal Characteristics

Light dependent upon selectable filters in position.

6.4.4.5 Data Acquisition Duty Cycle

Same as 6.4.2.5.

6.4.4.6 RFI, Magnetic Interference

Not susceptible, possible generation of minor RFI during switching operations.

6.4.4.7 Temperature Range

$+5^{o}$ to $+35^{o}$C.

6.4.4.8 Shock and Vibration

TBD.

6.4.4.9 Spectral Response

N/A

6.4.4.10 Resolution and Sensitivity

N/A

6.4.4.11 Control Requirements

1. Filter Change 5 positions.
2. Shutter Control 2 positions.
3. Calibrate Control 10 positions.

6.4.4.12 Housekeeping Data Requirement

1. Temperature, accuracy 1^{o} C.
2. Filter Position 5 positions.
3. Calibrate source intensity 10 positions.

6.5 SUBSYSTEM NO. 3 - VISIBLE-NEAR IR PHOTOMETER

6.5.1 General Description

Subsystem No. 3 will consist of a system for measuring the light intensity of various wavelengths of interest to research in the visible and near-infrared regions (3000 Å to 2.5 μm). An adjustable field of view will combine with a wide dynamic range and a fast response time to provide a versatile device for photometric observations from the spacecraft. The photometer subsystems will consist of five modules: 1) a scattered-light shield or baffling system with a mechanical shutter; 2) intensity calibration source; 3) a telescope with changeable field stops; 4) optical filters and 5) detectors. For economy and convenience, the basic configuration of the visible (subsystem No. 3) and ultraviolet (subsystem No. 4) models will be similar except for some differences in Modules 2, 4, and 5.

A manual mechanical shutter will provide protection for the entire optical and electronic system although it will be supplemented by an electronic high voltage turn-off activated by the upper count rate limit of the detectors. Calibration lamps will be mounted in front of the telescope and next to the detector so as to monitor changes in light gathering optics and detector systems which would affect the absolute calibration. For the visible range, a wavelength scanning filter with a band width of one Angstrom or more will be used although there will be provision for other types of optical interference filters. The telescope will be of a modified Cassegrain type with provision for changing the secondary mirror to provide different fields of view (aided also by adjustable field stops to change field shape for special experiments

such as limb scanning. The aperture (10 cm to 15 cm) will be large enough to provide a signal to noise ratio of one for a source brightness of 1 R/A at 5000 Å assuming a detector quantum efficiency of 10%. Scattered light shielding will be provided to reduce light scattered in the system by 10^{-10} for the sun at 20° and the sunlit earth 10° from the optic axis at full 2.5° field of view settings. Because of the relatively large size of the light shield (not less than 1.5 x 0.5 meters), several detector-filter combinations are proposed for each telescope so a single telescope can be used as a multiwavelength detector. Interchangeable, cooled detectors will be installed with pulse counting digital electronics providing a 10 MHz bandpass giving a continuous dynamic range of $> 5 \times 10^{6}$. Means for recording automatically peripheral information such as field of view, wavelength, direction, low voltage, high voltage, etc., will be provided for in the signal recording system.

The various modules of subsystem No. 3 are numbered according to the following list:

3.1 Light shield and mechanical shutter,

3.2 Intensity calibration system,

3.3 Light gathering optics and field stops,

3.4 Optical filters,

3.5 Detectors and electronics.

Engineering specifications are given in Section 6.5.2 following.

6.5.2 Engineering Characteristics of Module 3.1 (Light Shield and Shutter)

6.5.2.0 General Characteristics

The light shield module for the photometer subsystem will be of the same type as for the imaging subsystem. Refer therefore to

Section 6.3.4 for general engineering characteristics; also see Chapter 7.

6.5.3 Engineering Characteristics of Module No. 3.2 (Intensity Calibration)

6.5.3.0 General Characteristics

Two or more light sources (typically LED's) with constant power source to provide information on changes in the sensitivity of the light detecting system.

6.5.3.1 Weight

0.5 kg.

6.5.3.2 Stored and Operating Dimensions

N/A

6.5.3.3 Power Requirements

0.1 watt intermittant.

6.5.3.4 Output Signal Characteristics

N/A

6.5.3.5 Data Acquisition Duty Cycle

N/A

6.5.3.6 RFI or Magnetic Interference

None.

6.5.3.7 Temperature Range

Operating: 20 to 30° C.

Stored: -5° to +35°C.

6.5.3.8 Shock and Vibration

TBD.

6.5.3.9 Spectral Response

Emitting over spectral range of detector.

6.5.3.10 Resolution and Sensitivity

Resolution: Spatial: N/A.

Temporal: N/A.

Sensitivity: N/A.

6.5.3.11 Data Collection Rate

Intermittant.

6.5.3.12 Control Requirements

1. on-off (2 positions).
2. step intensity changes (5 positions).

6.5.3.13 Housekeeping Data

1. low voltage.
2. on-off.
3. intensity step.

6.5.3.14 Dynamic Range

N/A

6.5.3.15 Pre-launch Support

Cycled during pre-launch; test routine to be provided.

6.5.3.16 Design Life

Ten years with between mission-servicing.

6.5.3.17 Module Location

Sources near: 1. shutter.

2. detectors.

Power supply in command module.

6.5.4 Engineering Characteristics of Module No. 3.3 (Optics and Field Stops)

6.5.4.0 General Characteristics

A Cassegrain type telescope with stops defining full fields of

view from approximately 0.25 to 2.5 angular degrees, varying in shape.

6.5.4.1 Weight

Five kg.

6.5.4.2 Stored and Operating Dimensions

25 cm x 60 cm.

6.5.4.3 Power Requirements

Intermittant - 2 watts at 28 VDC to change aperture on manual command.

6.5.4.4 Output Signal Characteristics

Light beam varying in shape, with angular divergence between 0.25 and 2.5°.

6.5.4.5 Data Acquisition Duty Cycle

N/A

6.5.4.6 RFI or Magnetic Interference

Not susceptible, none produced.

6.5.4.7 Temperature Range

Operating: $\pm$ 5° C.

Stored: -10 to +35° C.

6.5.4.8 Shock and Vibration

TBD.

6.5.4.9 Spectral Response

Mirrors coated for 3000 to 2.5 µm.

6.5.4.10 Resolution and Sensitivity

Resolution: Spatial: 0.25° angular.

Temporal: N/A.

Sensitivity: N/A.

6.5.4.11 Data Collection Rate

N/A

6.5.4.12 Control Requirements

1. field stop type and size ($\sim$ 5 positions).
2. pointing direction unless bore-sited with Subsystems 1 and 2.

6.5.4.13 Housekeeping Data

1. temperature (to 1° C).
2. field stop type and size ($\sim$ 5 positions).
3. pointing direction $\pm$ 0.1° unless bore-sited with Subsystems 1 and 2.

6.5.4.14 Dynamic Range

N/A

6.5.4.15 Pre-launch Support

Same as 6.3.1.15.

6.5.4.16 Design Life

Ten years.

6.5.4.17 Module Location

Rigidly attached to 3.1.

6.5.5 Engineering Characteristics of Module No. 3.4 (Optical Filters)

6.5.5.0 General Characteristics

Optical bandpass limiters of various types, i.e., multi-layer interference filters, acoustically tuned filter, etc., to be mounted directly in front of the appropriate detectors.

6.5.5.1 Weight

0.5 kg.

6.5.5.2 Stored and Operating Dimensions

5 cm by 15 cm in diameter.

6.5.5.3 Power Requirements

None, except intermittent filter change.

6.5.5.4 Output Signal Characteristics

Light dependent upon filter characteristics.

6.5.5.5 Data Acquisition Duty Cycle

10 min to substantial portion of orbit.

6.5.5.6 RFI or Magnetic Interference

None.

6.5.5.7 Temperature Range

Operating: $\pm$ 0.5° C.

Stored: 0 to 35° C.

6.5.5.8 Shock and Vibration

TBD.

6.5.5.9 Spectral Response

Variable over visible band.

6.5.5.10 Resolution and Sensitivity

Resolution: Spatial: N/A.

Temporal: N/A.

Sensitivity: N/A.

6.5.5.11 Data Collection Rate

N/A

6.5.5.12 Control Requirements

1. wavelength position ($\sim$ 5 positions).

2. wavelength range - for tuned filter (probably analog or perhaps multi-position).

6.5.5.13 Housekeeping Data

1. temperature to + 1° C.

2. wavelength bandpass (analog or multi-position).

3. wavelength of peak (analog or multi-position).

6.5.5.14 Dynamic Range

N/A

6.5.5.15 Pre-launch Support

Simple operational tests with equipment to be provided.

6.5.5.16 Design Life

Ten years with between-mission servicing.

6.5.5.17 Module Location

Directly in front of detectors on optic axis.

6.5.6 Engineering Characteristics of Module No. 3.5 (Detectors and Electronics)

6.5.6.0 General Characteristics

One or more detectors with beam splitter/mirror and pulse counting electronics.

6.5.6.1 Weight

1 kg.

6.5.6.2 Operating and Stored Dimensions

20 cm x 20 cm x 40 cm.

6.5.6.3 Power Requirements

5 watts continuous at 28 vdc during operation.

6.5.6.4 Output Signal Characteristics

Binary 8 bit parallel output Non Return Zero or 16 bit if necessary to match Pulse Coded Modulation.

6.5.6.5 Data Acquisition Duty Cycle

Ten min to substantial fraction of orbit.

6.5.6.6 RFI or Magnetic Interference

None.

6.5.6.7 Temperature Range

Operating: 0° C to -20° C.

Stored:

6.5.6.8 Shock and Vibration

TBD.

6.5.6.9 Spectral Response

Selected between 3000 Å and 2.5 μm.

6.5.6.10 Resolution and Sensitivity

Resolution: Spatial: N/A.

Temporal: typically 1 millisecond.

Sensitivity: Signal count equals noise for source of 1 R/A. filling 2.5° full field with average detector at 5000 Å.

6.5.6.11 Data Collection Rate

Possible 10 MHz bandpass. Rate determined by needs of individual experiment. Depends on word length of PCM telemetry. For an 8 bit word, the data rate will not exceed 1000 words/sec for most observations (with housekeeping).

6.5.6.12 Control Requirements

1. on-off low voltage.
2. on-off high voltage.
3. integration period control.
4. detector type/combination.
5. integration period.

6.5.6.13 Housekeeping Data

1. temperature.
2. high voltage.
3. low voltage.
4. detector type/combination mode.
5. integration period.

6.5.6.14 Dynamic Range

Depends on data format

$> 5 \times 10^6$ available.

6.5.6.15 Pre-launch Support

Operational tests with test equipment to be provided.

6.5.6.16 Design Life

Five years with between-mission servicing.

6.5.6.17 Module Location

Detectors and beam splitter on optic axis at rear of photometer. Electronics nearby.

6.6 SUBSYSTEM NO. 4 - ULTRAVIOLET PHOTOMETER

6.6.0 General Characteristics

The plan of the ultraviolet photometer subsystem will be the same as No. 3 (visible photometer) and consist of five modules:

4.1 Scattered light shield with a mechanical shutter.

4.2 Intensity calibration source.

4.3 Optical filters.

4.5 Detectors with electronics.

Subsystem No. 4 will include the ultraviolet from around 300 Å to 3000 Å

and thus modules 2, 4 and 5 will be exchanged for physically different apparatus and the mirror in 4.3 will have a different coating. However, the basic configuration will be unchanged.

The intensity calibration source will vary, depending on the wavelength region and it will probably be a line emission in some cases. The mirror coating could have a reflectivity as low as 8% in the extreme ultraviolet but filter bandwidths are relatively large, cathode quantum efficiencies high and detector noise is low so the telescope aperture will probably not be increased. Filters are generally metal thin films, absorbing gas, or broad-band windows. Subtractive methods can be used to reduce the bandwidth, making necessary the use of two or more detectors simultaneously which could be difficult because of lack of beam splitters or signal. Two photometers could be deployed, however, because for most wavelengths in the region 300 Å to 1750 Å, a windowless photocathode and other "solar blind" detectors could be used, thereby considerably reducing the size of the light shield which would allow room for a second photometer.

6.6.1 Engineering Characteristics of Module 4.1 (Light Shield and Shutter)

6.6.1.0 General Characteristics

The light shield Module for the photometer subsystem will be of the same type as for the imaging subsystem. Refer therefore to Section 6.3.4 for Engineering Characteristics.

6.6.2 Engineering Characteristics of Module 4.2 (Calibration Source)

6.6.2.0 General Characteristics

Two or more light sources (typically gas discharge types)

with constant power source to provide information on changes in the sensitivity of the light detecting system.

6.6.2.1 Weight

0.5 kg.

6.6.2.2 Stored and Operating Dimensions

N/A

6.6.2.3 Power Requirements

0.1 watt intermittant.

6.6.2.4 Output Signal Characteristics

N/A

6.6.2.5 Data Acquisition Duty Cycle

N/A

6.6.2.6 RFI or Magnetic Interference

None.

6.6.2.7 Temperature Range

Operating: -20^{o} to 35^{o} C.

Stored:

6.6.2.8 Shock and Vibration

TBD.

6.6.2.9 Spectral Response

Emitting over spectral range of detector.

6.6.2.10 Resolution and Sensitivity

Resolution: Spatial: N/A.

Temporal: N/A.

Sensitivity: N/A.

6.6.2.11 Data Collection Rate

Intermittant.

6.6.2.12 Control Requirements

1. on-off (2).

2. step intensity changes (5).

6.6.2.13 Housekeeping Data

1. low voltage.

2. on-off.

3. intensity step.

6.6.2.14 Dynamic Range

N/A

6.6.2.15 Pre-launch Support

Cycled during pre-launch test routine to be provided.

6.6.2.16 Design Life

Five years with between-mission servicing.

6.6.2.17 Module Location

Sources near: 1. shutter.

2. detectors.

Power supply in command Module.

6.6.3 Engineering Characteristics of Module 4.3 (Optical System)

6.6.3.0 General Characteristics

A Cassegrain-type telescope with stop defining fields of view from approximately 0.25 to 2.5 angular degrees, varying in shape.

6.6.3.1 Weight

Five kg.

6.6.3.2 Stored and Operating Dimensions

25 cm x 60 cm.

6.6.3.3 Power Requirements

Intermittant 2 watts at 28 vdc to change aperture on manual command.

6.6.3.4 Output Signal Characteristics

Light beam varying in shape, with angular divergence between 0.25 and 2.5°.

6.6.3.5 Data Acquisition Duty Cycle

N/A

6.6.3.6 RFI or Magnetic Interference

None.

6.6.3.7 Temperature Range

Operating: $0 \pm 5^{\circ}$ C.

Stored: -10 to 35° C.

6.6.3.8 Shock and Vibration

TBD.

6.6.3.9 Spectral Response

Mirrors coated for 300 Å to 3000 Å.

6.6.3.10 Resolution and Sensitivity

Resolution: Spatial: 0.25° angular.

Temporal: N/A.

Sensitivity: N/A.

6.6.3.11 Data Collection Rate

N/A

6.6.3.12 Control Requirements

1. field stop type and size.

2. pointing direction (unless bore-sited with imagers).

6.6.3.13 Housekeeping Data

1. temperature.

2. field stop type and size.

3. pointing direction $\pm$ 0.1° (unless bore-sited with imagers).

6.6.3.14 Dynamic Range

N/A

6.6.3.15 Pre-launch Support

Same as 6.3.1.15.

6.6.3.16 Design Life

Ten years.

6.6.3.17 Module Location

Rigidly attached to 4.1.

6.6.4 Engineering Characteristics of Module 4.4 (Optical Filters)

6.6.4.0 General Characteristics

Optical bandpass limiters of various types, i.e., aluminum, beryllium, oxygen, LiF, CaF, etc., to be mounted directly in front of the appropriate detectors.

6.6.4.1 Weight

0.5 kg.

6.6.4.2 Stored and Operating Dimensions

5 cm by 15 cm diameter or less.

6.6.4.3 Power Requirements

None, except intermittent to change filters.

6.6.4.4 Output Signal Characteristics

N/A

6.6.4.5 Data Acquisition Duty Cycle

N/A

6.6.4.6 RFI or Magnetic Interference

None.

6.6.4.7 Temperature Range

Operating: $0 \pm 10^{\circ}$ C.

Stored: 0 to 35° C.

6.6.4.8 Shock and Vibration

TBD.

6.6.4.9 Spectral Response

Dependent upon filter.

6.6.4.10 Resolution and Sensitivity

Resolution: Spatial: N/A.

Temporal: N/A.

Sensitivity: N/A.

6.6.4.11 Data Collection Rate

N/A

6.6.4.12 Control Requirements

1. wavelength position.
2. wavelength range (for tuned filter).

6.6.4.13 Housekeeping Data

1. temperature $\pm 1^{\circ}$ C.
2. wavelength bandpass.
3. wavelength of peak.

6.6.4.14 Dynamic Range

N/A

6.6.4.15 Pre-launch Support

Simple operational tests with equipment to be provided.

6.6.4.16 Design Life

Five years with between-mission servicing.

6.6.4.17 Module Location

Directly in front of detectors on optic axis.

6.6.5 Engineering Characteristics of Module 4.5 (Detectors and Electronics)

6.6.5.0 General Characteristics

One or more detectors with beam splitter/deflector and pulse counting electronics.

6.6.5.1 Weight

1 kg.

6.6.5.2 Operating and Stored Dimensions

Not greater than 10 cm diameter by 25 cm.

6.6.5.3 Power Requirements

1 watt continuous at 27 vdc during operation.

6.6.5.4 Output Signal Characteristics

Binary 8 bit parallel output Non Return Zero or 16 bit if necessary to match Pulse Code Modulation.

6.6.5.5 Data Acquisition Duty Cycle

10 min to major portion of orbit.

6.6.5.6 RFI or Magnetic Interference

None.

6.6.5.7 Temperature Range

Operating: -20° C to $+20^{\circ}$ C.

Stored: $+5^{\circ}$ C to $+35^{\circ}$ C.

6.6.5.8 Shock and Vibration

TBD.

6.6.5.9 Spectral Response

Selected between 300 Å and 3000 Å.

6.6.5.10 Resolution and Sensitivity

Resolution: Spatial: N/A.

Temporal: typically 1 millisecond.

Sensitivity: TBD.

6.6.5.11 Data Collection Rate

Possible 10 MHz bandpass. Rate determined by needs of individual experiment. Depends on word length of PCM telemetry. For an 8 bit word, the data rate will not exceed 1000 words/sec for most observations (with housekeeping).

6.6.5.12 Control Requirements

1. on-off low voltage.
2. on-off high voltage.
3. integration period control.
4. detector type/combination.
5. integration period.

6.6.5.13 Housekeeping Data

1. temperature ($\pm$ 1° C).
2. high voltage.
3. low voltage.

4. detector type/combination mode.

5. integration period.

6.6.5.14 Dynamic Range

Depends on data format.

> 5×10^6 available.

6.6.5.15 Pre-launch Support

Operational tests with test equipment to be provided.

6.6.5.16 Design Life

Six months.

6.6.5.17 Module Location

Detectors and beam splitter on optic axis at rear of photometer. Electronics nearby.

6.7 ENGINEERING CHARACTERISTICS OF OBIPS CENTRAL CONTROL MODULE (CCM)

6.7.1 General Description

Figure 5.4 illustrates the general concept of the CCM. It receives inputs from the various OBIPS subsystems and from the Spacelab or Shuttle where it is installed. Except for the control functions contained within subsystems, the CCM contains all controls affecting the OBIPS, including pointing of subsystems. It also contains housekeeping displays and any necessary video displays that cannot be provided by the basic Spacelab or Shuttle. The primary outputs of the CCM are the video or digital signals and certain housekeeping data signals that need to be recorded on video tape or directly telemetered to ground.

The final configuration and the various essential functions of the CCM are dependent upon detailed characteristics of both the OBIPS subsystems and the Spacelab or Shuttle interfaces. For example, the CCM might or might not need to include computational ability for pointing control and perhaps video displays or video recording capability. The final design can also depend upon the desired level of crew member participation in such functions as temperature control of OBIPS subsystems or the monitoring of housekeeping functions. Most likely, it is best to minimize the need for crew attention to peripheral functions. The total CCM can be assembled from modular components having specific functions as follows:

1. Horizontal and vertical drive for Type I subsystems,
2. Composite synch for Type I subsystems,
3. Composite blanking for Type I subsystems,
4. Integration control for Type I subsystem,
5. Video switching control,
6. Video mixer,
7. Character generator for video display,
8. Video displays,
9. Time code decoder,
10. Subsystem pointing control,
11. Subsystem pointing indication,
12. Power processing or regulation (if necessary),
13. Housekeeping displays (temperature, filter and shutter placement, etc.),
14. Video or digital signal record,
15. Output signal processing.

These functions are described in following subsections.

6.7.1.0 Synchronization Generator (Horizontal and Vertical Drive and Blanking, Composite Synch and Blanking)

This provides the synch pulses which initiate the horizontal and vertical scans. The synch and blanking signals are also incorporated into the recorded or telemetered video signals to synchronize display monitors and to blank the monitors during horizontal and vertical retrace intervals. Synchronization pulses are provided to the character generator, integration control video mixer, video switcher, and output signal processor.

6.7.1.1 Reference Signal

(If needed for output signal reasons).

6.7.1.2 Integration Controllers

In some of the likely experiments there will be insufficient optical radiation to allow imaging with high temporal resolution. Experience with ground-based imaging systems has shown that their effective sensitivity can easily be extended by two to three orders of magnitude by the simple expedient of allowing the image to integrate for several seconds on a storage target within the detector tube. The image is subsequently read out in 1/30 sec. The integration controller determines the integration time by counting vertical synch pulses. Because the readout duration is only 1/30 sec, the integration controller should include either a disc recorder or a storage tube to hold the image so that the operator can view it critically. (Similar to the schemes being used in the airport security X-ray machines.)

6.7.1.3 Video Switching Control

There will be several sources of video signal - two or more imaging systems, one or more recorders, and a character generator. There will also be several possible receptors for video signals - two or more display monitors, waveform monitors, one or more tape recorders, one or more telemetry modules, and a video mixer. In order to retain full versatility, a video switcher should enable the operator to connect any video source to any video receptor.

6.7.1.4 Video Commutator

Depending on the total data storage capability and the transmission capability during an experiment, it may be desirable at times to commutate two imagers to share a single recorder or telemetry module. A likely situation is to have one imager producing fast time resolution images while another is operated in the integration mode. The fast imager could be interrupted once each second to insert a single readout frame from the integrator.

6.7.1.5 Video Character Generator

To permit cost- and time-effective analysis of video data, it is essential that time be displayed on each frame of video data and also that other parameters be so displayed. Examples of such other parameters are pointing data, time, particle accelerator beam on-off signals or other indicators of activation of various kinds of active experiments. The purpose of the character generator is to process decoded timing and other information into a format directly readable when inserted into a video signal.

6.7.1.6 Video Displays

Unless enough video display capability is provided by the Spacelab or Shuttle, the CCM will need to incorporate one or more convential video monitors to display Type I subsystem outputs.

6.7.1.7 Time Code Decoder

Decoded time fed to the video character generator is essential. If such signals are not available in proper format from the Spacelab or Shuttle, the CCM must contain a suitable decoder.

6.7.1.8 Subsystem Pointing Control

Manual or computer control of subsystem view directions is required. The complexity of such controls will depend upon the versatility desired in pointing, the simplest being for a mode in which all subsystems are on a common steerable mount. The pointing control can be part of the OBIPS CCM or it can be provided as a support function by Spacelab or Shuttle.

6.7.1.9 Subsystem Pointing Indicators

Regardless of the means of subsystem pointing control (see Section 6.7.1.8), a signal usable by the video character generator must be available to permit merging of the pointing data with the video signals.

6.7.1.10 Input Power Processing Option

It seems unlikely that the CCM will need to perform processing of input power (28 vdc or other) but it probably will need to serve as a power distribution point, perhaps with fusing.

6.7.1.11 Housekeeping Displays

Potentially the OBIPS has a large number of housekeeping

outputs that need relatively infrequent observation by the operating crew. Consequently it seems desirable to design a display scheme permitting manual command of the various housekeeping signals as needed and perhaps to include capability for essentially continuous display of selectable parameters. See also Section 6.8.

6.8 DATA HANDLING REQUIREMENTS

6.8.1 General Statement

The total OBIPS data handling requirement for a particular mission depends upon the number of subsystems flown. Requirements established in following sections are preliminary and are likely to be changed later. However, these requirements illustrate the general magnitude of the data handling task.

6.8.2 Imaging Subsystem Data Handling

With world time and astronomical look angles appearing within the raster, the peripheral data requirement is substantially reduced without serious degradation to the imaging data. It is reasonable at this stage to assume that the remaining 4 kbps of peripheral data can be packed into the vertical interval thus incorporating all relevant data to the subsystem within one channel. There presently exists sufficient information bandwidth within the vertical interval to easily accommodate the required data.

If transmission (or recording) bandwidth requirements do not permit more than one imaging system to operate at a time, field switching may be employed to matrix multiple sources to fit the requirements. This method is further enhanced when all peripheral data are packed in

the vertical interval giving each frame the ability to stand alone while remaining completely referenced.

Imaging Subsystem

Video Data

To include world time and look angles within raster via character generator.

Required bandwidth - 4 MHz

Peripheral Data	8 bit words		
Spacecraft position	480/sec	3.84 kbps	
Housekeeping			
Integration Mode		1 word/sec	0.04 kbps
Filter Selection			
Camera Temperature		1 word/sec	
Aperture		1 word/sec	
Shutter			
Calibration Light			
Filter Temperature		1 word/sec	
Source ID		1 word/sec	

Video Requirement - 4 MHz

Peripheral and Housekeeping - 3.88 kbps

6.8.3 Photometer Subsystem Data Handling

When operating at a typical dynamic range of 2.5×10^5, each photometer will generate roughly 8 kbps of raw data. If only one is operating then the total data requirement, including peripheral data,

would be roughly 20 kbps. With both operating the requirement increases to roughly 30 kbps (assuming spacecraft position and world time need not be redundant). Time and position data requirements have been formulated assuming readout every 0.01 sec. It is entirely feasible to reduce the data requirement by packing the information into the raw photometer data although this requires more signal processing onboard the spacecraft.

In order to handle the 5×10^6 dynamic range within the 8 bit word format it is necessary to generate 156.25 kbps of data with 50 μsec resolution. If, however, one can utilize the 16 bit word format the data requirement drops to 16 kbps with 0.001 sec resolution. In this case the subsystem data requirement would be reduced to roughly 28 kbps. With both subsystems in operation the data requirement would be roughly 44 kbps.

Parameters	Range	Resolution
World Time	365 days	0.01 sec
Spacecraft Position		
a) Latitude	$\pm 90^\circ$	0.001°
b) Longitude	360°	0.001°
c) Altitude	1000 km	0.1 km
Astronomical Look Angles		
a) 1st axis	360°	0.1°
b) 2nd axis	360°	0.1°
Filter Temperature	25°	0.1°
Camera Temperature	50°	0.2°
Field of View	2.5°	0.1°
Wavelength	6000 Å	1 Å

Photometer Subsystem

Raw Data

Dynamic Range	8 bit Format	16 bit Format
5×10^6 (max)	156.25 kbps	16 kbps
2.5×10^5 (typ)	8 kbps	16 kbps

all above provide at least 0.001 sec time resolution.

Time and Position	8 bit Format
Time (0.01 sec resolution) 600 words/sec	4.8 kbps
Spacecraft Position (0.01 sec time resolution) 800 words/sec	6.4 kbps
Look Angles (0.2 sec time resolution) 20 words/sec	0 .16 kbps
	11.36 kbps

Housekeeping

Field of View	1 word/sec	.04 kbps
Wavelength	2 words/sec	
Filter Temperature	1 word/sec	
Shutter, Calibration Lamp, Voltage Supplies	1 word/sec	

Photometer Subsystem

	8 bit	16 bit
Raw Data Channel	8-156.26 kbps	16 kbps
Peripheral and House-keeping	11.4 kbps	

Total requirement per subsystem

Dynamic Range	8 bit Format	16 bit Format
max	167.65 kbps	27.4 kbps
typ	19.4 kbps	27.4 kbps

7. A SERIOUS LIMIT TO OPTICAL OBSERVATION IN SPACE - STRAY LIGHT FROM SUNSHINE AND EARTHSHINE

7.1 STATEMENT OF THE PROBLEM

The earthbound observer of faint optical phenomena is well aware of the severe limitation imposed by the sunlit or moonlit atmosphere, so much so that at first thought it seems that all problems would be solved if only the observer could be above the atmosphere. Unfortunately, space observations can be seriously compromised by stray light on the detector from several sources:

1. Direct sunlight,
2. Direct moonshine,
3. Direct earthshine,
4. Direct starlight,
5. Aurora and airglow,
6. Light from the above sources reflected off the spacecraft.
7. Light from the various sources scattered from particulate matter in the vicinity of the spacecraft.

The important interference sources to avoid are sunlight and earthshine (and to a lesser extent, moonshine) falling on the detector or reflected on the detector from the spacecraft. One way to avoid the strong light problem on AMPS missions is to restrict the times of active experiments requiring optical diagnostics to the portions of orbits where the spacecraft is not in sunlight. The consequence of such a restriction is illustrated in Fig. 7.1, compiled for three orbits of inclination 50^{o} and spacecraft altitude 300 km for date July 14. Daily precession amounts to only a few degrees of longitude, so one of the orbits shown on Fig. 7.1 would

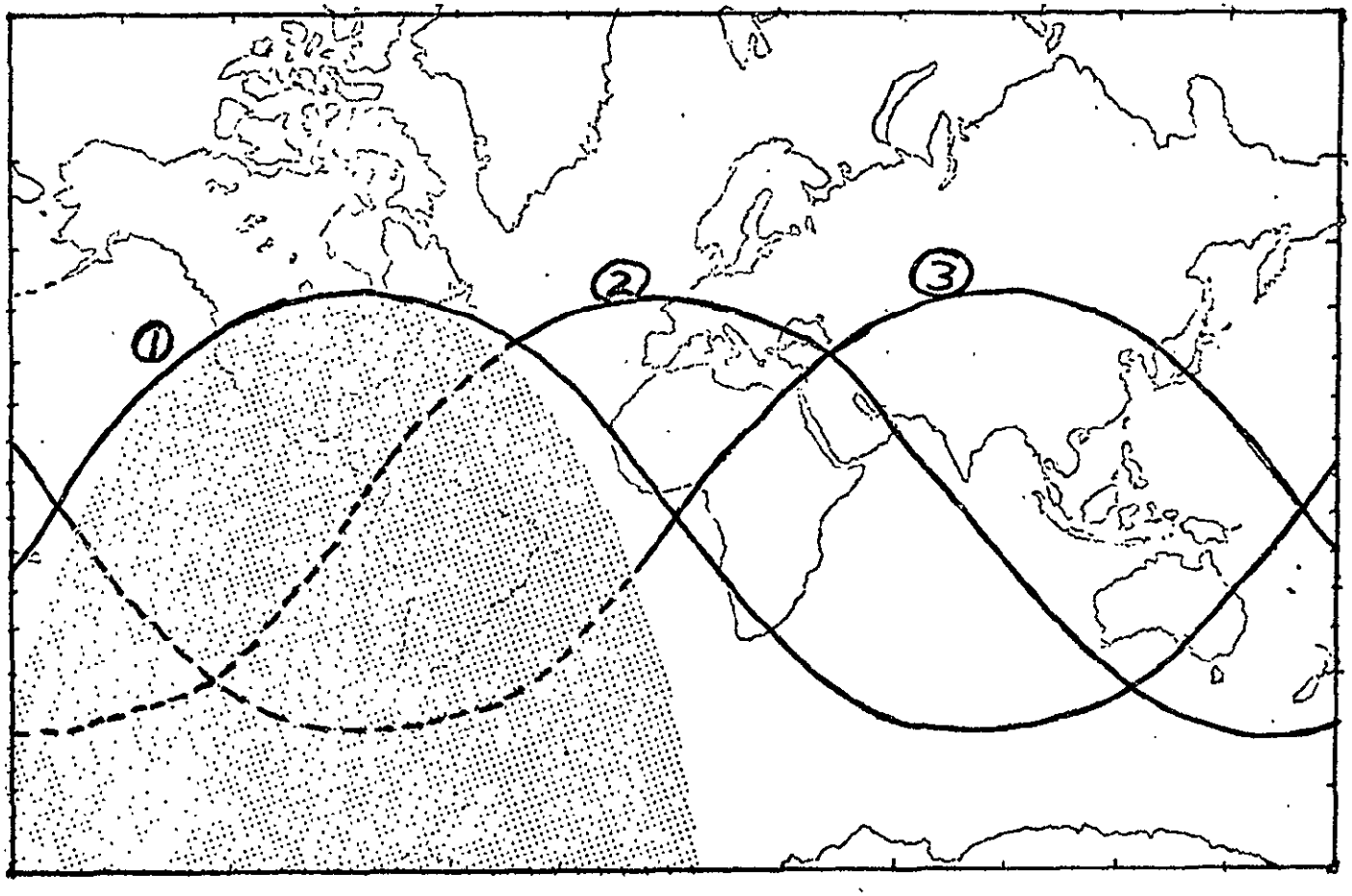

FIG. 7.1 Sample orbits with inclination 50° showing portions in darkness (shaded) for July 14.

approximate the track during a week-long AMPS mission; the particular track is determined by the local time of mission launch. The shaded portion of Fig. 7.1 is that region where the satellite is not in sunlight; near the edge of the region, the satellite is still exposed to earthshine. Therefore the portion of each orbit during which spacecraft detectors are shielded from both sunshine and earthshine is even less than the dashed-line portions of the orbits shown.

Note that it is possible to pick a launch time (Orbit No. 1) which completely precludes the spacecraft from ever being in darkness at this time of year. Even the most favorable case (Orbit No. 3) permits less than 40 minutes of darkness each orbit.

Very likely the technique of avoiding stray light by maintaining spacecraft darkness is too restrictive to be viable on AMPS missions. Therefore we must revert to stray light suppression techniques in order to extend the proportion of mission time during which we can perform active experiments requiring optical diagnostics. Owing to the physical size of the necessary light shields and other factors, the stray light problem significantly impacts the spacecraft interface, mission planning and design of active experiments.

The essential problem is that light falling on the front element of an optical system, whether it is a mirror, lens, filter or window will scatter a fraction of the light into 2π steradians. Special anti-reflective coatings can minimize the amount scattered from a lens surface into the detector, but when one is dealing with either direct sunlight or sunlight reflected from the earth vs. a faint source, the scattered light overwhelms the signal. Figure 7.2 after Leinert and Klüppelberg (1974), illustrates measured scattering coefficients for lenses

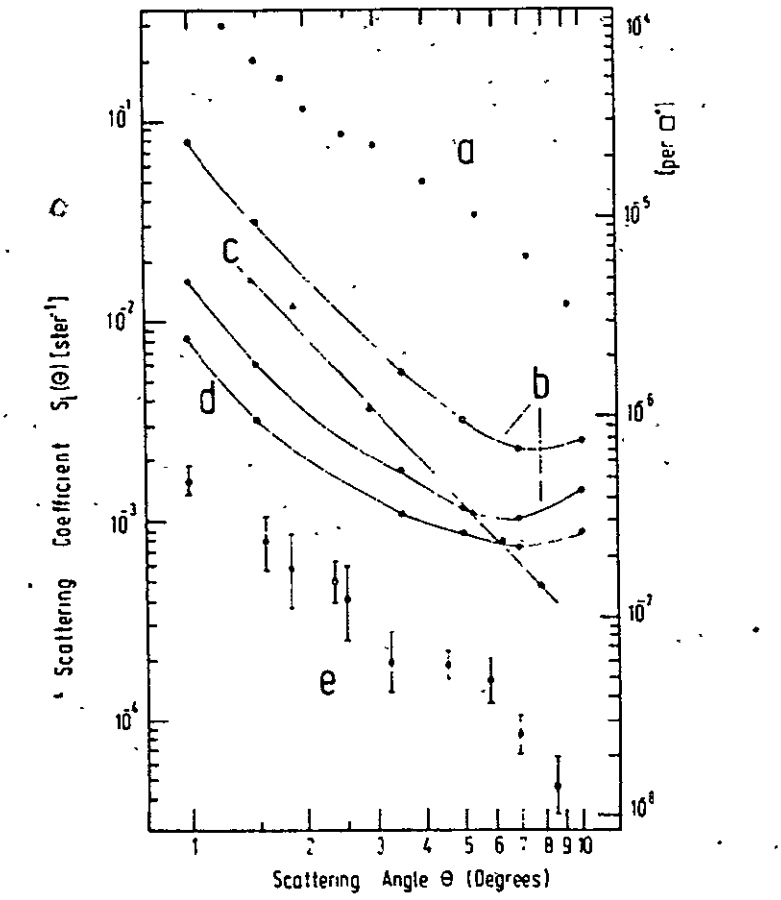

FIG. 7.2 Measured scattering Coefficients for lenses. The focal ratio of the lenses is f/D ≈ 4, the wavelengths 632.8 nm. Curve a is for a slightly dusty lens, b for a 50-mm standard quartz lens cleaned with collodium (o) or in an ultrasonic bath (0). For measurement c on a 66-mm standard glass lens the effect of internal double reflection was suppressed. Curve d is for a 40-mm quartz lens with higher surface quality, e for a carefully polished (λ/20) plane parallel plate of Suprasil I. The accuracy of an individual measurement, if not indicated in the figure, is ± 10%.
(After Leinert and Klüppelberg (1974)).

R. Parthasarathy
Space Sciences

RADIOWAVE IMAGING PROGRAM

This AFOSR supported program reached observational phase in October 1974. I had described the concept and technological details of this program in earlier talks to the Advisory Board. Briefly, our program aims to image a radiowave object field by means of a complex system of identical antennas, receivers, ultrasonic emitters and detectors and finally L.E.D. light bulbs.

The ten weeks of observations enable us to make the following conclusions:

1) Radiowave attenuation (30 MHz) through slim, discrete auroral arcs is negligible.
2) Active auroras, covering a greater part of the sky, do strongly engender radiowave absorption.
3) The radiowave attenuation is in general stronger in the southern sky when the displays are active overhead.

The advisors are welcome to drop by any time to see the records and films obtained in this program.

with various surface preparations. A slightly dusty lens is an order of magnitude worse than a similar one carefully cleaned with collodium. Contaminants resulting from Spacecraft maneuvering and effluvient dumps will appreciably exacerbate the scattering problem by depositing scatterers on the surface.

There is a local atmosphere of contaminants surrounding the spacecraft, but calculations and measurements have shown that the stray light scattered into an optical system from these particles is minor compared to more direct stray light.

Light scattered or reflected from parts of the spacecraft, including booms, antennas, solar panels, etc., also can contribute to untenable background levels.

If the orbit was such that the spacecraft was in the darkness most of the time, and experiments requiring optical instrumentation could be scheduled in darkness, then there is no need for a sunshade. However even a casual inspection of orbits with respect to season and relation to the sun line indicates that those possibilities are very limited. Particularly for a flight in northern hemisphere summer, both direct sun and earthshine are problems for experiments with ground station support or correlative measurements.

7.2 EFFECT OF WINDOW SCATTERING ON STAR DETECTION

A certain percentage of light passing through a window or other front optical surface is scattered into the surface with the effect of increasing the apparent background light level. Normally this is of no significance; however, if a bright source away from the direction of

observation is shining on the front surface, the apparent background light level due to the scattered light may be high enough to be detrimental to the intended observation.

It is now established that such scattering, together with lack of dark adaptation, is the reason why astronauts have not been able to see many stars when their spacecrafts have been in sunshine or earthshine. If windows are properly shielded from stray light, it is probable that stars down to the limit of the earthbound eye ($m_v \sim 6$-7) can be observed through spacecraft windows even in earthshine or sunshine.

It is possible to calculate the apparent background due to forward scattering (see Section 7.3) for a given geometrical relation between spacecraft optical surface, earth and sun. The results can be coupled with experimental values obtained by Ney and Hugh (1966) of the background against which a star of visual magnetide m_v can be seen. The background can be expressed in terms of Solar Surface Brightness (SSB) or in terms of apparent emission rate expressed in kilorayleighs/Å at a particular wavelength.

Since the barium ion line at 4554 Å is of special interest for certain active experiments, that wavelength is chosen to show the equivalency of the two means of expression.

The surface brightness of the sun at 4554 Å is:

$$B_{sun} = 3.14 \times 10^6 \text{ erg/ster cm}^2 \text{ sec Å}$$

$$= 7.19 \times 10^{17} \text{ photons/ster cm}^2 \text{ sec Å}$$

$$= 9.04 \times 10^9 \text{ kR/Å}$$

This relation is used to compile Table 7.1.

TABLE 7.1

Limiting Background Expressed in Units of Solar Surface Brightness (SSB) and in Apparent Emission Rate (kR/Å)

Visual Star Magnitude (m_v)	Limiting Background in SSB	Limiting Background in kR/Å (4554 Å)
-1	10^{7}	403
0	2×10^{-8}	181
1	10^{-8}	90
2	5×10^{-9}	14
3	8×10^{-10}	7.23
4	10^{-10}	0.90
5	10^{-12}	0.0090

7.3 FUNDAMENTALS OF SUNSHADE DESIGN

Since it is not possible to count on being able to eliminate earthshine in the visible by spacecraft maneuver, and requiring all optical experiments to be limited to portions of the orbit which are in total darkness is very restrictive, the optical package should have a sunshade.

Leinert and Klüppelberg (1974) have given an excellent review of stray light suppression in optical space experiments. The article is reproduced as Appendix 7A. Attentuation of incident stray light begins by simply positioning the spacecraft so that the optical device is in its' shadow. In cases where such maneuvers are not feasible during an AMPS mission, sunscreens might be deployed to shade the entrance to the baffle system from direct sun or earthshine.

The critical attenuation of the stray light is best accomplished

with a two-stage baffle system. The baffle system is designed for a certain field of view, and basically requires at least three reflections from absorbing surfaces for any photon coming from outside the field of view to reach the front optical surface. Figure 7.3 illustrates the basic design features of such a baffle system. All the baffle edges are outside the field of view of the optical device. Isotropic reflection and fresnel diffraction from the baffle edges are major sources of residual stray light, and the design should minimize the number of baffles required. State-of-the-art non-reflective surface treatments now approach reflectivities of 0.01 near normal incidence. If photons are required to undergo three reflections before reaching the lens, the flux is attenuated to 10^{-6}. Baffles have been tested with attenuation factors of up to 10^{-9}. For barium cloud and plasma gun observations detailed calculations of distance from the Shuttle to the object, brightness, angular dimensions are required to specify the signal to background requirements and the baffle requirements. Generally, attenuation to 10^{-6} is minimal and 10^{-7} more desirable.

The size of the sunshade is determined by the field of view and the diameter of the front optical surface. Wide fields of view and large apertures require large sunshades.

Design criteria must involve:

1. Field of view,
2. Rigidity of structure when deployed,
3. Minimum warping of the shield between solar illuminated and shaded sides,
4. State-of-art non-reflective surface preparation,

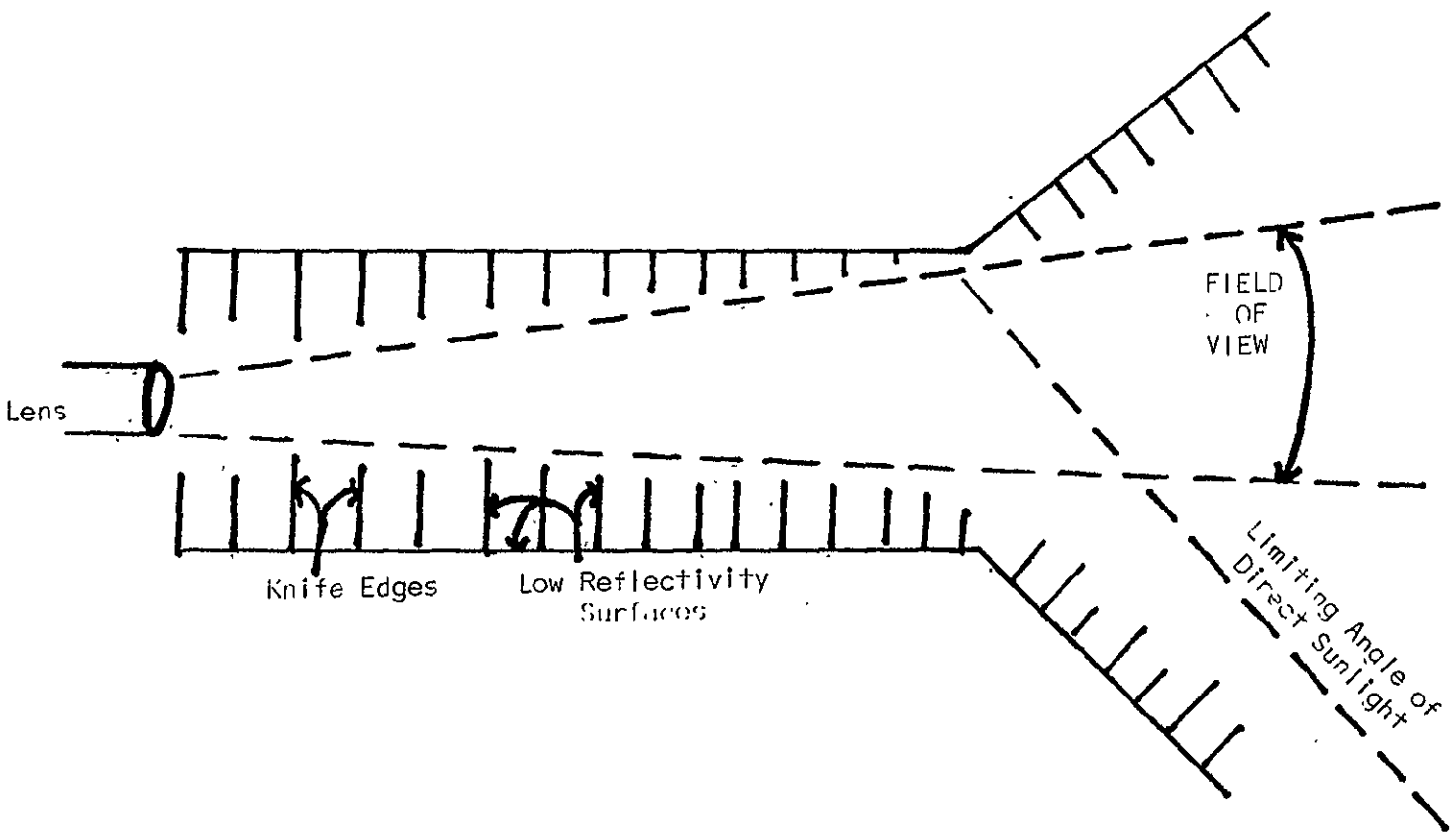
Lens
Knife Edges
Low Reflectivity
Surfaces
FIELD
OF
VIEW
Limiting Angle of
Direct Sunlight

FIG. 7.3

5. Outgassing properties,
6. Provision for protection of front optical surface from dust and other contamination.

7.4 A SAMPLE CALCULATION OF SUNSHIELD EFFECTIVENESS

The following calculations illustrate the effects of scattered light on optical measurement and the consequences of providing light shielding attainable with current technology. The example considers the observation of a thermite barium cloud with a spacecraft mounted television system. This particular series of calculations was prepared for an actual experiment considered for the ASTP Mission.

The sources of scattering and light are taken to be the sun and the earth which are both out of the camera field of view but which both illuminate the lens. A small (but appreciable) fraction of this illumination is scattered on to the TV photocathode by dust on the lens or by lens imperfections. First we consider the effect of the sun in the absence of any baffle system.

The sun's irradiance just outside the atmosphere is:

$$H_s = 1.39 \times 10^{-1} \text{ watts/cm}^2$$

(RCA Electro-Optics Handbook, p. 6-1).

During the experiment, the smallest expected angle between the observation point and the sun is 30°. By extrapolating the curve for a slightly dusty lens in Fig. 7.2 to 30°, one obtains the scattering coefficient:

$$S_\ell = 2 \times 10^{-3} \text{ ster}^{-1}$$

The total flux of scattered light is obtained by multiplying by the area of the lens A:

$$F_S = A\, H_s S_\ell \text{ watts/ster}$$

In terms of the f number and the focal length (FL),

$$A = \frac{\pi}{4}\left(\frac{FL}{f_{no}}\right)^2 \qquad \text{(FL in cm)}$$

$$F_S = \frac{\pi}{4}\left(\frac{FL}{f_{no}}\right)^2 H_S S_\ell \text{ watts/ster}$$

A circular area on the photocathode of area 1 cm^2 corresponds to a field of view given approximately by

$$\Delta\Omega = \frac{1 \text{ cm}^2}{(FL)^2}$$

Hence the intensity (I_S) of the light scattered on to the photocathode is:

$$I_s = \frac{\pi}{4}\left(\frac{FL}{f_{no}}\right)^2 S_\ell H_S \left(\frac{1}{FL}\right)^2 = \frac{\pi}{4}\,\frac{S_\ell H_S}{(f_{no})^2} \text{ watts/cm}^2$$

The photocathode current density is given by:

$$J_s = I_S\, \sigma_o\, M \text{ amps/cm}^2.$$

where σ_o is the photocathode response (amps/watt) at the peak of the spectral response curve) and

$$M = \frac{\int_o^\infty W(\lambda)R(\lambda)d\lambda}{\int_o^\infty W(\lambda)d\lambda}$$

$W(\lambda)$ is the spectral distribution of the illumination source and $R(\lambda)$ is the relative spectral response of the detector. The matching factor M is tabulated in the RCA photomultiplier manual (C131). For the sun and an S-20 photocathode,

$M = 0.406$

$\sigma_o = 0.068$ amp/watt

Combining the above expressions, we obtain finally:

$$J_S = \frac{\pi}{4} \frac{S_\ell H_S}{(f_{no})^2} \sigma_o M \text{ amp/cm}^2$$

Assuming an f1 lens:

$$J_s = \frac{\pi}{4} \frac{(2 \times 10^{-3})(1.39 \times 10^{-1})}{(1)^2} (0.068)(0.406) \text{ amp/cm}^2$$

$$J_s = 6.0 \times 10^{-6} \text{ amp/cm}^2$$

By comparison, the photocathode current density resulting from a 20 kR barium cloud is:

$$J_{4554} = \frac{(20 \times 10^{9})(4.364 \times 10^{-19})(0.066)}{16\ (f_{no})^2}$$

$$= 3.6 \times 10^{-11}\ \text{amp/cm}^2$$

which is five orders of magnitude less than the current due to stray light.

Now let us consider the earthshine problem. The illumination per cm^2 on the earth is

$$H \sin \gamma$$

where H is the solar flux at normal incidence and γ is the sun's elevation angle for the part of the earth which scatters light onto the TV camera lens. A proportion (δ) of this light is reflected by the earth. Since it is reflected isotropically, the reflected light per steradian is:

$$\frac{1}{\pi} H\delta \sin \gamma$$

The light falling on and scattered by the lens is:

$$F_E = \frac{1}{\pi} H \sin \gamma\ \delta\ \Omega_1\ A_2\ S_\ell\ (\theta)$$

Where Ω_1 is the angle subtended by the lens from the earth and A_2 is the area of the earth which contributes to the problem. It can be

easily shown geometrically that

$$\Omega_1 A_2 = \Omega_2 A_1 \cos \beta$$

where A_1 is the area of the lens, Ω_2 is the angle subtended at the camera by the illuminated earth, and β is the angle between the camera axis and the line from the camera to the illuminated earth. Hence

$$F_E = \frac{1}{\pi} H \sin \gamma \, \delta \, \Omega_2 A_1 \cos \beta \, S_\ell (\theta) \text{ watts/ster}$$

$$= \frac{1}{\pi} H \sin \gamma \, \delta \, \Omega_2 \cos \beta \, S_\ell (\theta) \frac{\pi}{4} \left(\frac{FL}{f_{no}} \right)^2 \text{ watts/ster}$$

Following the same reasoning as in the sun calculation, the photocathode current density is:

$$J_E = \frac{\pi}{4} \frac{S_\ell(\theta)}{(f_{no})^2} \frac{1}{\pi} H \sin \gamma \, \delta \, \Omega_2 \cos \beta \, (0.068)(0.406) \text{ amp/cm}^2$$

Let $S_\ell (15^o) = 4 \times 10^{-3}$

$f_{no} = 1$

$H = 1.39 \times 10^{-1}$

$\sin \gamma = \sin 35 = 0.57$

$\delta = 0.15$

$\Omega_2 = 0.05 \times$ (% Earth Illuminated)

$\cos \beta = \cos 15^o = 9.66 \times 10^{-1}$

$$J_E = \frac{4 \times 10^{-3}}{4} (0.139)(0.57)(0.15)(0.05 \times \text{\% Earth Illuminated})(0.966)(0.068)(0.406)$$

$$J_E = 1.6 \times 10^{-8} \times (\text{\% Earth Illuminated}) \text{ amp/cm}^2$$

In summary, the photo currents are:

20 kR cloud $J_{4554} = 3.6 \times 10^{-11}$ amp/cm^2

sun 30° off axis $J_S = 6 \times 10^{-6}$ amp/cm^2

1% of earth at 15° off axis $J_E = 1.6 \times 10^{-8}$ amp/cm^2

From the above derivation, it is clear that this particular barium cloud observation cannot be done without a carefully designed light baffle. (Other constraints precluded the use of narrow band optical filters.)

Now we look at the sun problem again, but with a baffle.

The light reaching the lens now is:

$$H' = H_S \alpha(\theta)$$

where $\alpha(\theta)$ is the baffle attenuation. The direction of H' is just outside the lens field of view since the scattering is primarily from the baffle knife edges; for this case the knife edges are considered to be on a cone of half angle $\sim 8^\circ$.

Using the same formula as before:

$$J_S' = \frac{\pi}{4} \frac{S_\ell(8^\circ)\, H'}{(f_{no})^2} \sigma_o M$$

$S_\ell(8^\circ) = 1.5 \times 10^{-2}$

$J_S' = \frac{\pi}{4} (1.5 \times 10^{-2})(1.39 \times 10^{-1}) \alpha\ (30^\circ)(0.068)(0.406)$ amp/cm^2

$J_S' = 4.5 \times 10^{-5}\ \alpha\ (30^\circ)$

We now turn to the earthshine problem with a baffle. Clearly the portion of the earth beyond 30^{o} contributes less than the sun. We will approximate the problem by lumping together 10% of the earth at an angle of 10^{o}.

$$J_e' = \frac{S_\ell(8^{o})}{4} \; H \sin(35^{o}) \; \delta \; \Omega_2 \; \alpha \; (10^{o})(0.068)(0.406) \; \text{amp/cm}^2$$

$$J_E' = \frac{1.5 \times 10^{-2}}{4} (0.139)(0.57)(0.15)(0.5) \; \alpha \; (10^{o})(0.068)(0.406)$$

$$= 6.1 \times 10^{-7} \; \alpha \; (10^{o})$$

It remains now to evaluate $\alpha(\theta)$ for $\theta = 10^{o}$ and 30^{o}. We have made laboratory measurements with a mockup baffle system to obtain the results given in Table 7.2.

Table 7.2

Observed Baffle Attenuation

Measurement Case	$\alpha(\theta)$
$\theta = 30^{o}$ (no knife edges visible)	1.1×10^{-6}
$\theta = 20^{o}$ (one knife edge visible)	2.6×10^{-6}
$\theta = 15^{o}$ (two knife edges visible)	5.0×10^{-6}
$\theta < 15^{o}$ (three knife edges visible)	7.6×10^{-6}

Additional measurements showed that aerosols in the laboratory and reflections from walls contributed an error near one-half but not greater than the light contributed by one knife edge. A measurement

made at $\theta = 30^{\circ}$ with reduced wall reflections yielded a value of $\alpha = 5.9 \times 10^{-7}$. On this basis, we adopt values for $\alpha(\theta)$ as follows:

$$\alpha(10^{\circ}) = 4 \times 10^{-6} \text{ and } \alpha(30^{\circ}) = 6 \times 10^{-7}.$$

Then $J_S' = (4.5 \times 10^{-5})(6 \times 10^{-7}) = 2.7 \times 10^{-11}$

and $J_E' = (6.1 \times 10^{-7})(4 \times 10^{-6}) = 2.4 \times 10^{-12}$

Table 7.3 presents a summary of the calculations. It shows the result that the observation of the barium cloud is impossible without the light baffling and marginally possible with baffling.

Table 7.3

Summary of Calculations

Source	Photocathode Current J amp/cm^2
20 kR barium cloud	$J_{4554} = 3.6 \times 10^{-11}$
Unshielded sun 30° off axis	$J_S = 6 \times 10^{-6}$
Unshielded earth (1% of earth 15° off axis)	$J_E = 1.6 \times 10^{-8}$
Shielded sun 30° off axis	$J_S' = 2.7 \times 10^{-11}$
Shielded earth (10% of earth 15° off axis)	$J_E' = 2.4 \times 10^{-12}$
Combined shielded earth and sun	$J_S' + J_E' = 2.9 \times 10^{-11}$

7.5 LIGHT SHADE DIMENSIONS

Following after the principles described by Leinert and Klüppelberg (1974) it is possible to design light baffling arrangements that provide

attenuation of 10^{-6} or perhaps as high as 10^{-9}. The basic design is as shown in Fig. 7.3; it consists of a first section and a second section which, if appropriatly chosen, permits maximum attenuation with a compromise between minimum length and minimum diameter of the sunshield. Presented here is a series of diagrams showing sunshield dimensions as a function of angle of protection for various fixed parameters - a) field of view, b) lens diameter and c) the angle between the viewing axis and the direction to the sun.

A key parameter is the lens diameter; the dimensions shown on the diagrams scale linearly as a function of lens diameter, consequently the curves can be scaled to fit any lens diameter.

Figure 7.4 shows the required length of the first section of a light shade as a function of the off axis protection angle for various fields of view. Figures 7.5A and 7.5B contain curves respectively showing the diameter and length of the light shade as a function of the angle of protection from earthshine or moonshine for optics having 0.5° field of view. Figures 7.6 and 7.7 are similar to Fig. 7.5 but are for fields of view 5° and 20°, respectively.

Notice that comparison of the A and B parts of each figure permits choice of a sunshield that provides the best compromise between diameter, length and angle of protection.

7.6 ALLOWED LOOK DIRECTIONS FOR OPTICAL INSTRUMENTS

Even when proper light shades are used with OBIPS subsystems or other optical instruments, the stray light problem potentially is a serious limitation to the conduct of active experiments requiring

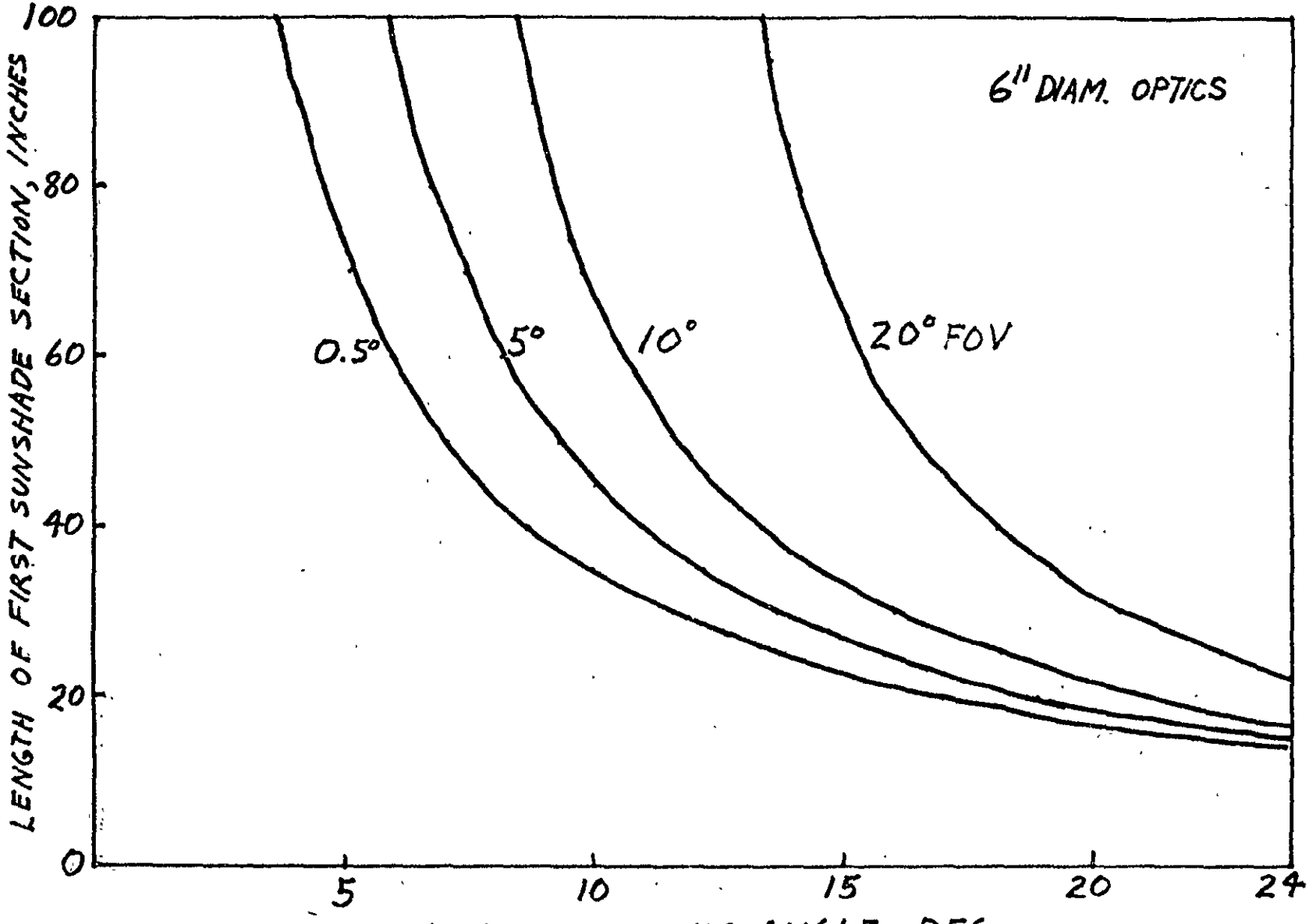

FIG. 7.4 LENGTH OF FIRST SUNSHADE SECTION VS. OFF-AXIS LIMIT FOR MOON- OR EARTHSHINE

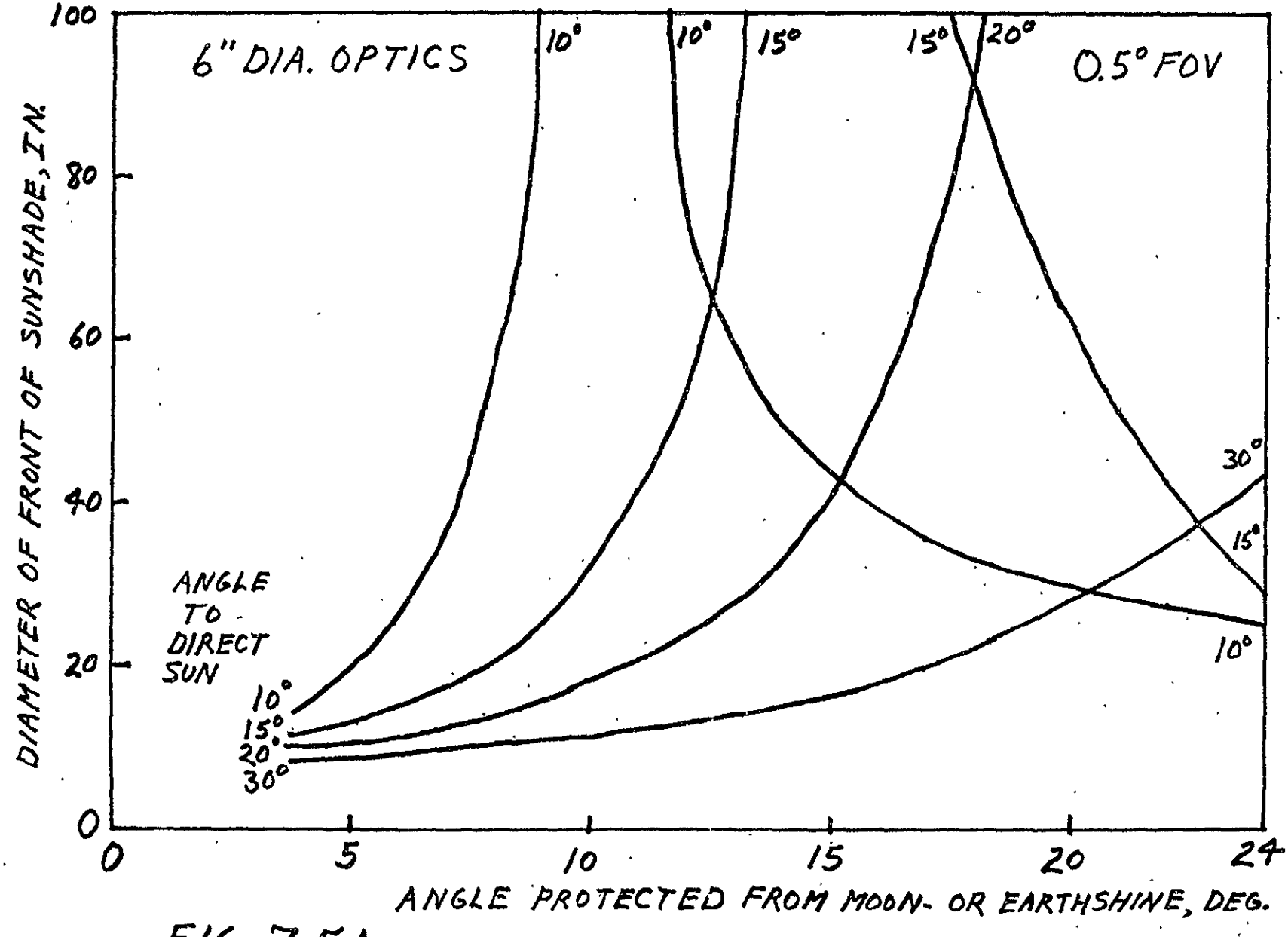
6" DIA. OPTICS
0.5° FOV
10°
10°
15°
15°
20°
30°
15°
10°
ANGLE TO DIRECT SUN
10°
15°
20°
30°
DIAMETER OF FRONT OF SUNSHADE, IN.
100
80
60
40
20
0
0
5
10
15
20
24
ANGLE PROTECTED FROM MOON- OR EARTHSHINE, DEG.

FIG. 7.5A

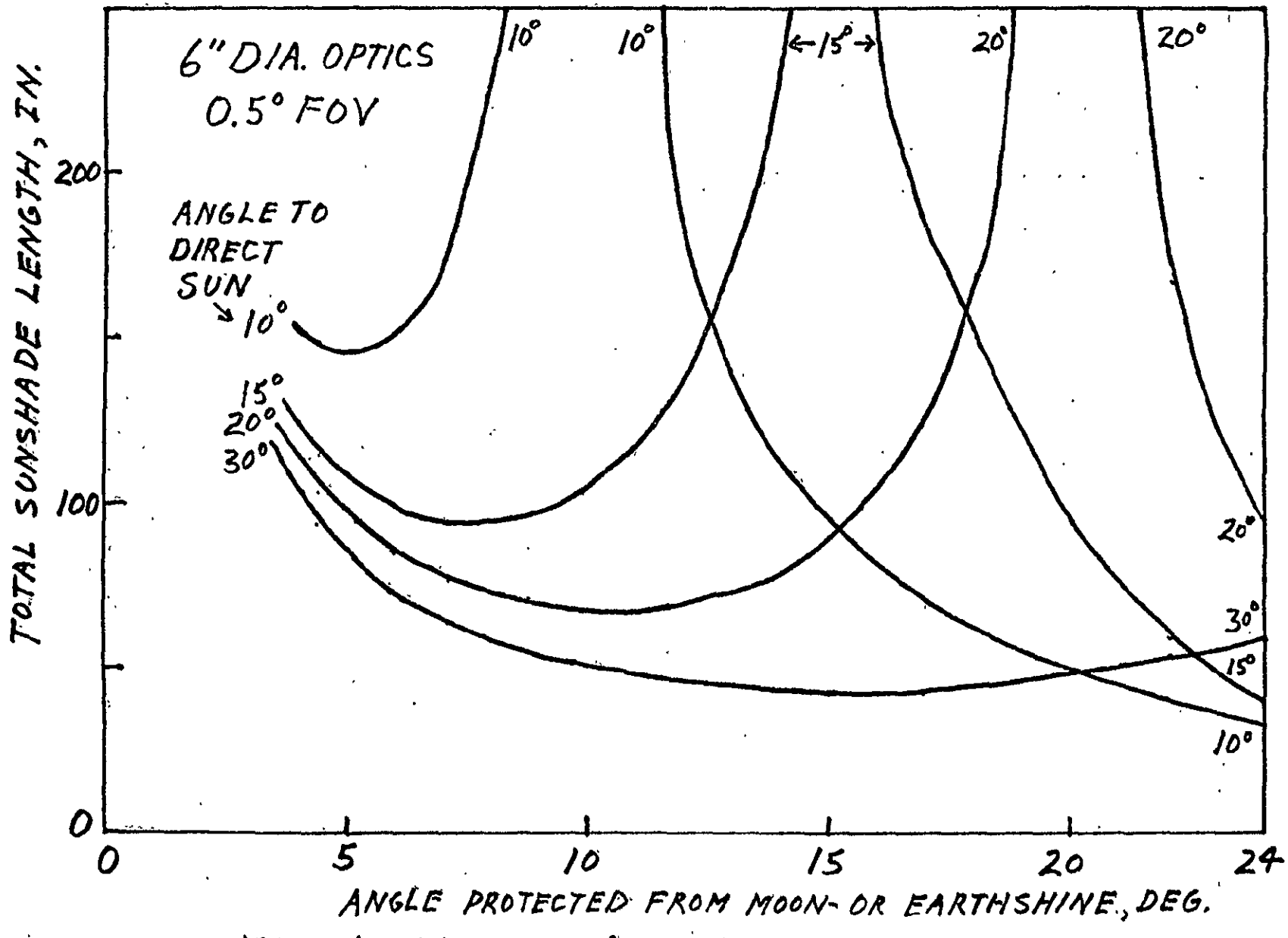

FIG. 7.5B 0.5° FOV

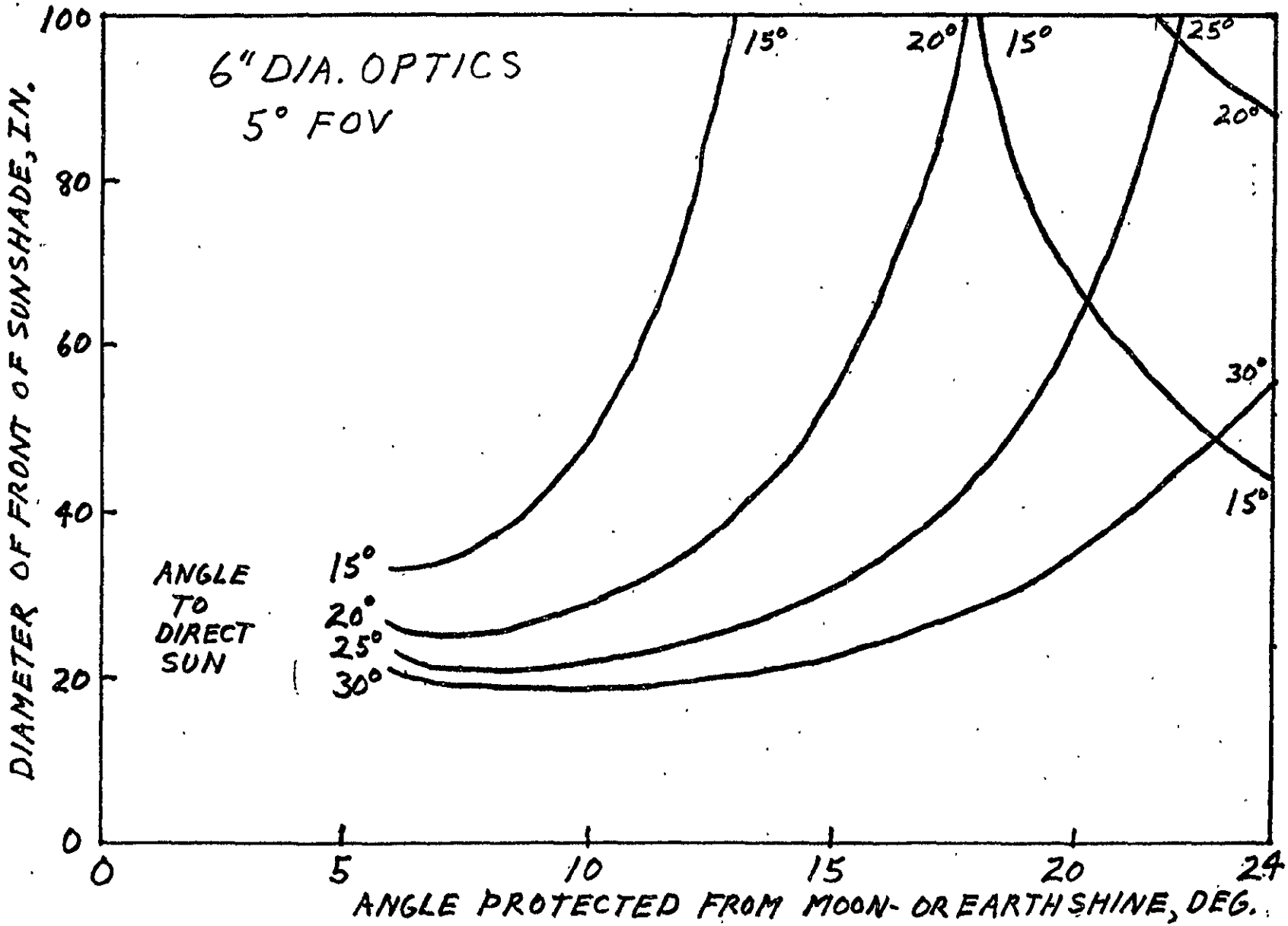
6" DIA. OPTICS
5° FOV
DIAMETER OF FRONT OF SUNSHADE, IN.
100
80
60
40
20
0
0
5
10
15
20
24
ANGLE PROTECTED FROM MOON- OR EARTHSHINE, DEG.
ANGLE TO DIRECT SUN
15°
20°
25°
30°
15°
20°
15°
25°
20°
30°
15°

FIG. 7.6A 5° FOV

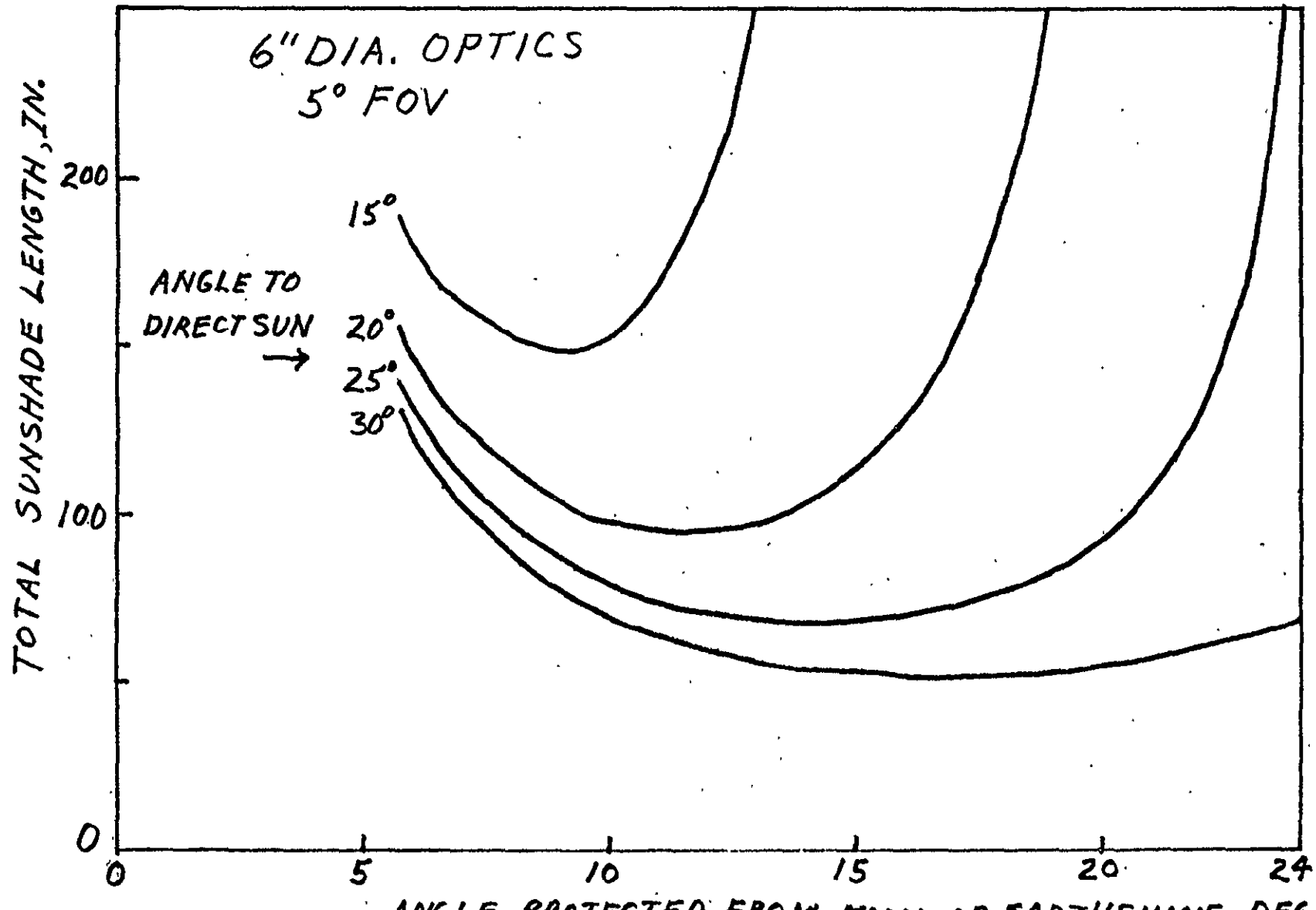
6" DIA. OPTICS
5° FOV
TOTAL SUNSHADE LENGTH, IN.
200
100
0
ANGLE TO DIRECT SUN →
15°
20°
25°
30°
0
5
10
15
20
24
ANGLE PROTECTED FROM MOON- OR EARTHSHINE, DEG.

FIG. 7.6B 5° FOV

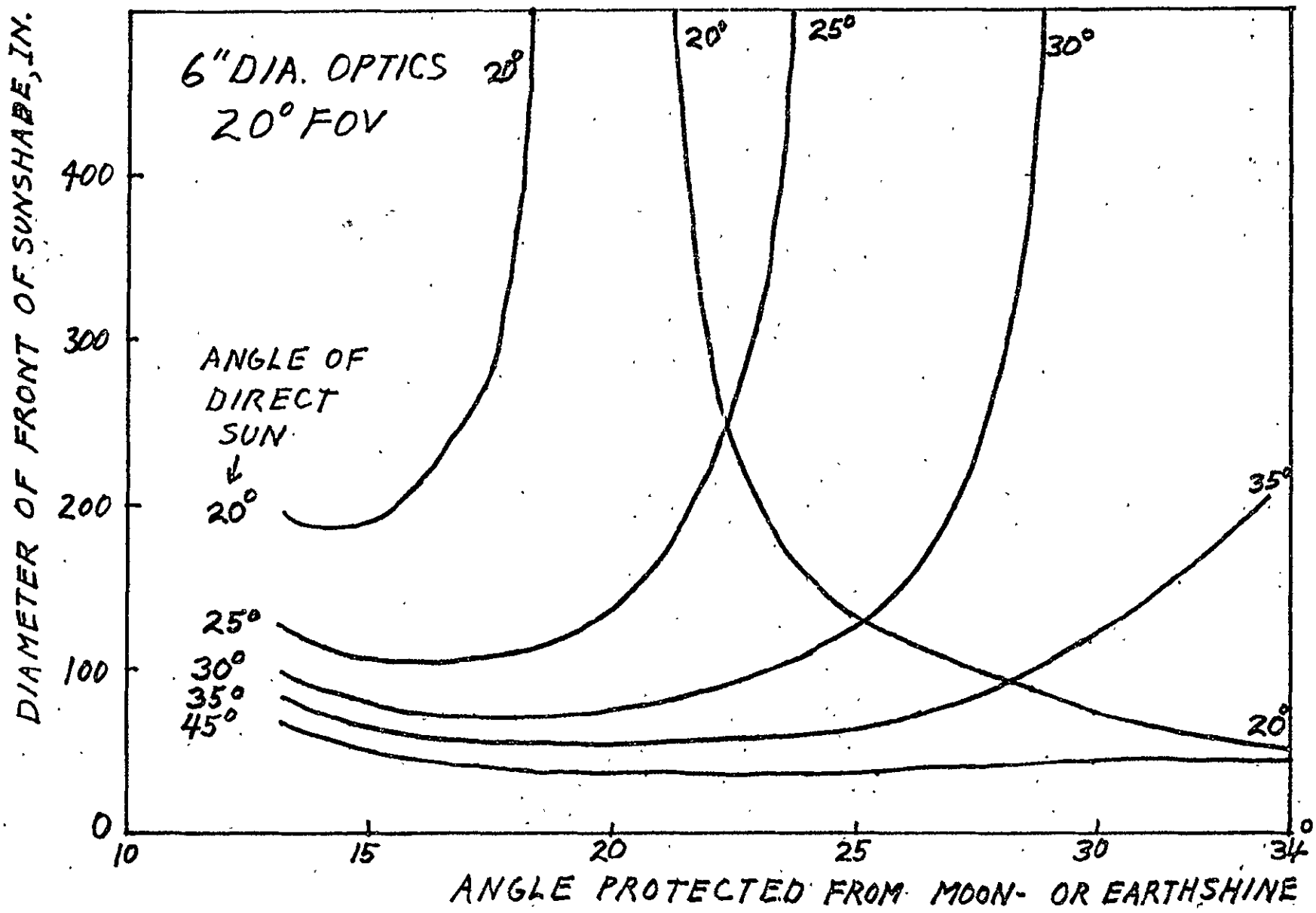

FIG 7.7A 20° FOV

optical diagnostics. As noted earlier, the problem is largely eliminated if the spacecraft is in darkness, yet this condition, at best, prevails only part of the time.

To illustrate the general nature of the effect of stray light, we examine the sample configuration shown in Fig. 7.8. A 50-meter boom with 50-meter antenna elements at its top extended along the y-axis is assumed.

Figure 7.9 shows the angular positions of the various obstructions to the field of view seen from the assumed OBIPS location shown on Fig. 7.8. The significant structures in this particular configuration are the edges of the payload bay, the Spacelab top, the Shuttle tail and the boom with antennas extended. If the structural elements shown in Fig. 7.9 are not illuminated by sunshine, moonshine or earthshine, these elements act only to block the field of view, (at least to a first approximation if we ignore starlight, airglow, aurora and city lights). However, if these elements are illuminated, they act as secondary sources of stray light. The intensity of the secondary sources will depend upon the intensity of the primary light source and the reflectance of the element surface. Black, absorbant surfaces are far better than silvery, shiny surfaces.

If the secondary source is relatively weak, it may be possible to observe to within 10° of the surface. In this case, the allowed view directions are as shown in Fig. 7.10. If the source is moderately bright (perhaps equivalent to the illuminated earth), viewing closer than 20° may not be feasible; see Fig. 7.11. In the case of a very bright reflective surface illuminated by direct sunlight, the secondary

C.2

NASA-S-72-2562-V

PAYLOAD BAY ENVELOPE

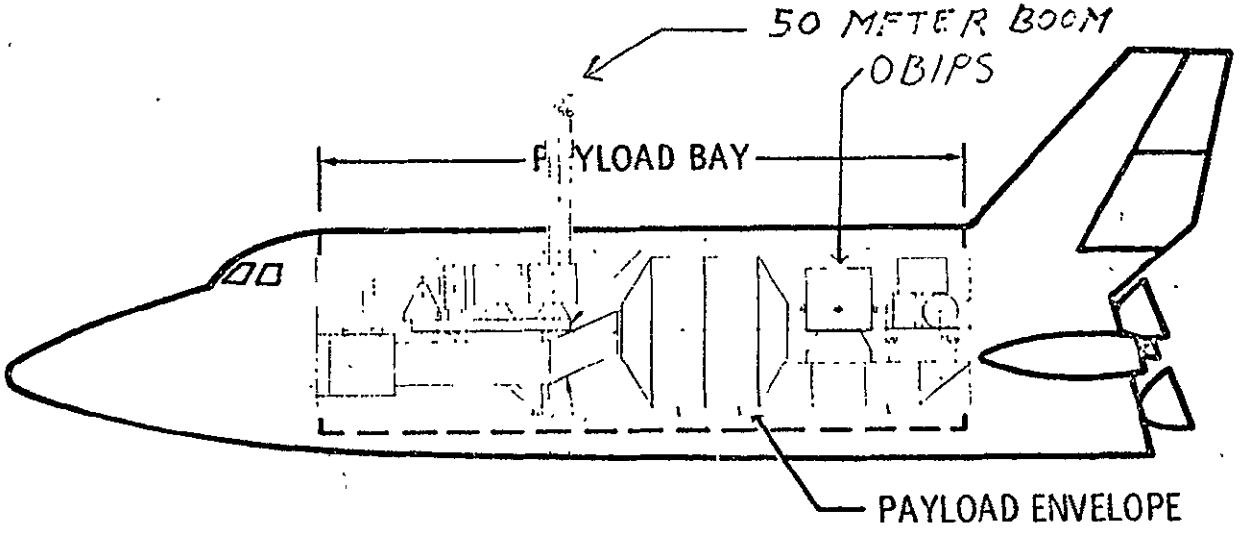

- PAYLOAD ENVELOPE
  - 15-FT DIAM x 60-FT LENGTH
  - INCLUDES THERMAL AND LOAD DEFLECTIONS
  - STRUCTURAL ATTACH POINTS EXTEND OUTSIDE ENVELOPE
  - UMBILICALS PENETRATE ENVELOPE

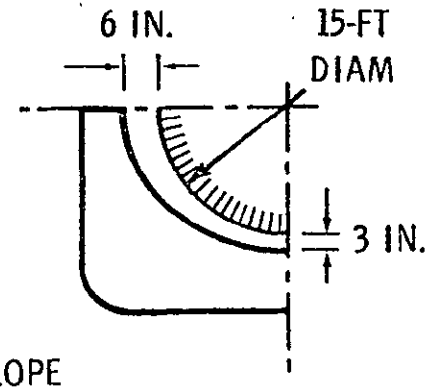

FIG. 7.8

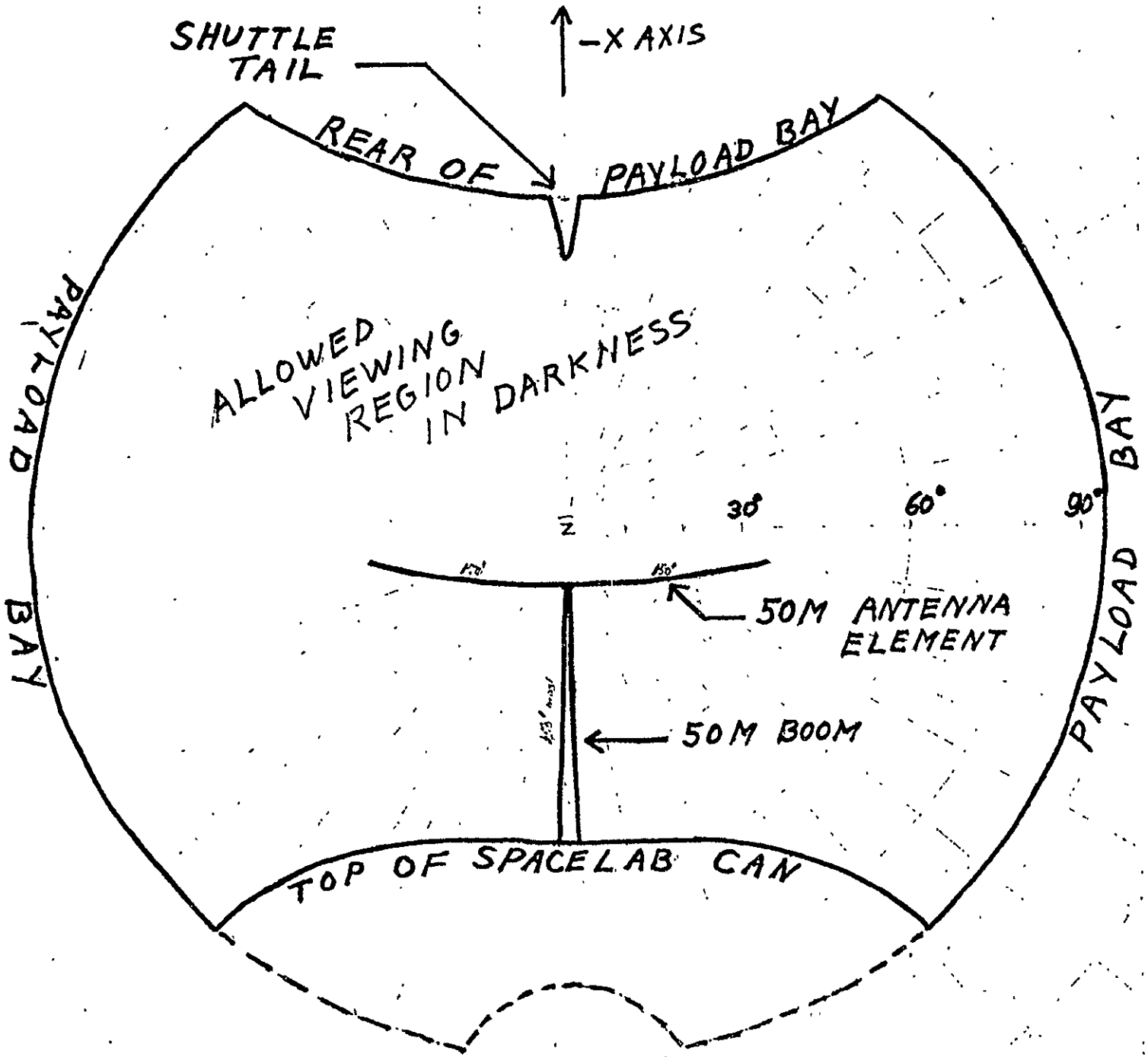
SHUTTLE TAIL
-X AXIS
REAR OF PAYLOAD BAY
PAYLOAD BAY
ALLOWED VIEWING REGION IN DARKNESS
30°
60°
90°
50M ANTENNA ELEMENT
50M BOOM
TOP OF SPACELAB CAN
PAYLOAD BAY

FIG. 7.9

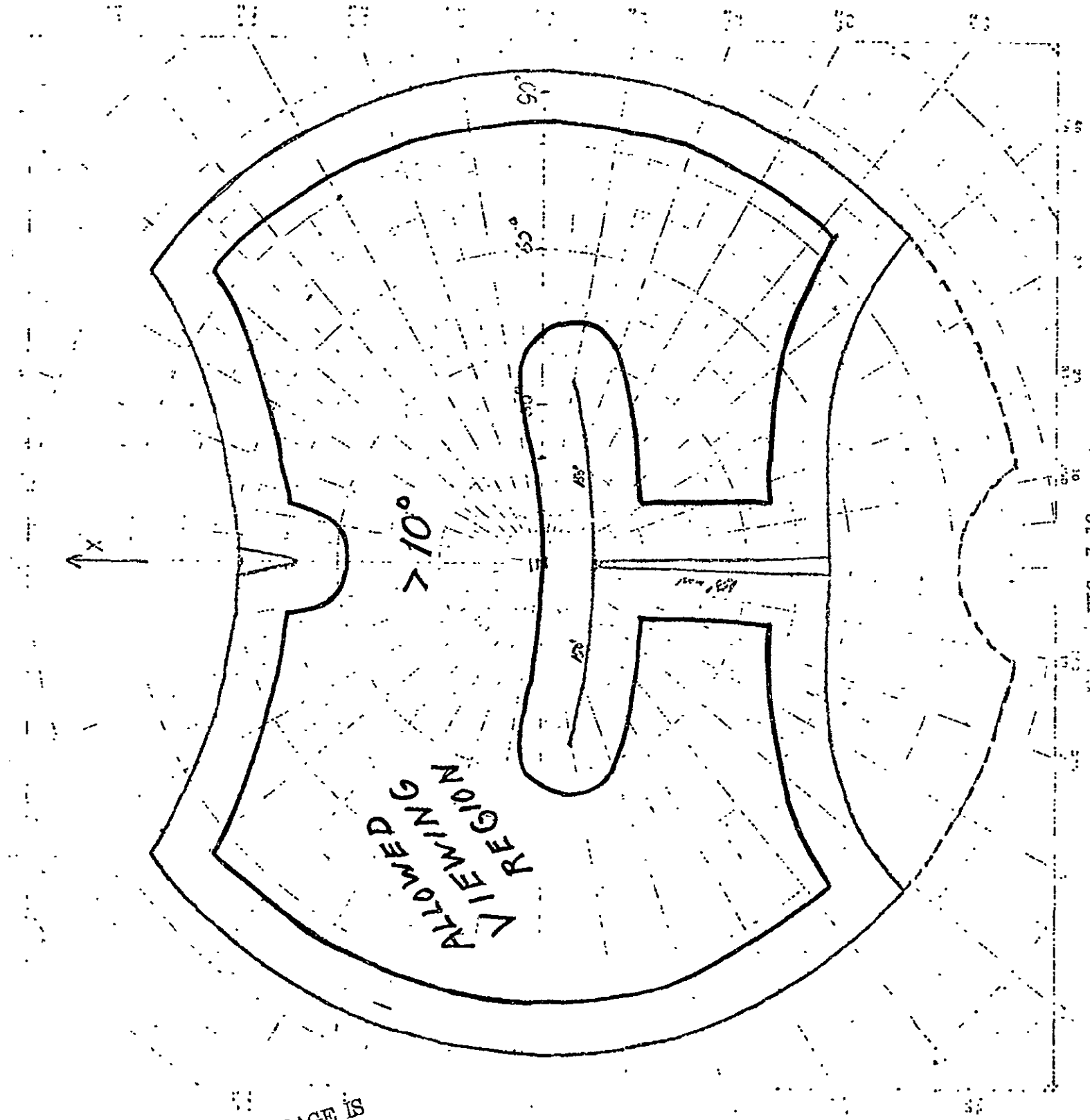

FIG. 7.10

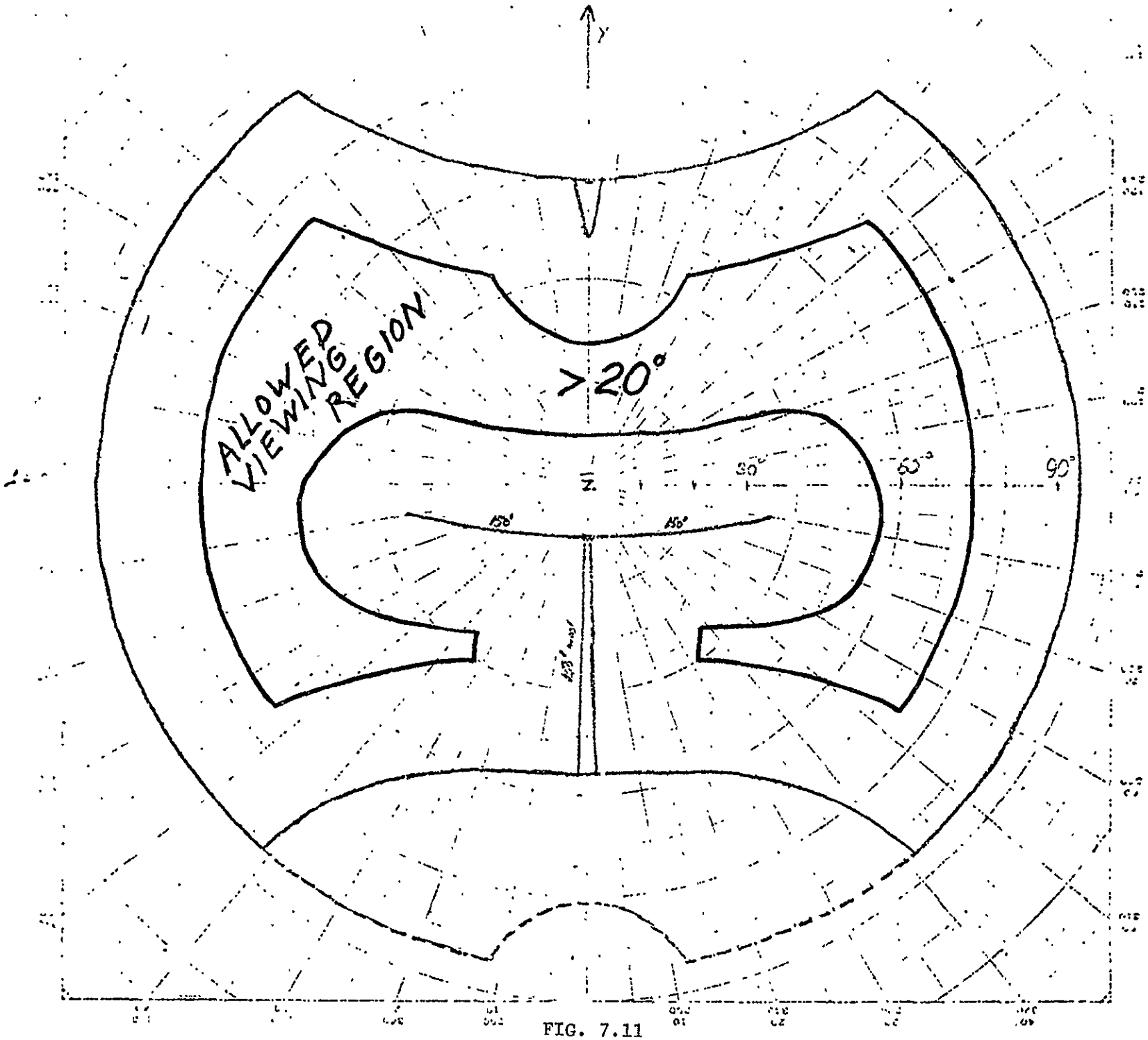

FIG. 7.11

source may preclude effective viewing closer than 30^{o}. Then, the permitted view directions are as shown in Fig. 7.12. A summary of Figs. 7.10, 7.11 and 7.12 is given in Fig. 7.13.

Figures 7.9 to 7.13 demonstrate the seriousness of the stray light problem. The problem is sufficiently severe to restrict certain experiments, and it suggests major efforts to reduce stray light sources by use of non-reflective coatings and placement of structured elements such as booms above the x-y plane of the Shuttle spacecraft.

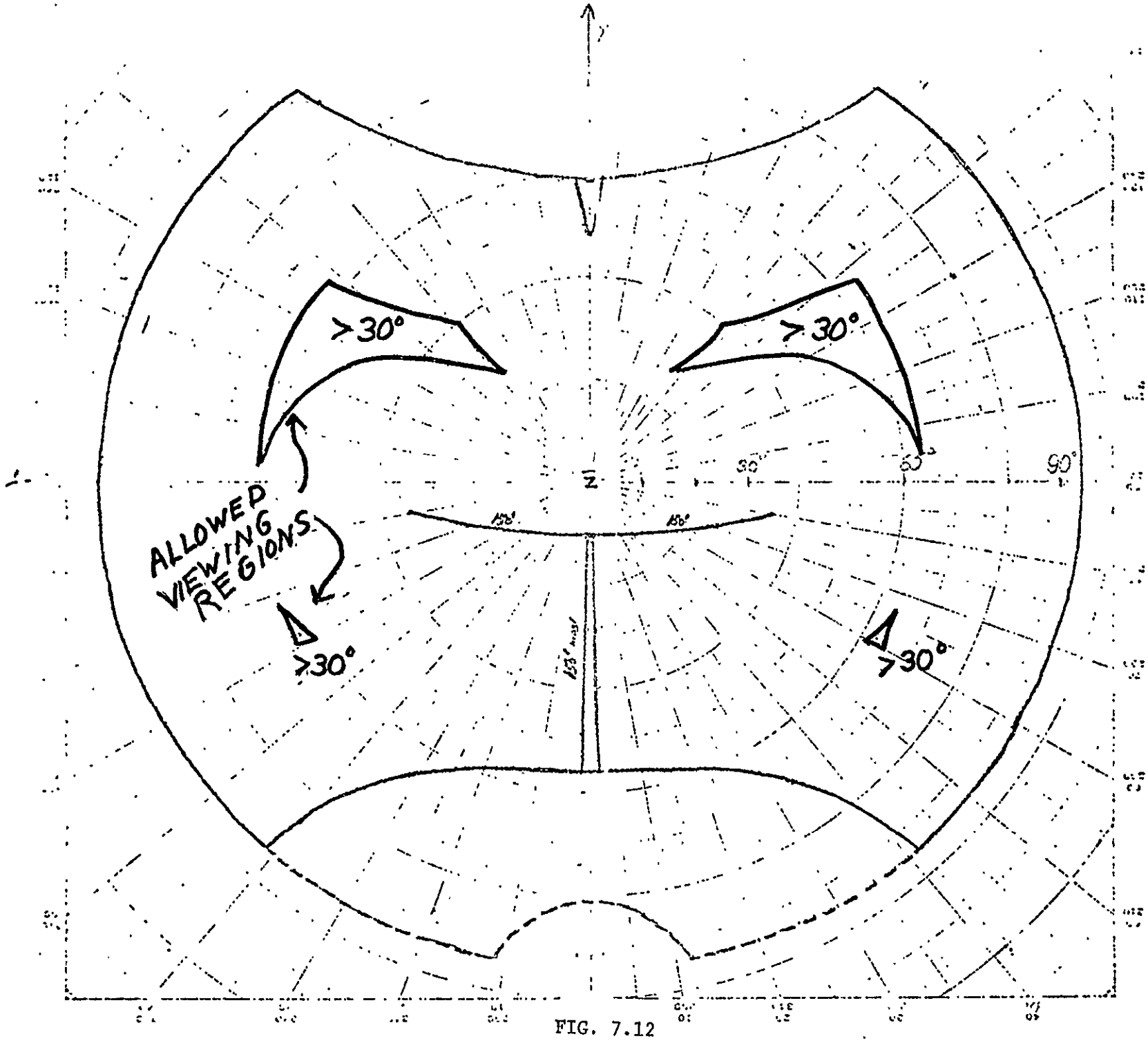

FIG. 7.12

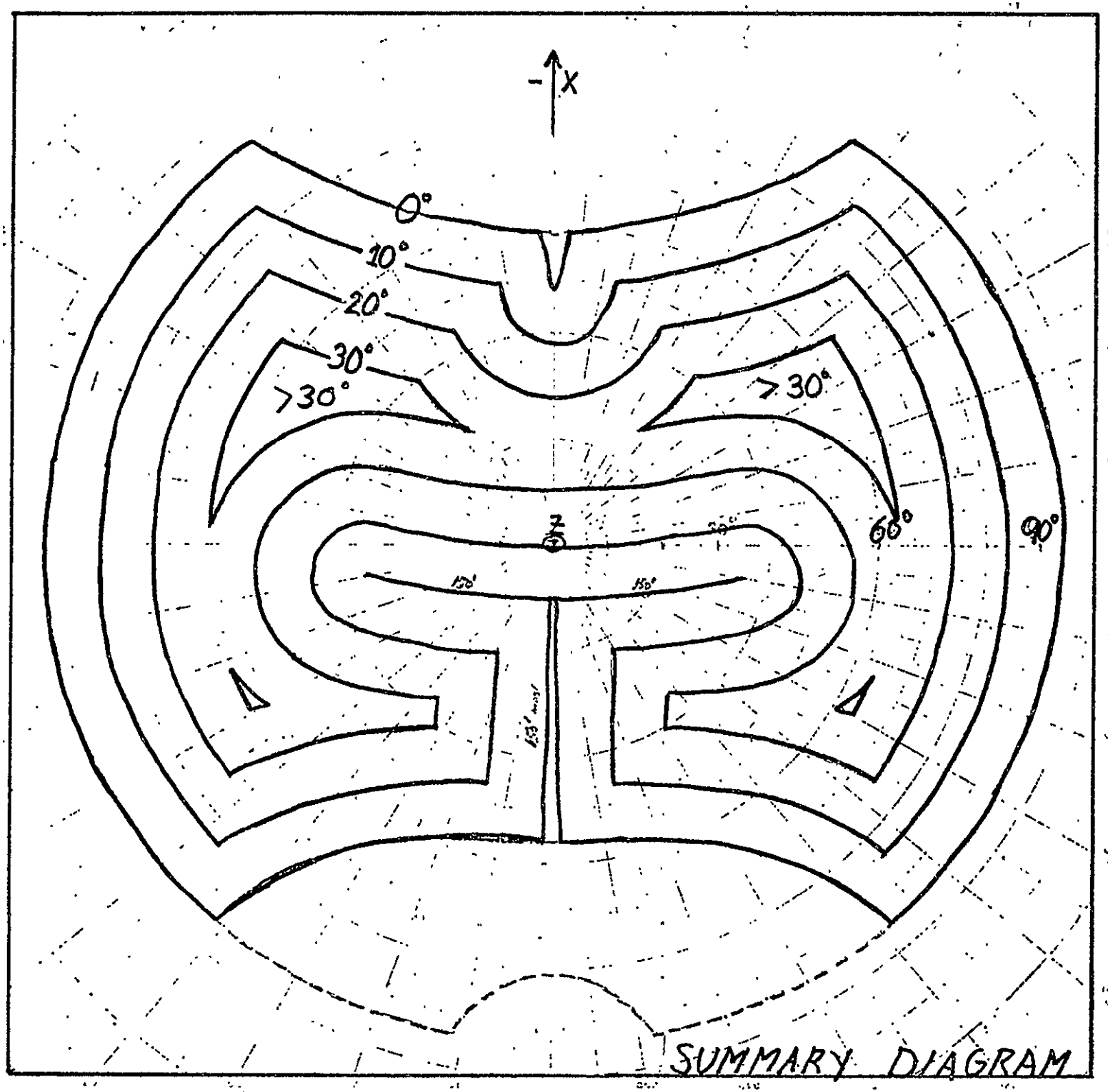

FIG. 7.13

APPENDIX 7A

Pages 96-104 are not reproduced here. In the original report these pages are a reproduction of a paper by C. Leinert and D. Klüppelberg entitled, "Stray Light Suppression in Optical Space Experiments", contained in Applied Optics, 13, 556, 1974.

individual air molecules is needed. In response to that need the use of sodium vapor for observing air motions in the height range 80-200 km was introduced in 1955. Sodium vapor emitted in trail form from a rocket is light enough to move with the air. It absorbs solar light and emits it at 5893 Å--yellow-orange light which is visible against a dark sky (Fig. 8.1). Observation of the trail is by ground-based triangulation photography. This method is restricted to twilight usage, but when trimethyl-aluminate (TMA) is substituted for sodium, sunlight is not necessary to produce a visible trail. Other tracer experiments have incorporated lithium which can be photographed in daylight, at least if the observations are made from aircraft at jet altitude (10 km). Consequently it is now possible to use the molecular tracer techniques to measure winds at twilight, at night and even, to a limited extent, in daylight.

8.2 TRACER TECHNIQUES FOR ELECTRIC FIELDS

A major advance in the use of tracer techniques began in 1963 when German scientists performed rocket experiments to eject barium and strontium vapor into the high atmosphere. By 1966 they had developed the technique to use a highly-efficient reaction to produce free barium atoms:

$$Ba + CuO \rightarrow Cu + BaO + \text{excess } Ba \ .$$

Exposed to sunlight in the high atmosphere, the neutral barium atoms absorb and re-emit green light. An appreciable fraction is quickly ionized by the ultraviolet sunlight, and the resulting Ba^+ ions emit red

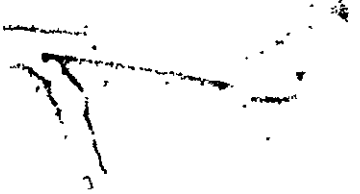

FIG. 8.1 A sodium vapor trail release showing deformation of the trail released on the rocket upleg and, at left center, a portion of the trail being released during the downleg part of the rocket flight. (Reproduced from an article by J. F. Bedinger.)

and blue light. The neutral Ba atoms rapidly take up the motion of the neutral atmosphere and so provide a tracer to measure the neutral wind. Most significant, however, is that an ion tracer is created. Such an ion is free to move unimpeded along the direction of the magnetic field $\vec{B}$, but its motion $\vec{V}_\perp$ in the transverse plane is governed by the equation

$$\vec{V}_\perp = \frac{1}{K}\frac{2}{1+\lambda^*}\left[\frac{\vec{E}_\perp}{B} + \frac{\vec{V}_n \times \vec{B}}{B}\right] + \frac{2}{1+\lambda^*}\left(\frac{\vec{E}_\perp \times \vec{B}}{B^2}\right) + \left(1 - \frac{2}{1+\lambda^*}\right)\vec{V}_n$$

where $\vec{V}_n$ is the motion of the neutral wind (and of neutral tracer atoms), K is the ratio of the ion-neutral collision frequency to the ion gyrofrequency, λ^* is the ratio of the Pedersen conductivity inside the tracer cloud to that outside and $\vec{E}_\perp$ is the electric field transverse to $\vec{B}$.

By releasing small amounts of tracer (e.g., 1-3 kg of Ba-CuO mixture) at high altitudes (above 200 km) the attempt is made to keep $\lambda^* \approx 1$ and K large so that the above equation reduces to

$$\vec{V}_\perp \approx \frac{\vec{E}_\perp \times \vec{B}}{B^2}$$

Hence, since $\vec{B}$ is known from magnetometer measurements and mathematical models, the observed motion of the ionized tracer allows determination of the electric field $\vec{E}_\perp$. Also observation of the tracer motion along $\vec{B}$ can be used, in principle, to measure the third component $E_\parallel$.

Various other methods--rocket- and satellite-borne probes, incoherent-scatter radar, observations of auroral motions and alignments, magnetic variations--are available to measure electric fields or to infer them.

Yet the barium ion tracer method has made the major contribution because of its unquestionable directness and the ease of use. Often, determinations of basic quantities, such as the electric field, are indirect or subject to uncertain errors. As there is little question about the validity of the ion tracer method, its impact on magnetospheric and ionospheric research has been very great. One reason for its impact is that the electric field is such an important quantity, it being crucial to many of the known or suspected acceleration processes that lead to auroral production or to increases in the magnetosphere's kinetic energy content during magnetospheric substorms.

The thermite barium release technique described above has been used during the past ten years at locations ranging from equatorial to polar; well over a hundred rockets carrying thermite barium releases have been flown. One of these, flown September 21, 1971 from Wallops Island, Virginia, cooperatively by NASA and Max Planck Institute groups carried a barium release cannister to a location 5 earth radii above the equator. The 16 kilogram release produced clouds visible to the naked eye and permitted measurement of the electric field in the magnetosphere. Even deeper in the magnetosphere was a release from the HEOS satellite at approximately 13 Re (earth radii) in the magnetospheric tail on March 18, 1969. Photographic observations from several locations in the northern and southern hemispheres permitted determination of the electric field in this region over a period of some minutes.

8.3 PERTURBATION USING BARIUM RELEASES

For reasons that are not yet totally understood, an ion cloud

produced from a barium release undergoes striation into an elongated region resembling a rayed auroral arc (Fig. 8.2). Irregular structures such as these can profoundly affect radio waves traversing them. Consequently, a thermite barium release permits a controlled way to study the effects of irregularly ionized regions on radio wave propagation in the ionosphere. Large (up to 350 kg) releases have been performed for the purpose of increasing the ion density and creating regions of contrasting ion and electron density. When used in this way the thermite release technique moves from the realm of tracer experiments to perturbation--an attempt to make controlled temporary changes in the medium being studied.

8.4 TRACER AND PERTURBATION USING DIRECTIONAL HEAVY IONS

Further progress in using barium as a tracer came as a result of the development of barium shaped charges. The thermite release technique ejects vapor in all directions at approximately 2,000^{o} K (i.e., the atoms travel at approximately 1 km sec^{-1}). However if pure barium metal is used as the conical liner of an appropriately configured shaped charge, a very-high velocity barium ion jet is created. The shaped charge is lifted to near 500 km altitude and aligned parallel upwards along the field line to avoid collisions with the atmosphere and to give the proper initial direction. Detonation commences at the rear of the cylinder of explosive by means of dual detonators activated by a timer. A plane wave shaper produces a detonation wave nearly planar which travels up the explosive at near 8 km sec^{-1}. As the wave impinges upon the tip of the cone, which has a full angle of 30^{o}, the wave collapses the cone inward, vaporizing it and increasing the forward velocity. The

FIG. 8.2 A large barium release (48 kg) from Poker Flat in March 1969. The ball-like green neutral cloud moves with the wind while the reddish ion cloud, showing extensive striation structure, is constrained to move under the influence of the electric and magnetic fields.

resulting vapor jet proceeds upwards with peak velocity near 13.5 km sec^{-1}. As escape velocity from the earth at 500 km altitude is near 10 km sec^{-1}, all of the atoms travelling faster than that can traverse entire magnetic field lines unless stopped by collisions or electric fields. With barium liners weighing 1 kg, nearly one mole (6×10^{24}) of ions is generated by the explosion and subsequent ultraviolet irradiation. Calculations show that if the plasma remains in the same magnetic flux tube, it should be visible out to the magnetic equator if fired along auroral zone field lines.

After pioneering experiments by the Max Planck Institute group and at the University of Alaska, the first long distance tracing experiments were carried out jointly by the University of Alaska and Los Alamos Scientific Laboratory from Kauai, Hawaii. The field line originating 500 km over Kauai is about 7,000 km long with a conjugate point in the South Pacific south of Samoa. The experiment was done three times and on each occasion the streak, from Hawaii, could be seen as far south as the equator; and then on beyond there to its precipitation in the atmosphere it was observed aboard a pair of instrumented jet aircraft. Figure 8.3 comprises TV composites from one of the aircraft of the third experiment at two times, and showing distance from the burst point. Subsequent drift of the ion clouds at the conjugates in one of the experiments showed a significant difference in the conjugate electric field, implying either decoupling of the hemispheres or parallel electric fields.

The next experiment, OOSIK, was carried out near L = 6 from Poker Flat. The barium streak was tracked by TVs out to near 3 Re and was

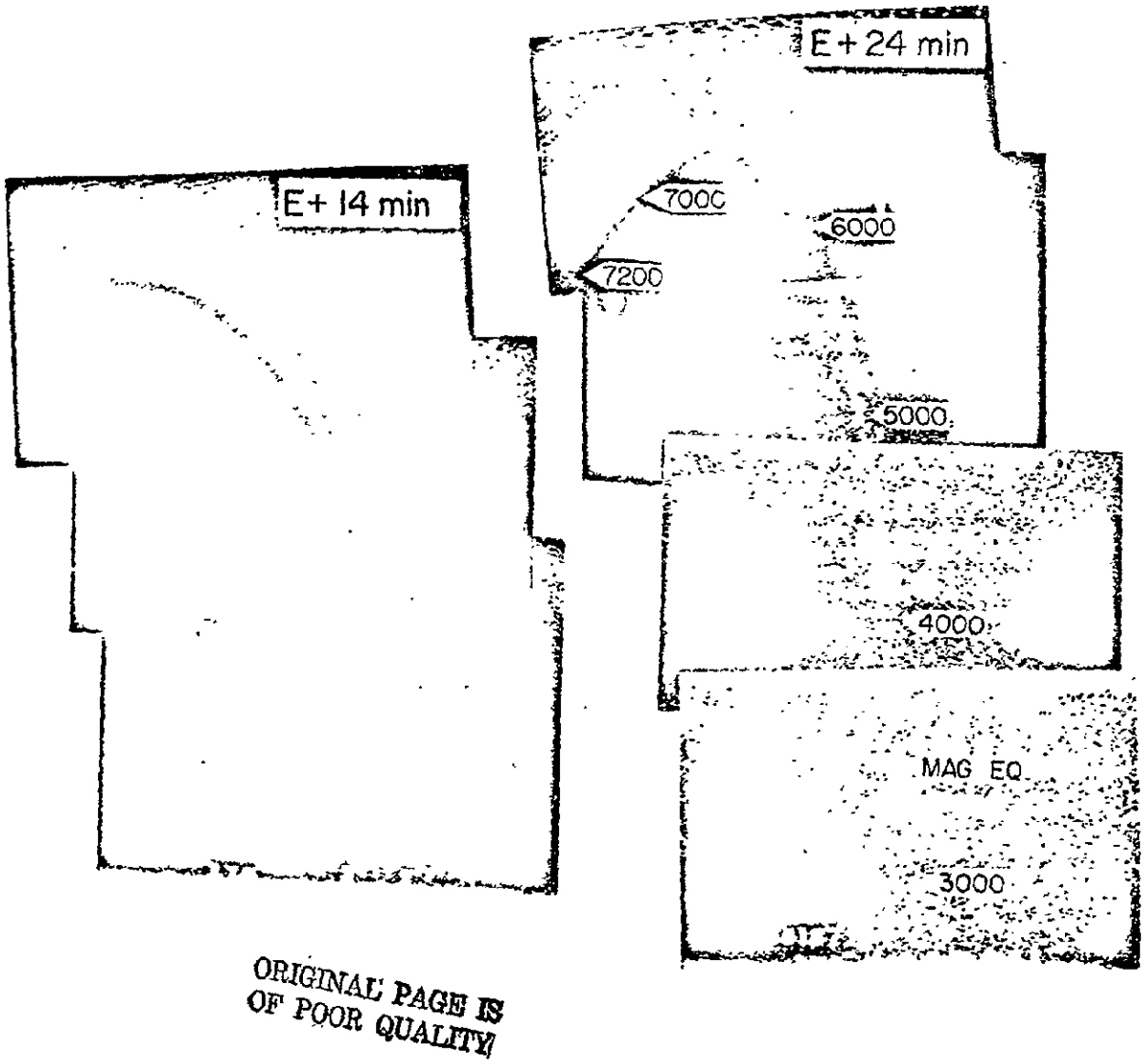

FIG. 8.3 Composites of TV images showing the appearance of a barium-painted field line. At the fainter bottoms of the images the field line is high over the equator and at the brighter top the barium is penetrating the atmosphere near the aircraft.

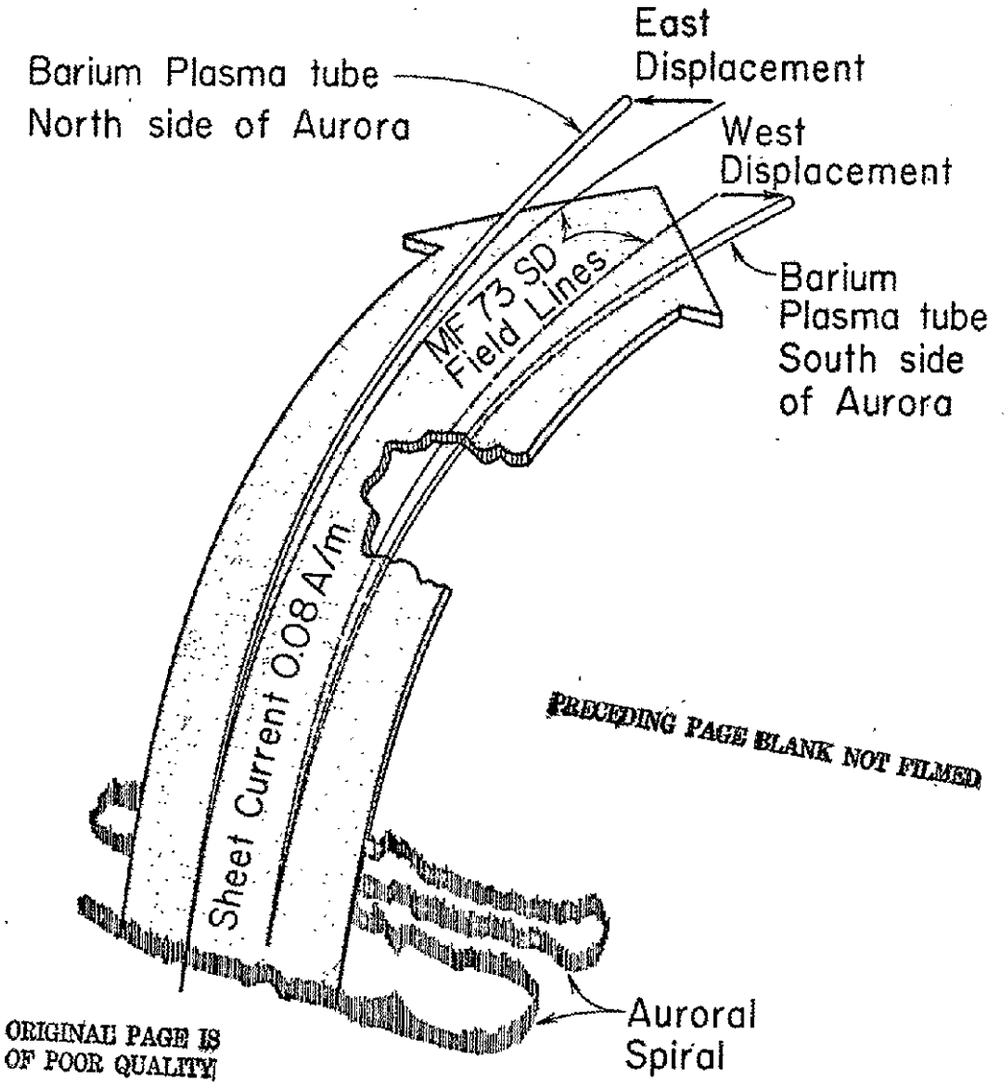

FIG. 8.4 A schematic diagram showing how field-aligned currents over an aurora deform the magnetic field to give the observed relative displacements of barium streaks on either side of the aurora.

FIG. 8.5 Photograph from SKYLAB III showing the barium streak (between arrows), three and a half minutes after injection, rising above the horizontal bright airglow near the earth and through the constellation Cygnus.

and dynamics of the dayside polar cusp regions with the barium shaped charge technique. The anti-solar polar cap convection was vividly demonstrated for over 2,500 km and 40 minutes in one experiment from Cape Parry, N.W.T., Canada, conducted by LASL and the University of Alaska. Other experiments from there and by the M.P.I. group from Greenland found varying fields in the cusp region. During one of the M.P.I. experiments the barium experienced a velocity increase above altitude 3,000 km indicating that the ions were accelerated by a potential drop of 170 volts, but the distance and time involved are not known so a magnitude cannot be assigned to the parallel electric field.

As with thermite releases, a small shaped charge acts as a non-perturbing tracer while a larger injection serves as a controlled perturbation. In the spring of 1974 two attempts were made to inject massive amounts of barium plasma into the magnetosphere. The introduction of such cold plasma was predicted to result in release of stored magnetospheric energy in the form of precipitating trapped electrons. Rocket failures doomed the attempts, but similar experiments at Poker Flat, Alaska are planned for March, 1976. Another such injection-precipitation scheme calls for the introduction of large numbers of light-weight lithium ions which might cause precipitation of electrons, protons and alpha particles.

8.5 HIGH VOLTAGE ELECTRON AND ION ACCELERATOR EXPERIMENTS

Yet another major class of active experiments involves the use of high-vol accelerators to eject precisely controlled beams of electrons or positive ions. In principle, the beams of charged particles can be used to investigate a variety of magnetospheric and ionospheric characteristics

and also for more general studies of the propagation of beams through an ambient medium. Energetic charged particle beams released above the atmosphere should travel along the direction of the magnetic field until the particles either reach a mirror point or intersect the atmosphere where the particles will excite an artificial aurora. Optical observations permit the location of the aurora to be determined, as well as the intensities of the various emissions produced. From such observations it is possible to study the spreading of the beam, backscattering coefficients, and time-dependent emission spectra as functions of beam energy, pitch angle (angle between the particle direction and the magnetic field), magnetic dip angle, atmospheric composition and beam current. Observation of the orientation and location of the artificial aurora allows precise determination of the orientation of the magnetic field in the atmosphere. Upward ejection of the charged particles allows mapping of the magnetic field from one hemisphere to the other, and enables the field line length to be measured by noting the travel time. Additionally, use of different beam energies allows determination of both the electric field and particle drifts due to gradients in the geomagnetic field, since the $\vec{E} \times \vec{B}$ drift is independent of particle velocity, whereas the gradient drift is proportional to particle velocity.

The first electron accelerator experiment was conducted at Wallops Island, Virginia, in 1969 by a group led by Wilmot N. Hess of NASA. The accelerator was flown on a rocket to altitudes near 350 km and oriented to eject downward beams of electrons lasting up to one second and with current and energy up to 490 ma and 9.7 kev, respectively. Though some scientists speculated that the beam would interact with the ambient

plasma and thereby lose its energy before creating detectable aurora, this did not happen. The resulting auroras could not be seen by eye but they were detected by sensitive image orthicon television systems located in Virginia and Maryland (Fig. 8.6a). Aside from proving the feasibility of the technique and showing that electron beams do propagate along the magnetic field without significant losses, this first experiment yielded a precise determination of the magnetic field orientation and experimental verification of theoretical predictions of the beam spreading and penetration into the atmosphere. It also raised (still unanswered) questions about the energies and paths of electrons entering the accelerator to maintain its approximate neutrality.

The same group conducted a follow-on experiment in 1972 using a similar but potentially more powerful accelerator to eject electrons upwards from locations over Hawaii. Television systems were deployed on jet aircraft near the conjugate region south of Samoa in the southern hemisphere to observe the auroras expected there when the electrons arrived a fraction of a second after ejection and after having traveled a distance of approximately 7,000 km. For unknown reasons, only one of the nearly 200 expected auroras was observed (Fig. 8.6b). Others may have occurred without detection, but in many other cases it is obvious that the electron beams did not escape the accelerator. The one observed aurora was of the expected shape and intensity but its location was a surprise. Prior to this experiment there was a general opinion that the configuration of the magnetic field was well known at this low-latitude location. The observed auroral position, some 30 km away from the expected, showed that there is error in the way that models of the time-dependent magnetic field are calculated.

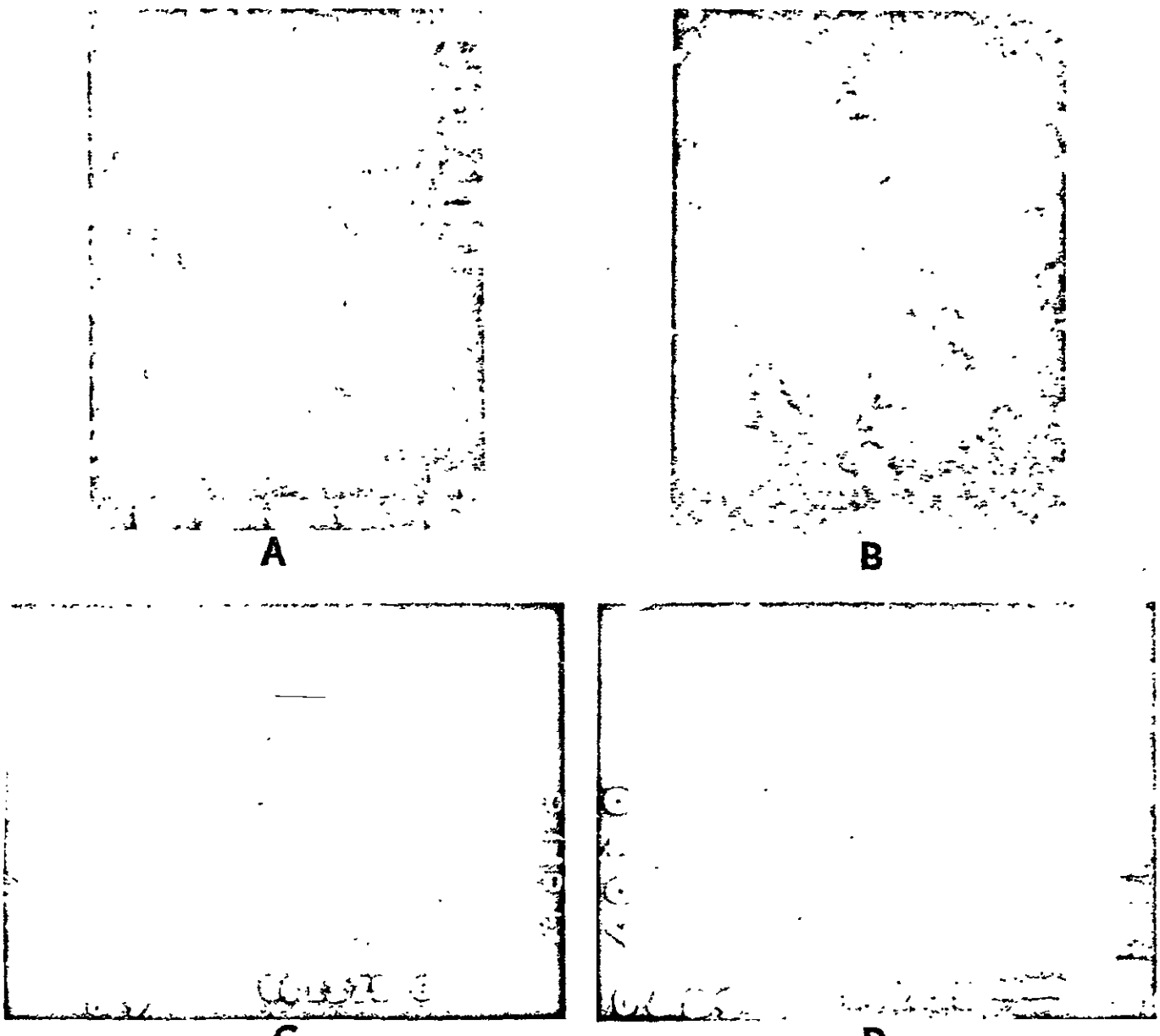

FIG. 8.6 Artificial auroras detected by TV systems: a) Aurora generated downfield near Wallops Island, Virginia in 1969; b) aurora created in the southern conjugate region from an accelerator flown from Hawaii in 1972; c) and d) low-latitude aurora above and below an accelerator flown from Poker Flat in April, 1975.

Dr. John R. Winckler and his co-workers at the University of Minnesota have now flown a series of three rocket accelerators to investigate the location, intensity and timing of electron beams returned by mirroring from the location conjugate to the rocket accelerator. Called the Electron Echo experiment, the method uses low current and high energy (about 80 ma and 40 kev) and it depends primarily upon direct detection of the mirrored particles by electron detectors flown on the rocket vehicle or small packages ejected from it. Successful detection of the echo beam requires placement of a detection package in the echo beam, the location of which depends upon the beam drift due to the ambient electric field and the gradient in the magnetic field--quantities that are uncertain, especially at high-latitudes. Fully successful Electron Echo experiments were conducted first at Wallops Island and then at Poker Flat in April, 1974. The next experiment is planned for January of 1976; the University of Alaska's television systems will be used in an attempt to detect and record the location of artificial auroras produced by the direct electron beam and by the beam echoed back from the southern hemisphere.

Within the last two years there have been several successful electron accelerator experiments in the Soviet Union, and in early 1975 a French-Soviet team launched two rockets carrying electron accelerators from Kerguelen Island in the southern Indian Ocean (ARAKS Experiment). Electron beams of 0.5 amp, 30 kev and 1.0 amp, 15 kev traveled across the equator to the Soviet Union where radars detected ionization produced when the beams struck the atmosphere.

Probably the most powerful rocket-borne electron accelerator yet

flown was launched by the Air Force Cambridge Research Laboratories at Poker Flat on April 13, 1975 (Fig. 8.6c,d). Ten ampere, 3 kev beams ejected at altitudes near 120 km produced auroras readily detected by television systems and which were perhaps marginally visible to the naked eye. This group plans to fly additional high-power accelerators from Poker Flat during the next two years.

Medium- and low-power particle accelerators are finding use also in another form of full-scale experiment directly applicable to the space environment but which is conducted on the earth's surface. In March, 1975, we placed two of our television systems inside a large vacuum tank to observe beams from electron accelerators. This tank, located at NASA's Plum Brook Station near Sandusky, Ohio, is 30 meters in diameter and 38 meters high. It can be rapidly pumped down to simulate altitudes as high as 300 km. The experimental configuration permitted observation of the electron beam's interaction with the air inside the tank and with an aluminum Faraday cup while varying the tank pressure, the beam current voltage, focusing and direction, and the retarding potential on the Faraday cup. The group, led by Dr. William Bernstein of NOAA, obtained several interesting results. A major result leads to the suggestion that beam-beam rather than beam-plasma interactions may be responsible for certain radio-frequency emissions associated with natural auroral production.

8.6 THE FUTURE

Even before being fully developed and applied, several techniques for tracer experiments, including shaped-charge barium releases and

electron accelerators, are now being expanded in hopes of using them for perturbation experiments. Accelerator technology is just reaching the point where it may be feasible to produce sufficiently intense particle beams to cause significant perturbation effects. The breakover point between a tracer and a perturbation beam is probably near 50 kilowatt (e.g., 5 amp at 10 kev). only fractionally larger than achieved so far. There is, of course, a long-available means to produce high-power semi-controlled particle beams using nuclear explosions in the high atmosphere. Such devices were used in 1962, and these did produce major perturbation effects. However, it seems unlikely that this technique will soon be used for scientific experimentation in the magnetosphere.

9. OPTICAL OBSERVATION OF ACTIVE EXPERIMENTS

9.1 INTRODUCTION

Crucial both to the design of experiments and to the design of experiment-producing equipment, i.e., particle accelerators or other devices, is a knowledge of the useful capability of optical detection devices. The purpose here is to provide that knowledge as best we can using both theoretical and experimental approaches. A variety of factors must be considered; these are outlined in the flow diagram, Fig. 9.1. At each step along the way there are uncertainties which can preclude quantitative statements about the scientific information expected to result from a particular experimental configuration. In the following discussion we attempt to retain generality, but often it is necessary to examine specific cases with narrow treatments to arrive at the desired design information.

In general, an active experiment that is to be observed optically will produce in some region of space an emitting volume. The emitting volume may be determined by magnetic and electric field configurations, by the velocity distribution of experiment gases or exciting particles, by atmospheric density and perhaps by diffusion. The determination of the emitting volume must be performed for each separate experiment because it is so dependent upon the nature of the experiment. In some cases an objective of the experiment will be to measure the emitting volume.

Within the emitting volume will be a rate of <u>volume emission</u>: that is, the number of photons per unit volume per unit time. Whether the experiment be one involving particle-particle, wave-particle or

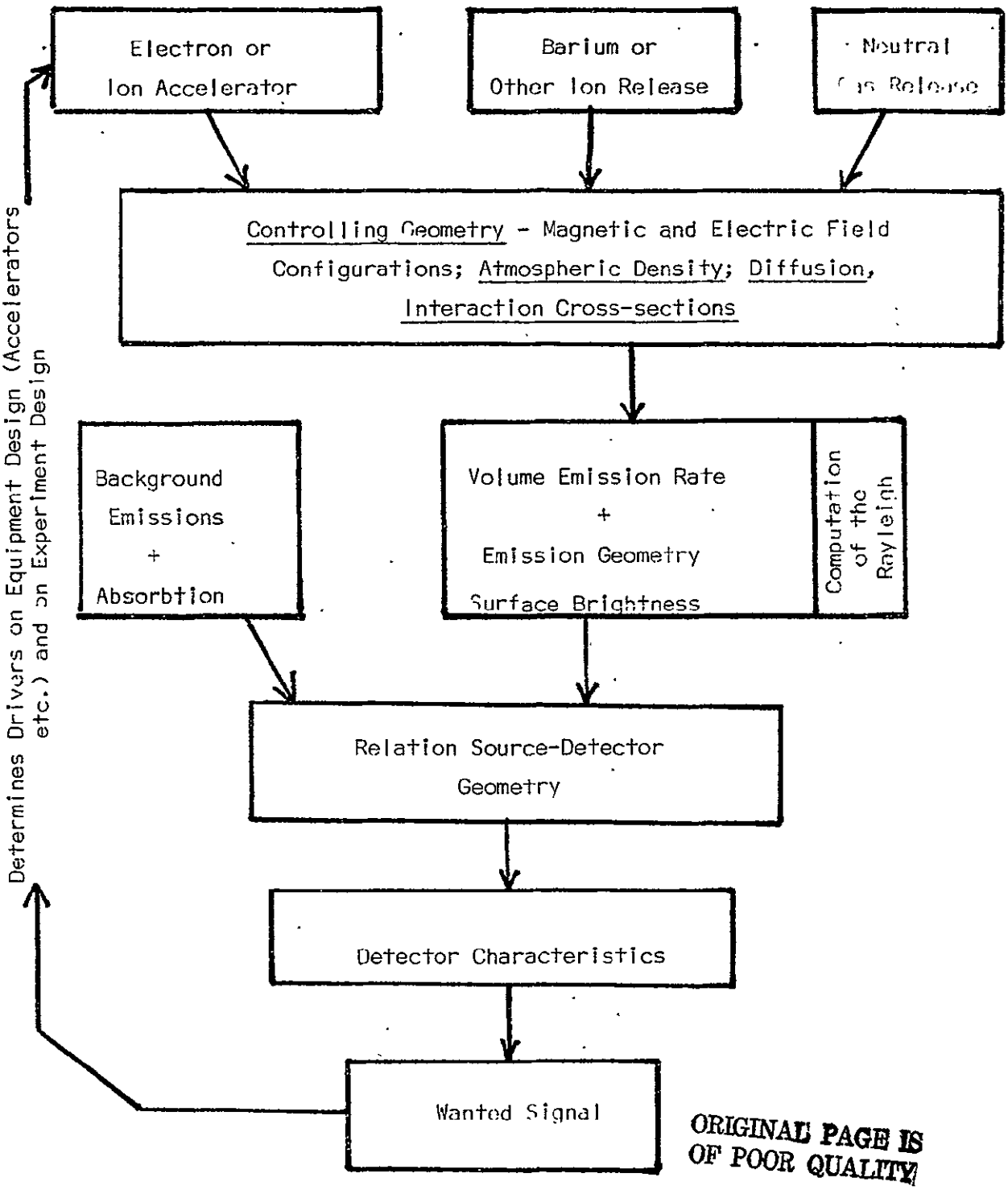

Fig. 9.1 Flow Diagram for Optical Observation of Active Experiments

photon-particle interactions, the *a priori* determination of the volume emission rate is likely to depend upon a combination of theoretical prediction and emperical experience.

9.2 EMISSION FROM A SOURCE (DEFINITION OF THE RAYLEIGH)

Here we will use as a unit of apparent emission the rayleigh, a unit used almost exclusively in aurora and airglow study.

The rayleigh is a unit of apparent emission of a source, that is, the total emission in all directions, i.e., over 4π steradians. In practice one cannot directly measure this total apparent emission; to do so would require a detector that completely surrounds the source so as to measure the emission coming out in all directions. But one can look at the source from one direction and measure the number of photons entering a detector pointed at the source.

Consider a detector which has an opening of area A cm^2 that defines a field of view 2α where α is the half angle of the field of view (Fig. 9.2).

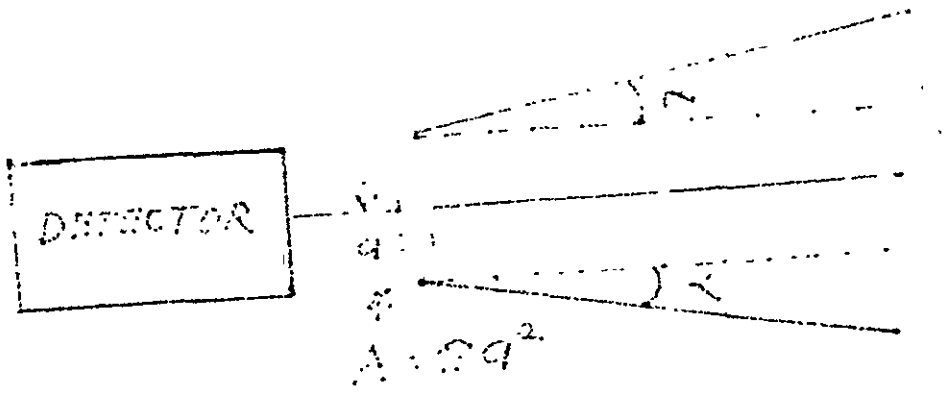

FIG. 9.2

The detector of area A subtends a solid angle as seen by a point in the source at distance r of A/r^2 ster as shown in Fig. 9.3.

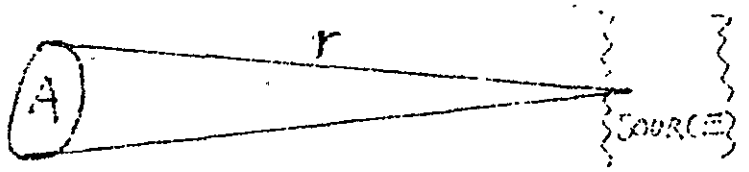

FIG. 9.3

The solid angle Ω of the field of view of a system with half angle α is $\Omega = 2\pi (1-\cos \alpha)$. (This is so since the curved surface area of a spherical segment is $2\pi rh$ and $h = r (1-\cos \alpha)$ (see Fig. 9.4).

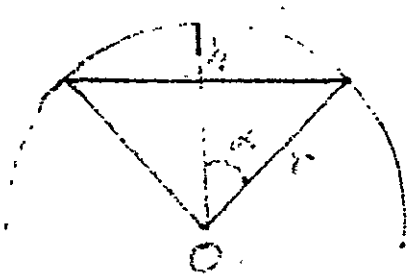

FIG. 9.4

So the area of curved surface intersected by field of view of half angle α is $2\pi r^2 (1-\cos \alpha)$.= Solid angle is area of intersected surface/r^2 = $2\pi (1-\cos \alpha)$. Using this relation we have

$\alpha = 1^\circ$	5°	20°	40°	60°	90° (all-sky camera)
$\Omega = 9\times10^{-4}$	0.024	0.379	1.47	$\pi = 3.14$	$2\pi = 6.28$ ster

Now let there be a source region S which emits in a single wavelength (or wavelength increment) F(r) photons/cm^3 sec (total emission over 4π ster). Assume the source is isotropic, i.e. emits uniformly in all directions, The number of photons from one cubic centimeter falling on the detector (per sec) is F(r) times the solid angle subtended by the

detector at the source divided by 4π ster. (The division by 4π is necessary because F(r) is defined as the emission per 4π ster, i.e., total emission in all directions.) If the detector completely encircled the source cubic centimeter it would detect all the photons emitted, i.e., F(r) photons/sec. The solid angle subtended by the detector is A/r^2 ster. If it had a solid angle of 4π ster it would surround the source and in this case its area would be $A = 4\pi r^2$ (area of a sphere of radius r). Thus the number of photons falling on the detector per sec would be $(4\pi r^2/r^2) \cdot (F(r)/4\pi) = F(r))$.

So the number of photons falling on the detector (per sec) from 1 cubic centimeter is $(A/4\pi r^2) \cdot (F(r))$. But we assume that the source is large enough to cover the field of view of the detector and that the source is uniform over that field. Therefore the number of photons falling on the detector and coming from distance r is $(A/4\pi r^2)(F(r))$ times the area of the source intersected by the field of view. That area is $\Omega\ r^2$. Thus the number of photons falling on the detector from distance r in the source is

$$\frac{\Omega A}{4\pi} \cdot F(r) \text{ photons/sec ster}$$

The total emission coming to the detector is then obtained by integrating along the line of sight, i.e., along the column. It is

$$\frac{\Omega A}{4\pi} \int^{\infty} F(r)\, dr \text{ photons/sec}$$

Notice that this expression is dependent upon $\int_0^{\infty} F(r)\, dr$, which is a function of the source alone and also is dependent upon Ω and A which

are determined only by the observing instrument characteristics. By dividing the expression by ΩA (ster cm^2) we have a quantity I

$$I = \frac{1}{4\pi} \int_0^\infty F(r)\, dr \text{ photons/sec } cm^2 \text{ ster}$$

which depends only upon the source but which obviously also is related to the direction from which we view the source. Multiplying both sides by 4π ster we have

$$4\pi I = \int_0^\infty F(r)\, dr \text{ photons/}cm^2 \text{ sec}$$

which is the emission rate (in all directions) of the source. (This multiplication then implies that we should get the same answer regardless of the view direction.) Notice that the quantity measured is I which has units of photons/cm^2 sec ster but that the emission rate ($4\pi I$) is in units of photons/cm^2 sec.

A rayleigh is defined as an apparent emission rate of 10^6 photons/cm^2 (column) sec. (The word "column" is inserted to emphasize that this is integrated emission rate from the column along the line of sight and is not a flux.)

I is called the surface brightness. It is the number of photons crossing one square centimeter of the source surface per sec per ster.

The Apparent Emission Rate (in rayleighs) = Surface brightness x 4π ster.

Note that surface brightness is independent of the distance of the observer. A particular field of view moved twice as far away gets ¼ as

much light per unit area of surface but sees 4 times as much surface area.

The relationship between apparent emission of the source and the surface brightness assumes no radiative transfer problems, that is that the source region is not optically thick at the wavelength being viewed. This problem does not appear in active experiments involving the production of artificial aurora except perhaps in certain wavelengths in the UV part of the emission spectrum. However, thermite barium clouds are optically thick in the major lines such as 4554 Å; in essence the optical thickness problem puts an upper limit on the surface brightness of a barium cloud. From a practical viewpoint, the optical thickness problem does not affect shaped charge or ion engine ejections of suprathermal ion materials such as barium because of the elongated geometry and typically low ion density within most of the optically emitting region. By convention, the term rayleigh is used even in optically thick situations, but it is simply 4π times the surface brightness and no longer has any simple relationship to the volume emission rate if the source is optically thick.

Except in the unusual case of a spherical emitting volume, the apparent surface brightness will depend upon the direction from which that volume is viewed. For most active experiments the emitting volume is more likely to be approximately cylindrical. Figure 9.5 illustrates the case of a uniformly emitting cylinder of diameter unity and length $L \gg 1$. The apparent surface brightness is proportional to the path length through the cylinder along the view direction, i.e., $\propto 1/\sin\theta$.

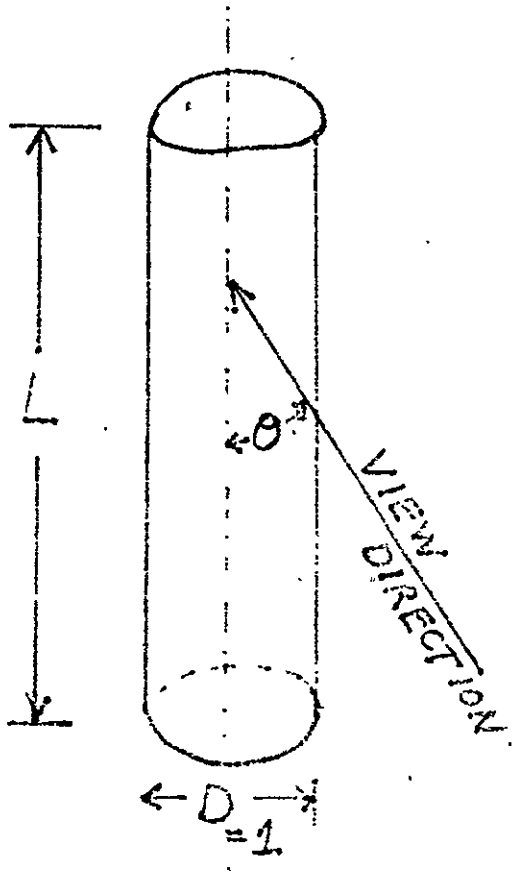

θ°	PATH LENGTH
0	L
5	11.5
10	5.76
20	2.92
30	2.00
40	1.56
50	1.31
60	1.15
70	1.06
90	D = 1

FIG. 9.5

In an actual case, an artificial aurora produced in 1969 had a ratio of L/D $10^4/133 = 75$. Hence the surface brightness viewed end on was 75 times greater than the surface brightness viewed perpendicular to the ray.

9.3 PRODUCTION OF LIGHT BY ELECTRON IMPACT ON THE ATMOSPHERE

During a recent AMPS Working Group meeting, there arose the question of the relative efficiency of different energy electrons in producing observable emissions. The question is important in experiment and equipment design since there is a wide range of achievable electron energy that electron accelerators can be designed for. Calculations were available showing the light production efficiency per unit energy deposition over the energy range from fractional kev to 10 kev. As accelerator voltages greater than 10 kev are being considered for use on AMPS missions, we examine here the efficiency question over a range extending to 300 kev. The calculations are performed for the N_2^+ 1NG band at 4278 Å, an emission resulting from electron impact in an easily observed part of the visible spectrum.

The calculation of the slowing down of electrons incident on the atmosphere has been carried out by several methods. Of interest here is a method by Rees (1963) based on laboratory measurements of Grün (1957). The latter author found an empirical relation between the penetration depth, R, and the energy of the incident electron, E (in kev):

$$R = 4.57 \times 10^{-3} E^{1.75} \text{ mg cm}^{-2} \quad (1)$$

Physically, this simply means that the energetic electron travels into the atmosphere roughly according to the 1.75 power of the particle energy. According to Eq. 1, a monoenergetic electron of energy E_o = 5.6 kev travels to where the atmosphere is 9.316338×10^{-2} mg cm^2. The atmospheric depth (mg cm^{-2}) versus altitude (km), plotted in Fig. 9.6 for a typical model atmosphere shows this value to correspond to an altitude of 109 km. The atmospheric density there is $\rho = 1.32 \times 10^{-7}$ mg cm^{-3} and the range in atmospheric-centimeters (atmo-cm.: the equivalent depth of atmosphere in cm. at STP) is r_o given by

$$r_o = \frac{R}{\rho} = 7.8 \times 10^5 \text{ atmo-cm.}$$

This quantity is given as a function of altitude in Fig. 9.7.

The rate at which the incoming electrons are ionizing the atmospheric constitutents per unit volume per incident unit electron flux (f), is:

$$\frac{q_{E_o}}{f} = \frac{E_o}{r_o \Delta E} \lambda(Z/R) \cdot \frac{[O_2]_z + 0.92\,[N_2]_z + 0.56\,[O]_z}{[O_2]_R + 0.92\,[N_2]_R + 0.56\,[O]_R} \quad cm^{-3} sec^{-1} \quad (3)$$

where ΔE is the average energy (in ev) lost by the incoming electron per ionization. This quantity has been shown to be almost independent of electron energy and equal to 35 ev, λ (Z/R) is the normalized energy distribution function or the fraction of energy lost at an altitude Z above the final altitude R, (λ(Z/R) = 1 when Z=R). A graph of λ (Z/R) is given in Fig. 9.8. $[X]_z$ and $[X]_R$ are the number densities (cm^{-3}) at Z and R respectively. The coefficients take into account the differences

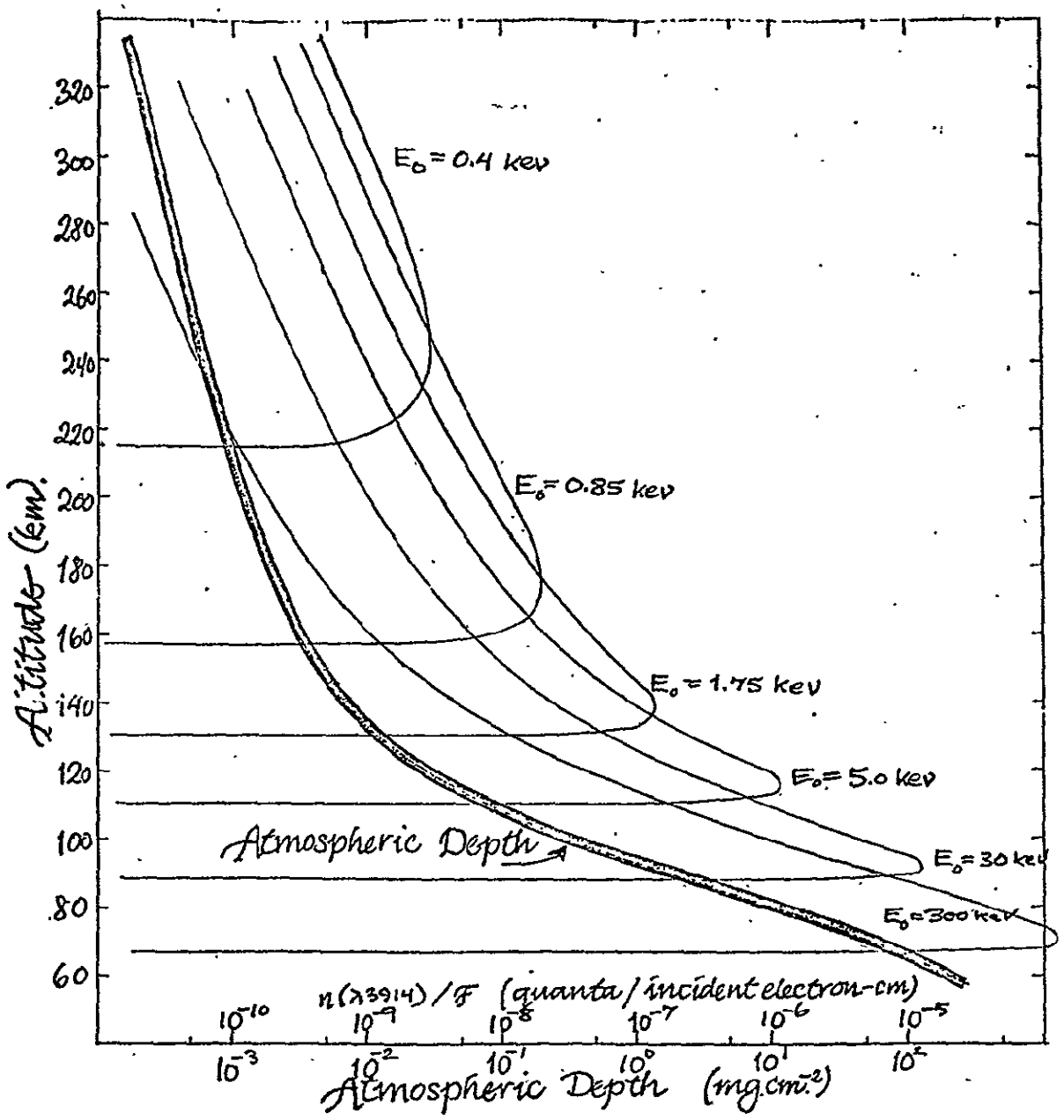

FIG. 9.6

Showing the atmospheric depth, D, as a function of altitude. Shown also are altitude profiles of N_2^+ 1NG 3914 Å emission in the atmosphere for electrons of various energies.

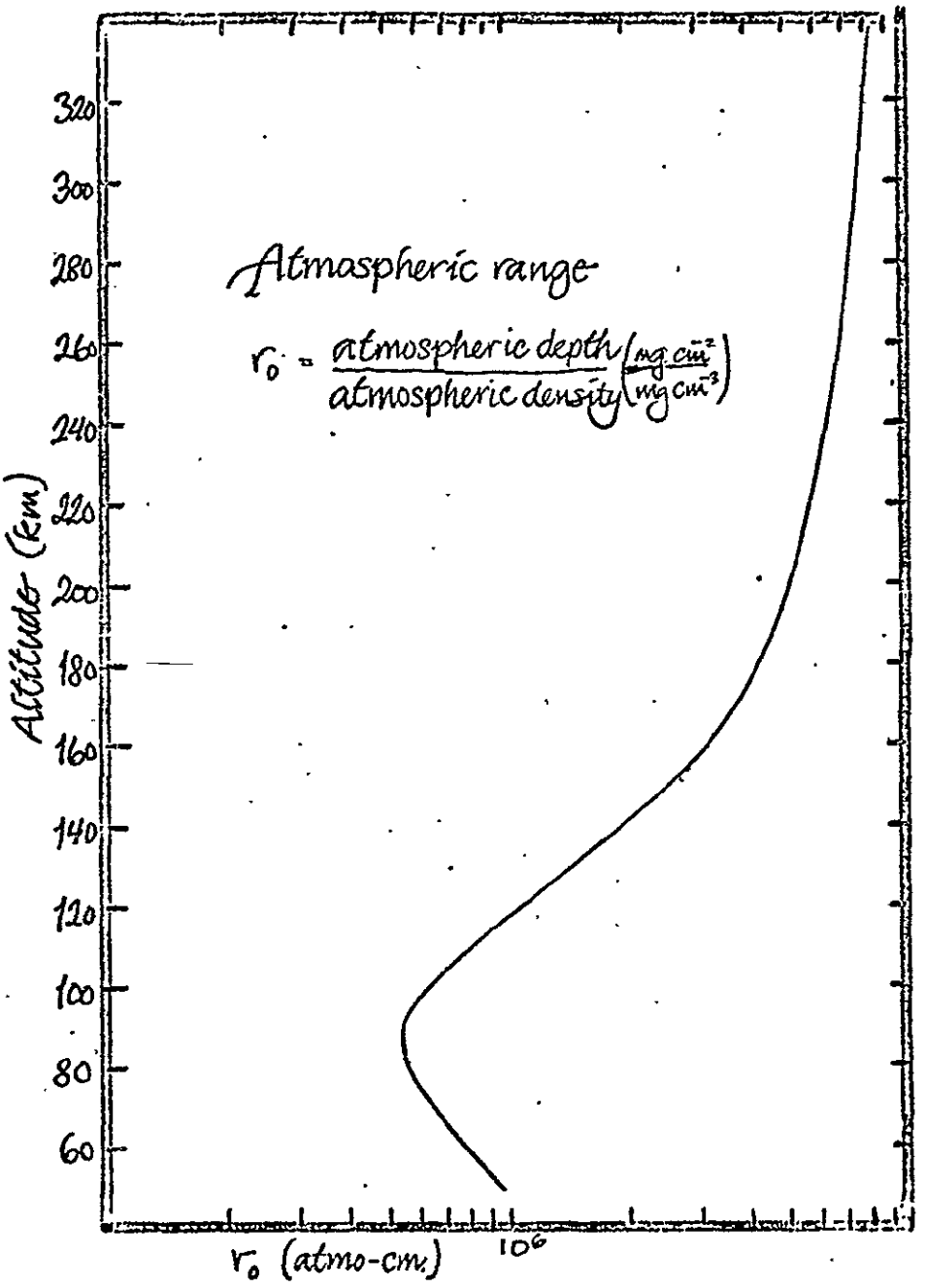
Atmospheric range
r_0 = atmospheric depth / atmospheric density
(mg cm⁻² / mg cm⁻³)
Altitude (km)
320
300
280
260
240
220
200
180
160
140
120
100
80
60
r_0 (atmo-cm.)
10^6

FIG. 9.7

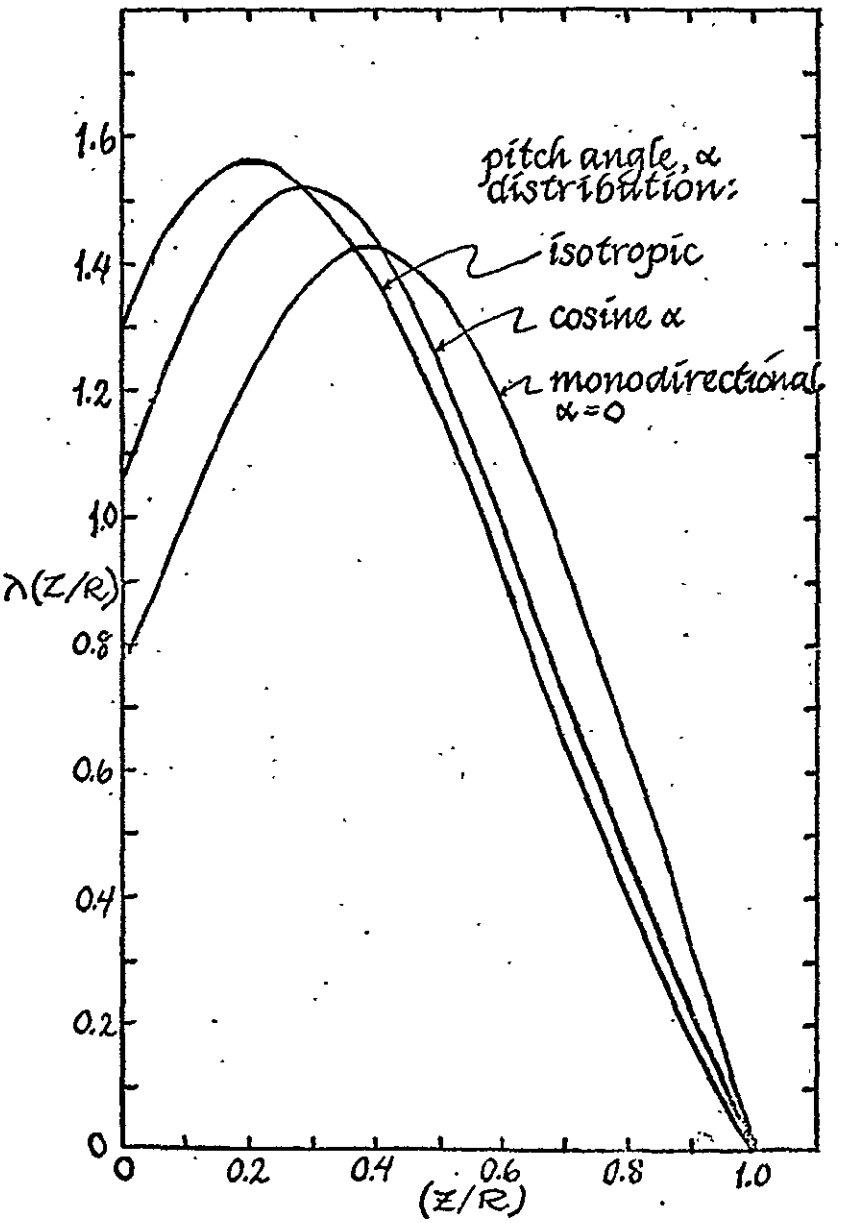

FIG. 9.8

The energy dissipation function for three different pitch angle distributions.

in the ionization efficiency of the atmospheric constituents.

For each 50 ionizations, one quantum of 3914A N_2^+ 1NG emission is emitted. Thus, the volume emission rate can be calculated by inserting a factor to take this into account. For the 4278A N_2^+ 1NG band, this factor is 0.013, and the volume emission rate at Z due to electrons of energy E_o is:

$$\frac{N_{E_o}(Z)\ (4278A\ N_2^+\ 1NG)\ (\text{quanta cm}^{-3}\ \text{sec})}{F_{E_o}\ (\text{electrons cm}^{-2}\ \text{sec}^{-1})}$$

$$= \frac{(0.013)\ E_o}{r_o \Delta E}\ \lambda\ (Z/R)\ \frac{[O_2]_Z + 0.92[N_2]_Z + 0.56[O]_Z}{[O_2]_R + 0.92[N_2]_R + 0.56[O]_R} \tag{4}$$

To find the volume emission rate at Z due to electrons with an energy spectrum g(E)

$$N(Z) = \int_{Emin}^{Emax} g(E)\ N_{E_o}\ dE\ \text{cm}^{-3}\text{sec}^{-1} \tag{5}$$

The total zenith emission intensity in rayleighs is then

$$4\pi I = (4\pi \times 10^6) \int_{Z=R}^{Zmax} N(Z)\ dZ \tag{6}$$

In the case of spacecraft-borne electron accelerators, the electron pulses are monoenergetic and the equation for the volume emission rate at altitude Z is of the form of Eq. 4. The emission rate as a function of altitude for various representative energies is shown in Fig. 9.6. A first impression of Fig. 9.6 is that the higher the characteristic energy (for constant current) the greater the total emission rate. It

is of obvious interest to determine the relationship of total emission rate to particle energy for a wide range of energies.

Figure 9.9 shows the total 4278 Å emission rate versus the characteristic energy of an incoming electron energy spectrum of a Maxwellian form at a constant particle form or current. Note, however, that the slope of this line is less than 1 so that the efficiency of producing N_2^+ 1NG emission becomes less with increasing particle energy.

To illustrate this result more clearly, the total volume emission rate per unit electron energy flux has been plotted versus the characteristic energy of the electrons in Fig. 9.10. This plot (from Rees and Luckey, 1974) has been extended beyond 30 kev to show that there is little gain in total emission per unit input energy for energies greater than approximately 5 kev.

The 4278 Å emission rate per unit energy deposition rate, or radiant efficiency, has been used in the analysis of satellite auroral observations of electron energy input and optical radiation output (Deehr, et al., 1973). This efficiency was assumed to be constant and equal to 280 R erg^{-1} sec cm^2 (Dalgarno, et al., 1965). Eather and Mende (1971) modified this conversion to account for aurora excited at higher altitudes by lower energy electrons by changing it according to the fractional content of N_2 with height. Rees and Luckey (1974) put this on a more general basis; their theoretical calculations show that the efficiency increases from 160 R erg^{-1} cm^2sec at characteristic energy 1 kev to 210 R $erg^{-1}cm^2$sec at 10 kev (Fig. 9.10). This increase is due to the increasing percentage of N_2 in the total neutral gas composition from the high altitudes (low electron energies) down to approximately 100 km

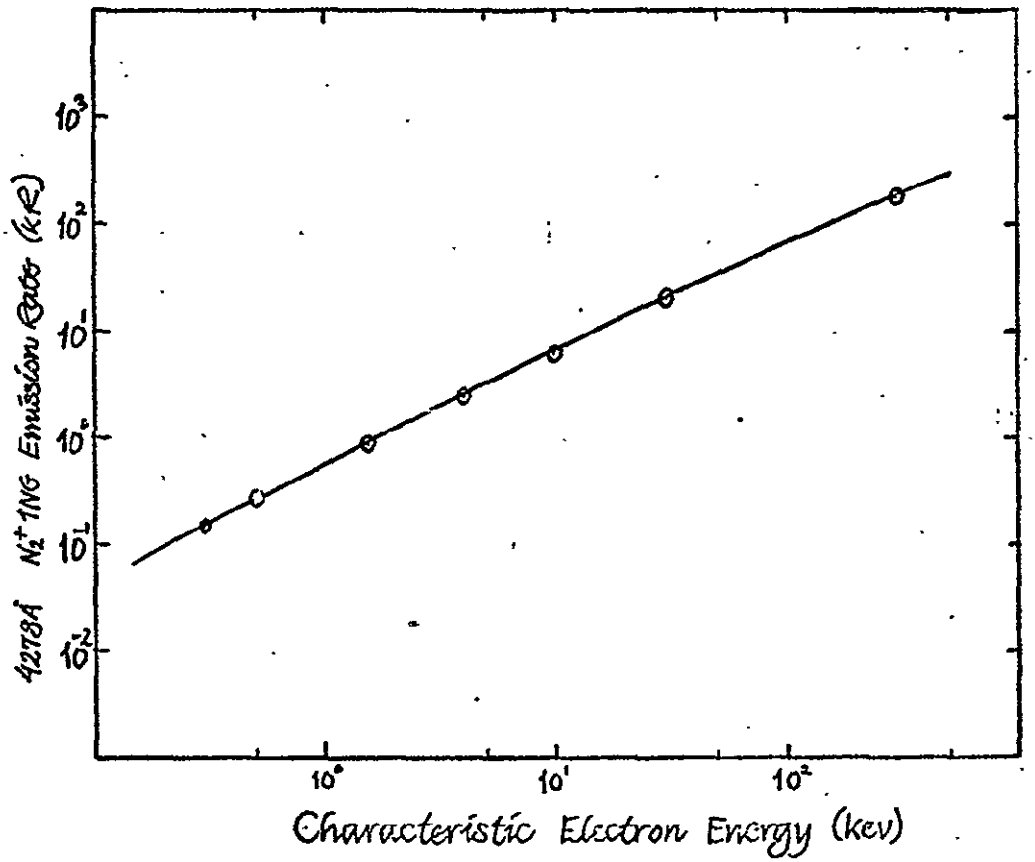

FIG. 9.9

Total emission rate of 4278 Å n_2^+ due to an incoming flux of 10^9 electrons cm^{-2} sec^{-1} as a function of electron energy.

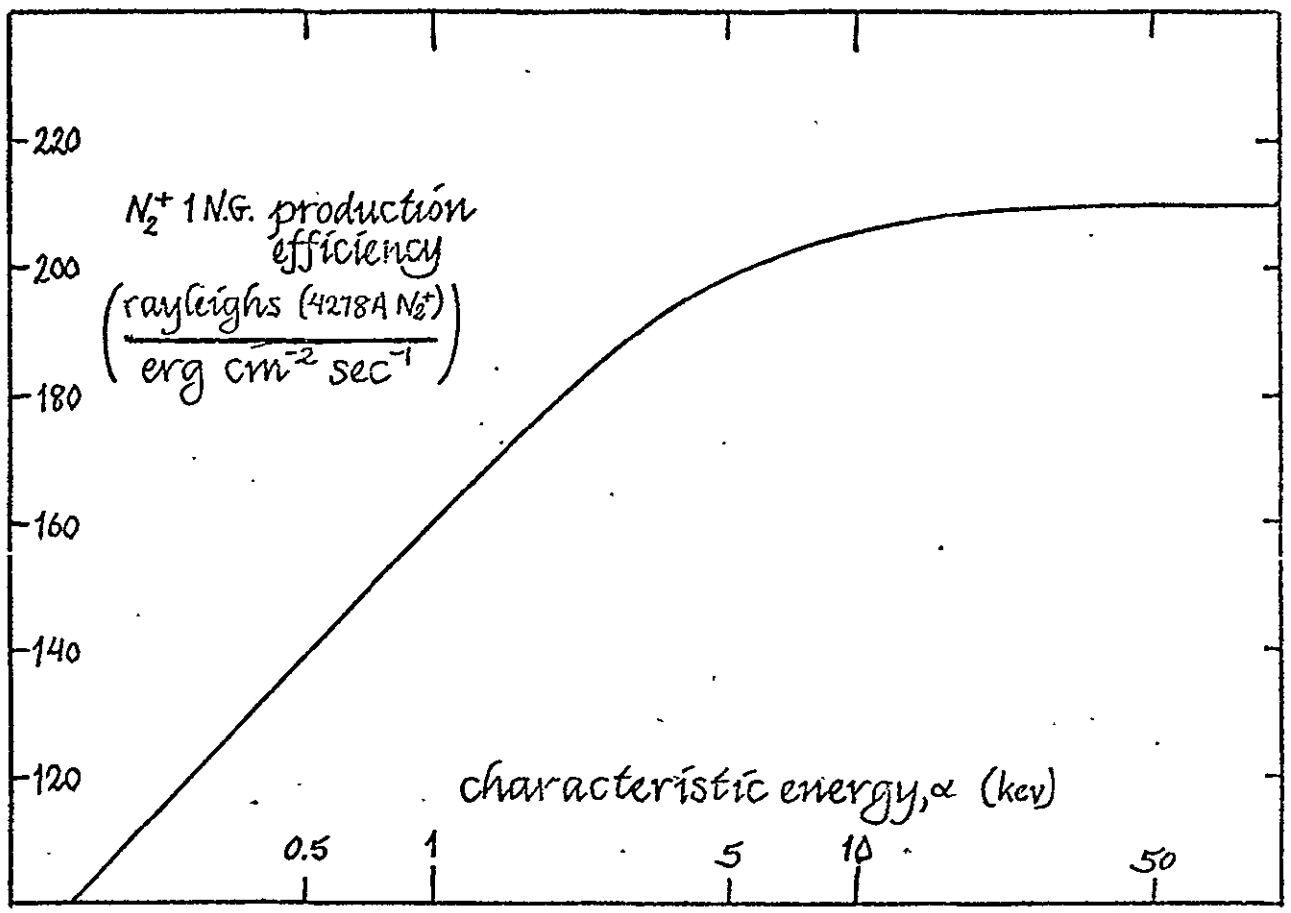

FIG. 9.10

The production efficiency of 4278 Å N_2^+ emission as a function of characteristic incoming electron energy.

altitude where N_2 becomes almost a constant percentage of the total composition. At this point (the altitude for maximum deposition of 10 kev electrons) the efficiency of N_2^+ 1NG production becomes constant, reflecting the constant ratio of N_2 population to total neutral composition. This extension of the curve to 300 kev in this study shows this fact graphically. At even higher energies the curve will turn over because even the short-lived N_2^+ 1NG emissions are quenched below 60 km altitude. However, this is not of interest for most auroral studies. Transfer of electron energy to the ambient electron population is a secondary effect, but under high ($> 10^6$ cm^{-3}) densities it could perhaps change the efficiency curve measurably. The major absorber of incoming particle energy under any conditions, however, is the neutral particle population.

On the basis of the calculations made here and those referred to, one can conclude that there is virtually no difference in the efficiency of production of the N_2^+ 1NG band emissions over the range 10 kev to 300 kev. Thus a 50 kw accelerator operating at 10 kev will produce the same light (N_2^+ 1NG) emission as one at 100 kev. Below 10 kev, the production efficiency does substantially decline, as is shown in Fig. 9.10.

Note that the same conclusion does not necessarily pertain to other emissions., For example, the OI 5577 Å emission is quenched below altitude 100 km. Therefore, the set production efficiency of OI 5577 emission per unit energy deposition falls off for characteristic energy above approximately 10 kev, the characteristic energy of electrons stopping near altitude 100 km. Owing to the long lifetime of the parent state of

the OI 5577 Å emission, the decreased net efficiency at high accelerator voltages may be of little consequence in AMPS experiments involving high cross-magnetic field vehicle velocities.

9.4 SOURCE - DETECTOR GEOMETRY

Given an optical source with an apparent emission rate (in rayleighs) we now examine the effects of source geometry and instrumental geometry without regard to how photons are processed inside the optical detector.

A key concept is that of instrument resolution. A photometer has a single resolution element identical to the photometer field of view. An imager has a large number of resolution elements the areal sum of which is equal to the two-dimensional field of view of the imager optics. The effective angular size of a resolution element is determined by the field of view of the optics and the inherent characteristics of the image tube. In a very real sense an imager can be thought of as being an array of photometers having very small fields of view.

Note from the definition of the rayleigh given in Section 9.2 that the apparent surface brightness of a source is independent of the distance between the source and the observing instrument. This statement pertains only as long as the resolution element field of view is entirely covered by the source. If the separation is increased to the point where the field of view just corresponds to the apparent size of the source, further separation leaves unchanged the area of the source observed, but the light per unit area of the source surface falling into the resolution element falls as the square of the distance. A practical consequence of this matter is illustrated by the following example.

$$P_1 = I_1 \frac{A\,S}{R^2} + I_b \frac{A}{R^2} \cdot \Omega_1 R^2 = \frac{I_1 AS}{R^2} + I_b A\Omega_1 \qquad (9.4.2)$$

Similarly, the number of photons entering a resolution element of the imager is

$$P_2 = (I_1 + I_b) \frac{A}{R^2} \cdot \Omega_2 R^2 = (I_1 + I_b)\, A \cdot \frac{\Omega_1}{625} \qquad (9.4.3)$$

for all values of R such that $R_o < R < R_1 = 25\ R_o$, since at $R = 25\ R_o$ the field of view of the imager resolution element just covers the source area S. Beyond R_1 Eq. 9.4.2 holds for P_2 with substitution of Ω_2 for Ω_1.

Notice from the form of Eq. 9.4.2 that, as R increases, the contribution from the background remains fixed while the contribution from the wanted source decreases with the square of R. By holding $S \cdot I_1 = F/4\pi$ constant and letting $S \to 0$, Eq. 9.4.2 reduces to the case of a point source with total emission F rayleighs. (Strictly speaking, going to the limit S = 0 negates the use of rayleighs as a unit. The conventional treatment is to replace F (in rayleighs) by a point source of P_t megaphotons.)

$$P_1 = \frac{FA}{4\pi R^2} + \Omega_1 I_b \quad \text{(photons sec}^{-1}\text{)} \qquad (9.4.3)$$

In the intermediate case of a linear source of width W and infinite length, the source area falling in the field of view of half angle α for a given separation distance R is $2WR \tan \alpha$. For values of R smaller than $R_1 = W/(2 \tan \alpha)$ the number of photons falling into the resolution element is

$$P_1 = (I_1 + I_b) \cdot A\Omega_1 \tag{9.4.5}$$

For $R > R_1$ the field of view exceeds the width of the linear source object. Then

$$P_1 = \frac{2I_1\ AW \tan \alpha}{R} + I_b A\Omega \tag{9.4.6}$$

Since $\Omega = 2\pi\ (1 - \cos \alpha)$, Eq. 9.4.6 can be expressed in terms of either α or Ω. Also in the above, the surface brightness has been used. In order to express the emission sources in rayleighs set $I_1 = F_1/4\pi$ and $I_b = F_b/4\pi$.

Fig. 9.11 illustrates how the light entering a detector from point, circular and line sources immersed in a background emission falls off with distance and the fact that the light from the background remains constant. In this particular case the surface brightness of the source is taken to be 10 times that of the background. Notice that only when the source-detector separation is less than some distance R_o such that the source covers the resolution element (or photometer field of view) is the ratio between source and background maintained. That ratio is commonly referred to in the term <u>contrast</u> defined as follows:

$$\% \text{ Contrast} = \frac{\text{scene highlight-background}}{\text{scene highlight}} \times 100 \tag{9.4.7}$$

Expressed as a function of apparent emission rates (in rayleighs)

$$\% \text{ Contrast} = \frac{F_{source}}{F_{source} + F_{background}} \times 100 \tag{9.4.8}$$

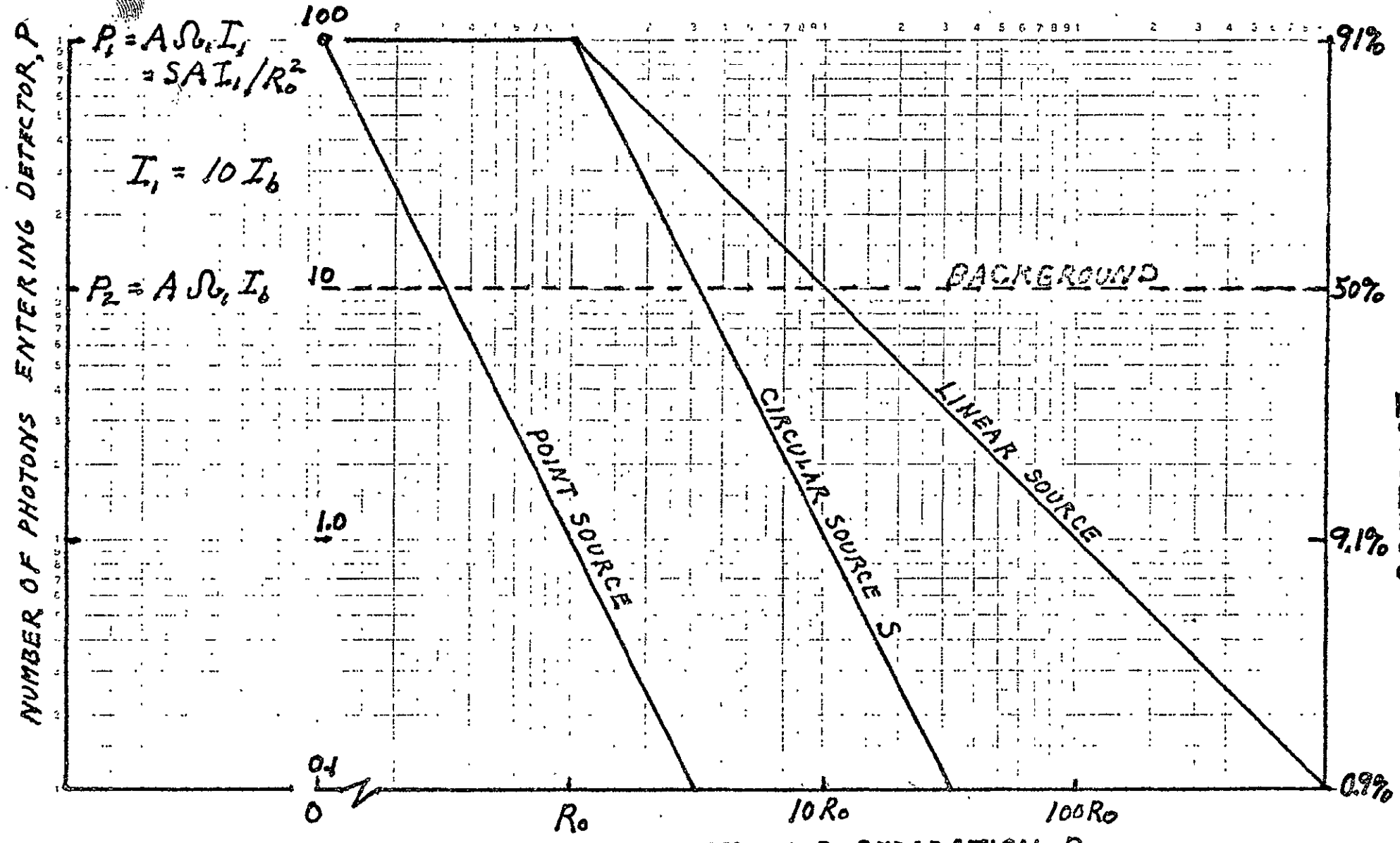

FIG. 9.3 PHOTONS ENTERING A DETECTOR AS A FUNCTION OF SEPARATION FOR POINT, LINEAR AND CIRCULAR SOURCES

Beyond R_o the 'effective' contrast falls off simply because the detector resolution element receives a higher proportion of background emission. It is for this reason that an imaging device with its multitude of tiny resolution elements can be effective in situations where a photometer is not. Also this is the reason why it is desirable to use the smallest field possible on a photometer except when observing very large source regions, such as an airglow layer seen from the ground or looking straight down from above.

9.5 PHOTO-ELECTRIC DETECTOR GEOMETRY AND CONVERSION OF LIGHT TO CURRENT

Given an apparent emission rate F (source + background) rayleighs, the number of photons crossing one cm^2 of the source surface is 10^6 F/4π photons sec^{-1} $ster^{-1}$. If the source region covers the field of view of a resolution element of solid angle Ω, the number of photons falling into an optical system with lens area A is $P = 10^6$ F A Ω/4π. Since $A = \pi(D/2)^2$ where D is the lens diameter and, for small fields of view $\Omega = \pi \tan^2 \alpha$, the number of incident photons can be expressed as

$$P = \frac{10^6 F\pi D^2}{16} \tan^2 \alpha .$$

This light, assumed to be from a distant source, is focused on the optical focal plane at a distance L from the lens plane. The lens focal ratio f is the ratio L/D. Photons entering the resolution element of half angle α fall on the focal plane in a circle of radius $X = L \tan \alpha$, consequently $\tan^2 \alpha$ can be expressed as $(X/L)^2$.

$$\text{Hence } P = \frac{10^6 F\pi D^2}{16} \quad \frac{X^2}{L^2} = \frac{10^6 F\pi X^2}{16f^2}$$

The quantity πX^2 is the area of the detector intercepting P photons. Thus setting $\pi X^2 = 1\ cm^2$ we obtain the expression that relates the number of photons per square cm of detector surface to the source emission rate F (in rayleighs) and the focal ratio of the lens f:

$$P = \frac{10^6\ F}{16\ f^2}\ \text{(photons cm}^{-2}\ \text{sec}^{-1}\text{)} \tag{9.5.1}$$

This expression is independent of the solid angle of a resolution element, so its direct use assumes that the source of apparent emission F covers the resolution element field of view. If that is not the case, Eq. 9.5.1 may still be used by setting

$$F = F_1 \cdot \frac{S}{\Omega R^2} + F_b \tag{9.5.2}$$

to account for the fact that the wanted source of emission rate F and area S covers only the fraction $S/\Omega R^2$ of the resolution element field of view. As $\Omega = \pi \tan^2\alpha$, the expression $P = 10^6\ F\ \pi\ D^2\ \tan^2\alpha/16$ then becomes

$$P = \frac{10^6\ \pi\ D^2}{16}\ \tan^2\alpha\left(\frac{F_1\ S}{\pi\ \tan^2\alpha\ R^2}\right) + F_b$$

Let $F_b = 0$ so as to examine only the source F_1. Then, as before, let $F_1 \cdot S = F^1$, a constant quantity, while requiring $S \to 0$. The expression then becomes

$$P = \frac{10^6\ F^1\ D^2}{16\ R^2}\ \text{(photons sec}^{-1}\text{)} \tag{9.5.3}$$

In the above derivation of Eq. 9.5.3 for a point source, the quantity $F_1 S/\Omega$ conceptually has been replaced by a quantity F^1 representing the total apparent emission and thinking of the resulting photons as being spread over one resolution element of the detector. Strictly speaking, the number of photons entering a detector from a point source depends only upon the source emission rate, the source-detector separation and the aperture, but not the focal ratio f. Note that for a fixed point source, separation and lens area, an increase in f requires an increase in the focal length L but no change in the area (πX^2) of the focal plane receiving the light, this area always being zero if the optics are perfect. However, the image of the point source will, in practice have an area defined by the size of the detector resolution element.

Note the difference in units between Eqs. 9.5.2 and 9.5.3.

For observation of active experiments from below the atmosphere, account generally must be taken for absorption and scattering of the light from the source. Absorption also may be significant for spacecraft observation if the view direction is a long atmospheric path.

9.6 TRANSMISSION OF LIGHT THROUGH DETECTOR OPTICS

Before arriving at the detecting element, photons must be transmitted through the instrument's optical system where wavelength-dependent losses will occur. An example of the transmission characteristics of a visible band lens, one that has been used in the observation of numerous active experiments, is shown in Fig. 9.6.1. In addition, certain observations will require the use of filters that may cut the transmission in half even at the wavelength of maximum transmission. Despite such losses, the use of a filter can substantially improve scene contrast and hence improve the signal-to-noise.

FIG 9.6.1 RELATIVE TRANSMISSION Vs. WAVELENGTH
DELFT RAYXAR LENS
E105/0.75

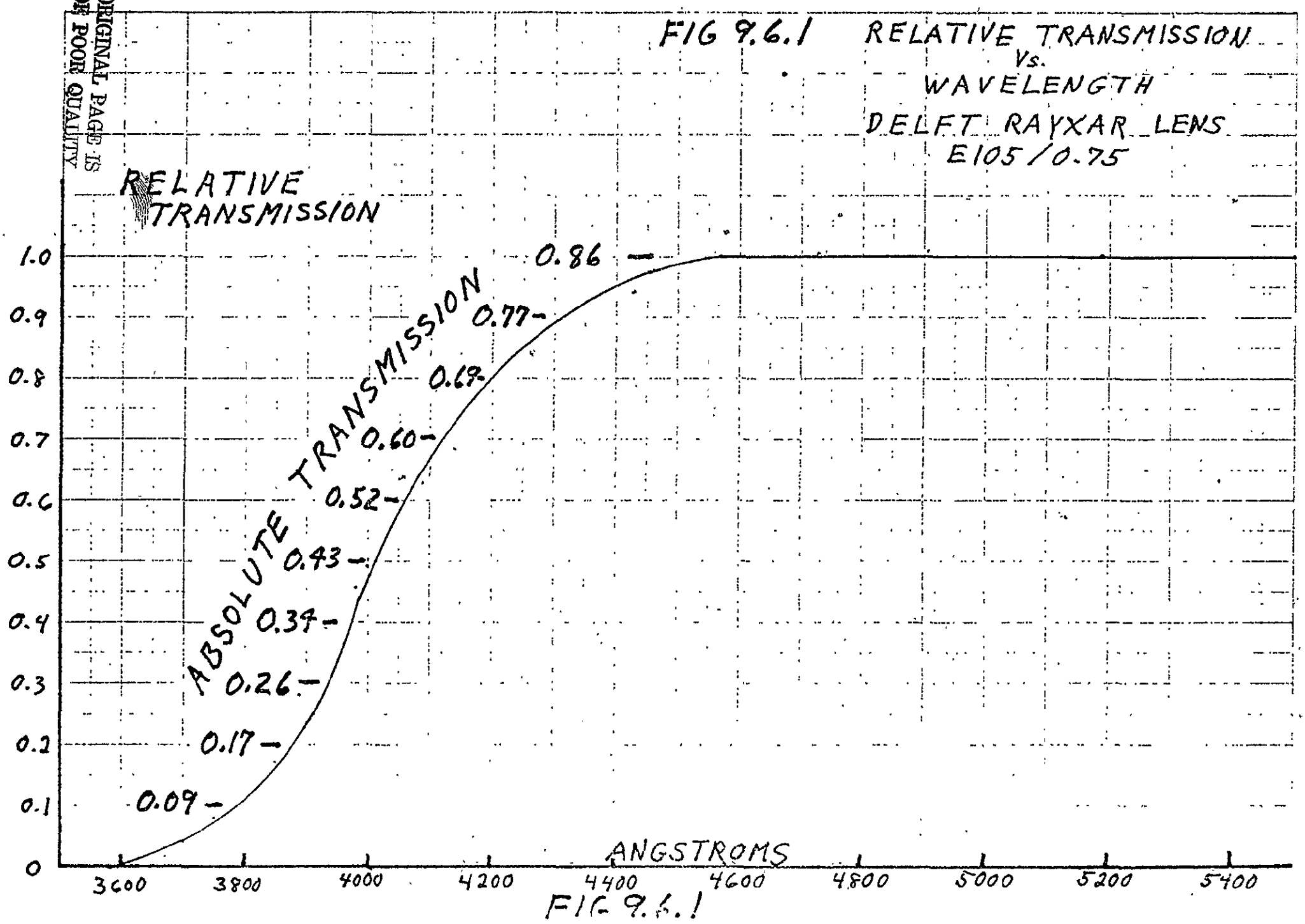

FIG 9.6.1

9.7 CONVERSION OF LIGHT TO ELECTRICAL SIGNAL: DETECTOR SENSITIVITY AND RESOLUTION

By the use of Eq. 9.5.1, appropriately corrected for path absorbtion and transmittance of the optical system, one can determine the number of photons per unit area falling on a photon detector from the wanted source and the surrounding background. Then by use of a curve of the type shown in Figs. 9.7.1 and 9.7.2 the conversion from photons cm^{-2} sec^{-1} to photocathode current per cm^2 sec is accomplished. This is a convenient quantity to work with to determine the system resolution and hence the ability to detect the wanted emission during an active experiment.

The following discussion emphasizes imager techniques but the principles apply equally to photometric detectors.

A very useful indicator of an imaging system's capabilities is a plot of its limiting resolution as a function of light level. Such curves are widely used in the electro-optics industry where the illumination is expressed in foot candles. (Sometimes foot candles are replaced by watts/cm^2. This is arrived at by using the conversion 20 lumens equals one watt, or 1 foot candle equals 0.54 watts/m^2. This equivalence is only valid for a detector having the same spectral response as the photopic eye and a source with the same spectral emittance characteristics as a tungsten bulb maintained at a color temperature of 2856^{o} K.) For most situations anticipated on AMPS missions, the foot candle is an entirely inappropriate unit. Where the source of illumination is other than 'standard white light', the expected resolution must be determined by a three-step process.

First, the photocathode illumination in photons/cm^2 sec is determined for each wavelength present in the source, taking the lens charac-

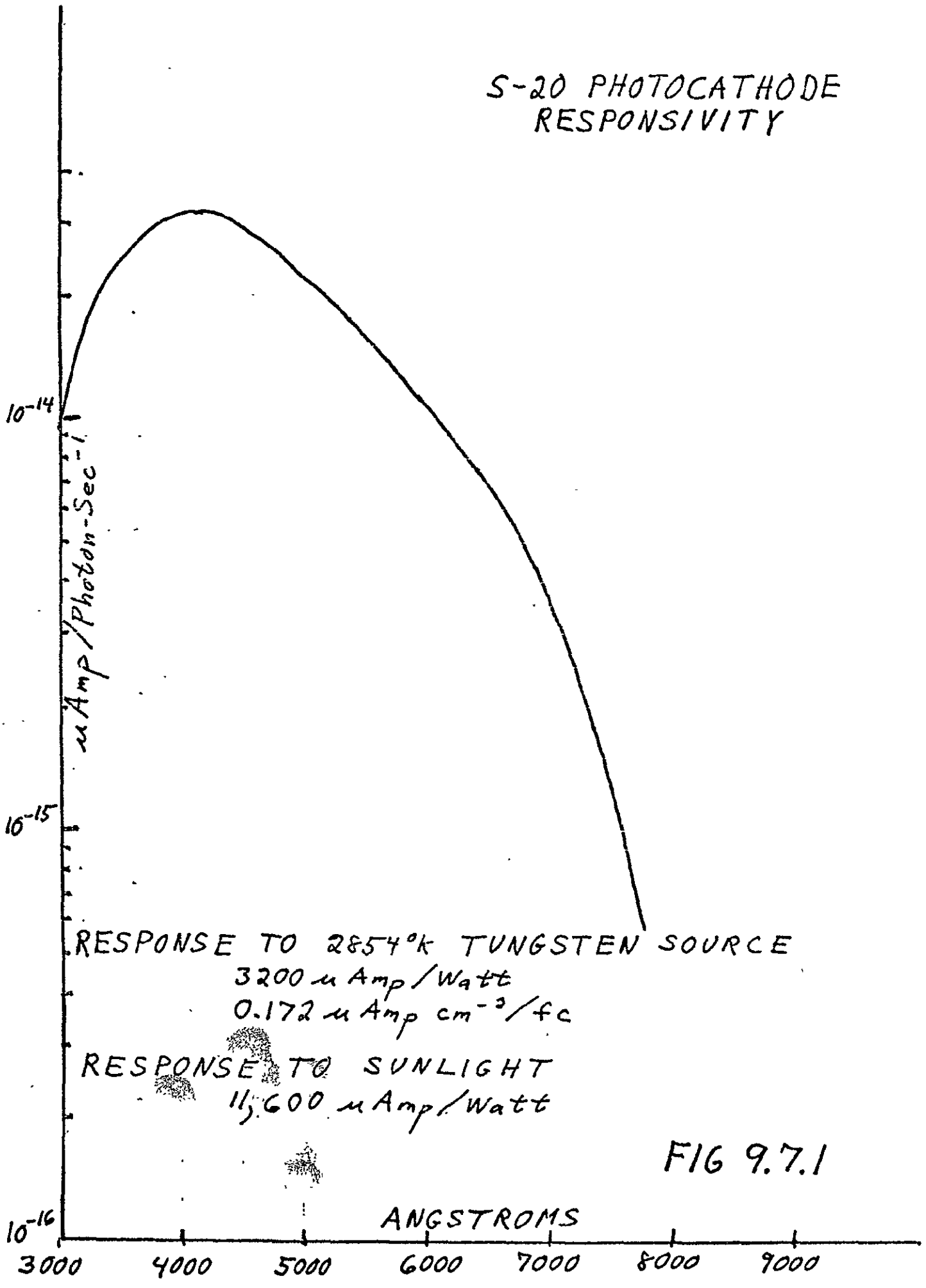
S-20 PHOTOCATHODE
RESPONSIVITY
10^{-14}
10^{-15}
10^{-16}
uAmp/Photon-Sec^{-1}
RESPONSE TO 2854°K TUNGSTEN SOURCE
3200 u Amp/Watt
0.172 u Amp cm^{-2}/fc
RESPONSE TO SUNLIGHT
11,600 u Amp/Watt
ANGSTROMS
3000
4000
5000
6000
7000
8000
9000

FIG 9.7.1

S-25 PHOTOCATHODE RESPONSIVITY

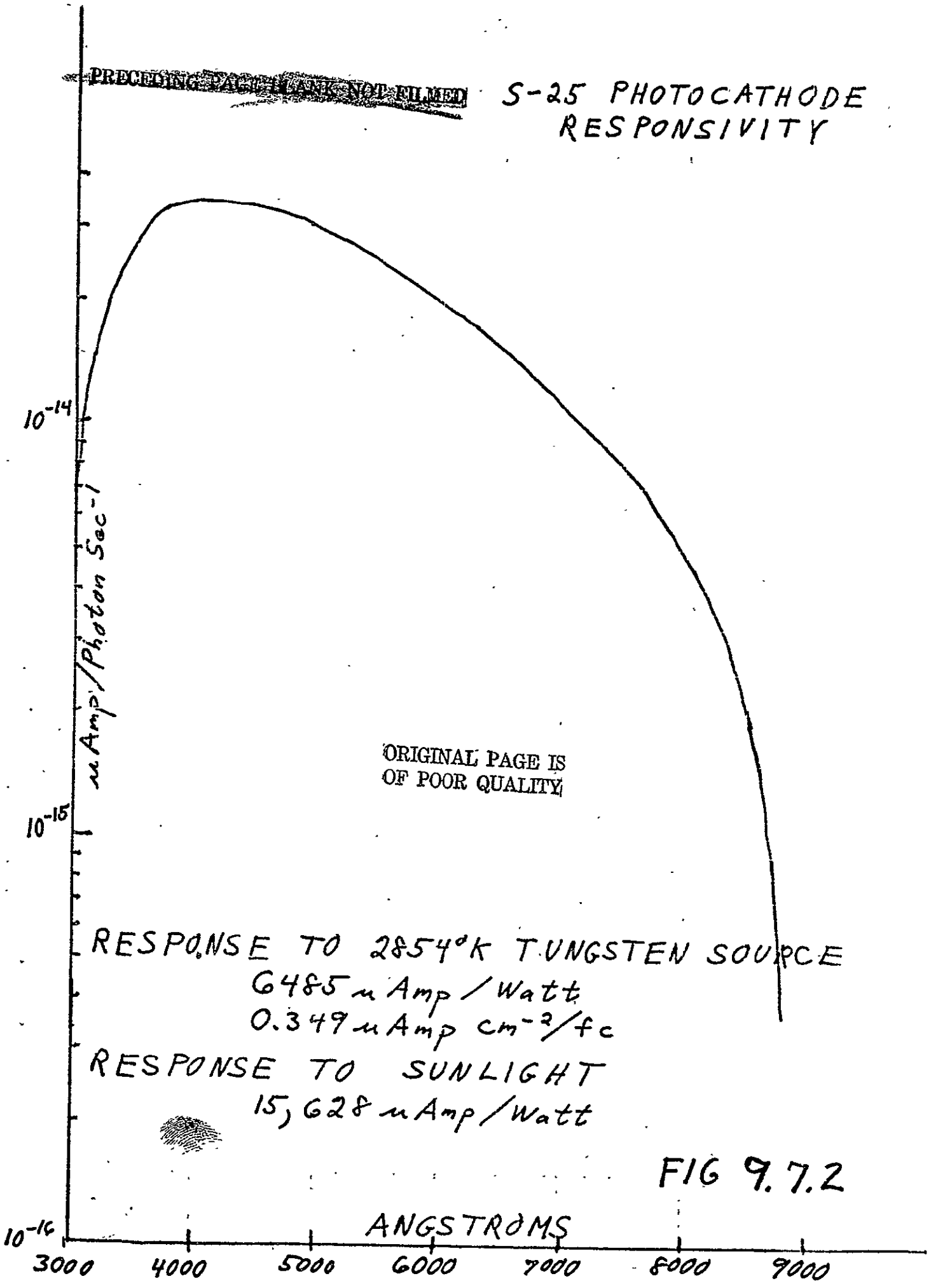

RESPONSE TO 2854°K TUNGSTEN SOURCE
6485 μAmp / Watt
0.349 μAmp cm^{-2}/fc

RESPONSE TO SUNLIGHT
15,628 μAmp / Watt

FIG 9.7.2

teristics into account. Then, the expected photocurrent density is calculated taking into account the spectral response of the photocathode. The curves in Figs. 9.7.1 and 9.7.2 are typical of photocathodes available on imaging cameras. Figure 9.7.1 is derived from data provided by RCA for an SIT (EBS)(C21117C) type camera tube with an S-20 photocathode. Figure 9.7.2 is based on similar data provided by General Electric for an image orthicon tube (7987) with an extended red S-25 photocathode. In addition to the actual responsivity curves, approximate equivalences are given in the diagrams for sunlight and incandescent light. These are based on the matching factors tabulated in the RCA Photomultiplier Manual.

Once the photocurrent density has been determined, the expected resolution may be read directly from the appropriate resolution vs. photocurrent curve. Figure 9.7.3 is derived from Westinghouse data for SIT (EBS) tube with a 40 mm photocathode diameter. A photocathode sensitivity of 160 ua/lumen is assumed. It is expected that visual-band detectors available for the early AMPS missions will have performances similar to that shown in Fig. 9.7.3. The theoretical limit for an ideal detector is also shown (photoelectron noise limit). This is based on recognition statistics (RCA Electro-Optics Handbook).

Figure 9.7.4 shows the resolution vs. photocurrent for image orthicon tubes based on General Electric data. (The 7967 tube type has an S-20 photocathode, and the curves also apply for the type 7807 with the S-10 photocathode since the scale is photocurrent rather than light level.) The image orthicon is not recommended for the Shuttle, but the curves are included because most optical data on AMPS-type experiments to date

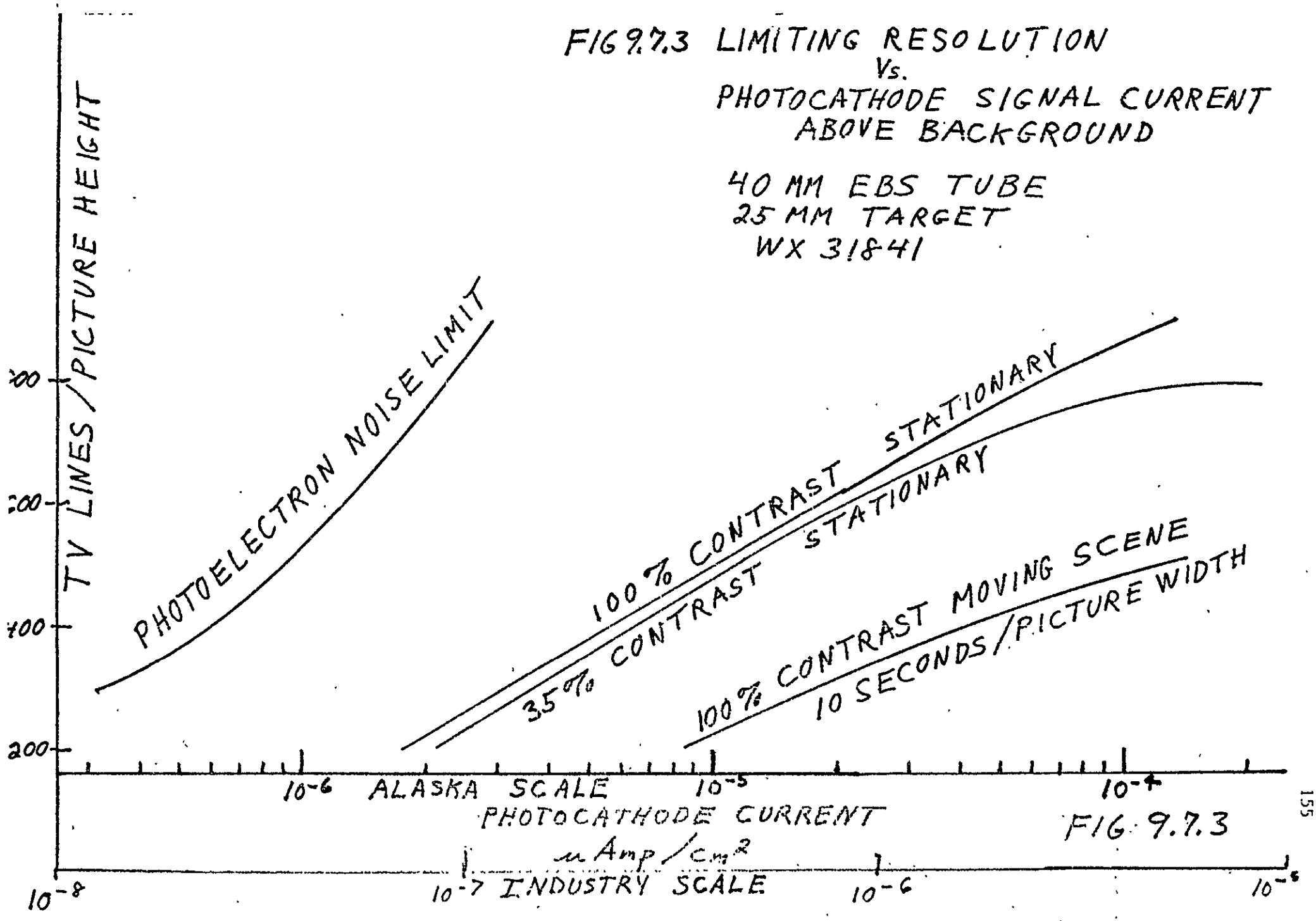
FIG 9.7.3 LIMITING RESOLUTION
Vs.
PHOTOCATHODE SIGNAL CURRENT
ABOVE BACKGROUND
40 MM EBS TUBE
25 MM TARGET
WX 31841
TV LINES / PICTURE HEIGHT
300
200
400
200
PHOTOELECTRON NOISE LIMIT
100 % CONTRAST STATIONARY
35 % CONTRAST STATIONARY
100 % CONTRAST MOVING SCENE
10 SECONDS / PICTURE WIDTH
10-6 ALASKA SCALE 10-5 10-4
PHOTOCATHODE CURRENT
μ Amp / cm2
10-8 10-7 INDUSTRY SCALE 10-6 10-5

FIG 9.7.3

FIG 9.7.4 LIMITING RESOLUTION
Vs.
PHOTOCATHODE SIGNAL CURRENT
ABOVE BACKGROUND
7967 IMAGE ORTHICON TUBE

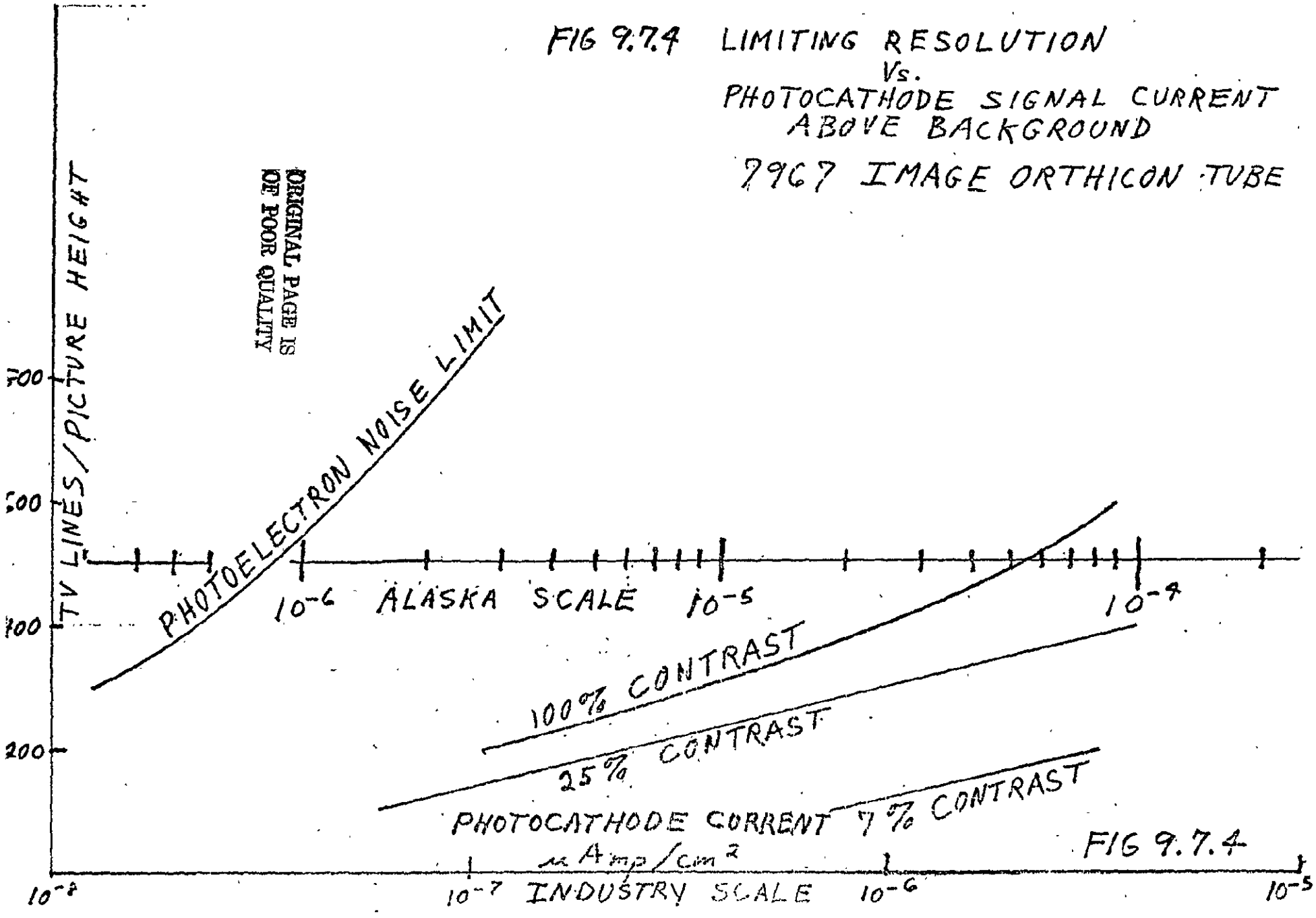

FIG 9.7.4

have been obtained with image orthicons. The empirical knowledge obtained from previous experiments thereby can be compared to predictions based on an analytical approach.

Figure 9.7.3 shows that the photocurrent required for a given resolution is an order of magnitude greater than the limit set by the photoelectron statistics. One method commonly used to more closely approach that limit is to add an image intensifier in front of the camera tube photocathode. Figure 9.7.5 shows the resolution which results from two such combinations. One pair of curves is from information published in the RCA Electro-Optics Handbook. The other pair is based on material supplied by RCA in a private communication. The discrepancies between the two 100% curves have not yet been resolved.

9.8 EFFECT OF SCENE MOTION

The resolution vs. photocurrent curves are the result of observations of a fixed test pattern. If the test pattern is moving, the effective sensitivity is reduced. This reduction results partly from the decrease in effective integration time, but more so from a variety of poorly understood factors that have to do with the ability to completely read out all of the information on a storage target in a single raster scan. These factors are usually referred to collectively as stickiness or lag. Figure 9.7.3 shows that moving the test pattern across the picture in a 10 sec period is equivalent to reducing the light level by a factor of six. This will probably be improved slightly before the early AMPS missions, but conservative experiment planning should be based on the lag characteristics of the WX31841 tube, as shown.

FIG 9.7.5 LIMITING RESOLUTION Vs PHOTOCATHODE SIGNAL CURRENT ABOVE BACKGROUND 40 MM SIT TUBE COUPLED TO 40MM IMAGE INTENSIFIER

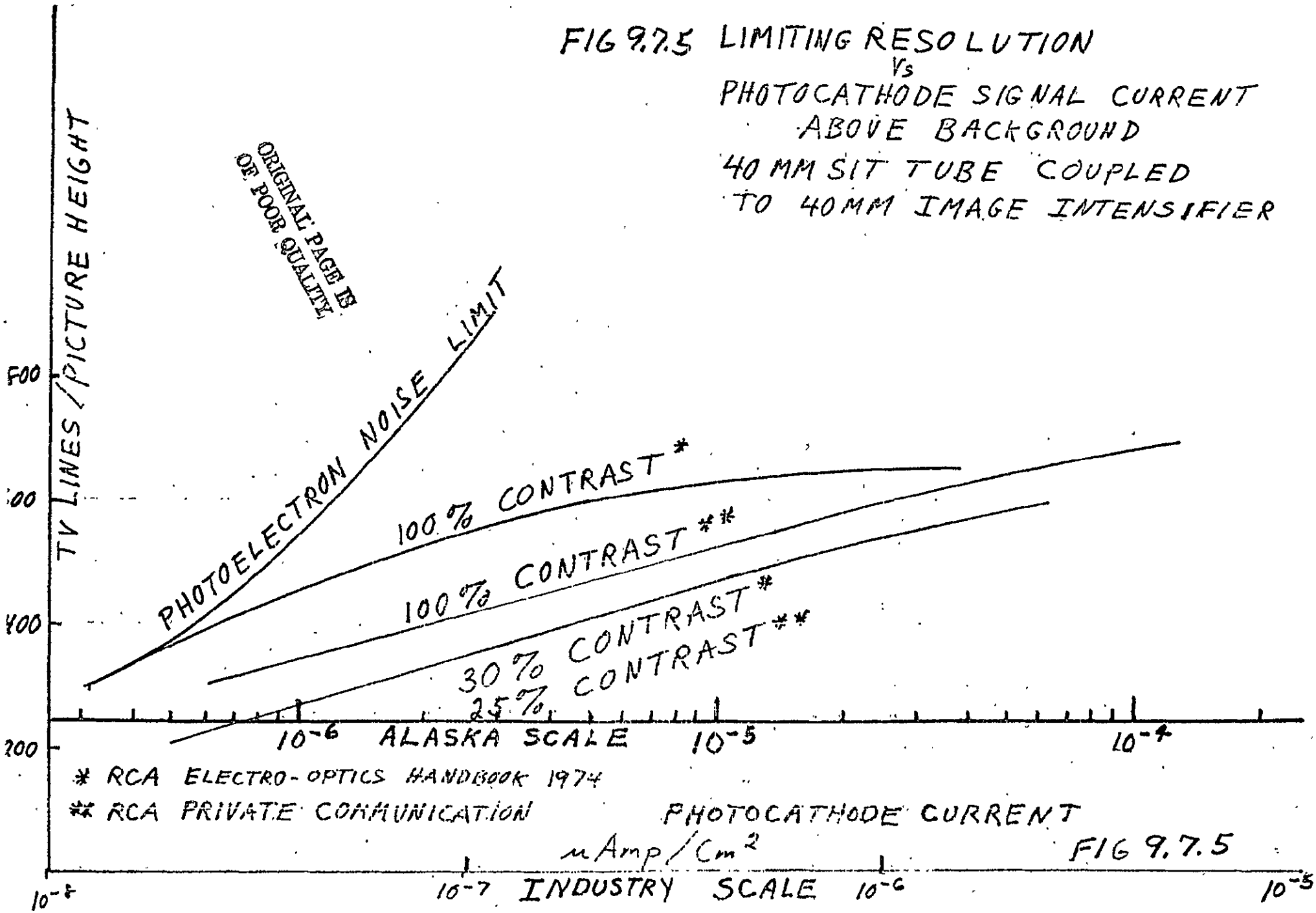

FIG 9.7.5

9.9 CONTRAST

Most of the sensitivity information provided by manufacturers refers to 100% contrast test patterns. Unfortunately, real scenes never have 100% contrast, and AMPS experiments will probably have very low contrast. When tube or camera manufacturers do provide low contrast data they invariably plot the resolution as a function of highlight illumination. However, the ability to discern an object depends primarily on the intensity of the object itself (signal) rather than on the highlight illumination (signal plus background). Consequently, Figs. 9.7.3, 9.7.4 and 9.7.5 are all plotted as functions of signal current rather than highlight current. The EBS (SIT) tube suffers little degradation when the contrast is reduced from 100% to 35% (Fig. 9.7.3) except at relatively high light levels. It appears that the only problem occurs when the background exceeds the saturation level of the tube ($\sim 6 \times 10^{-6}$ $\mu a/cm^2$). Since the smallest useful signal is approximately 6×10^{-8} amps, the minimum useful contrast is $\sim$ 1%. A contrast of 5% -10% is probably quite acceptable for many experiments.

Other detectors do not function as well under low contrast situations. According to Fig. 9,7,4, the image orthicon operated at 7% contrast requires 14 times as much source brightness as when operated at 100% contrast. The maximum obtainable resolution at 7% contrast is $\sim$ 300 TV lines. From this it is inferred that past experiments have generally been contrast limited rather than signal limited.

The image intensifier - SIT combination seems like a good approach when judged at 100% contrast. However, a comparison of Figs. 9.7.3 and 9.7.5 illustrates that at low-contrast values there is little advantage (and sometimes a disadvantage) in using the intensifier.

FIG 9.10.1 SIGNAL CURRENT REQUIRED TO IMAGE POINT SOURCE Vs INTEGRATION TIME WL-30893 SEC TUBE

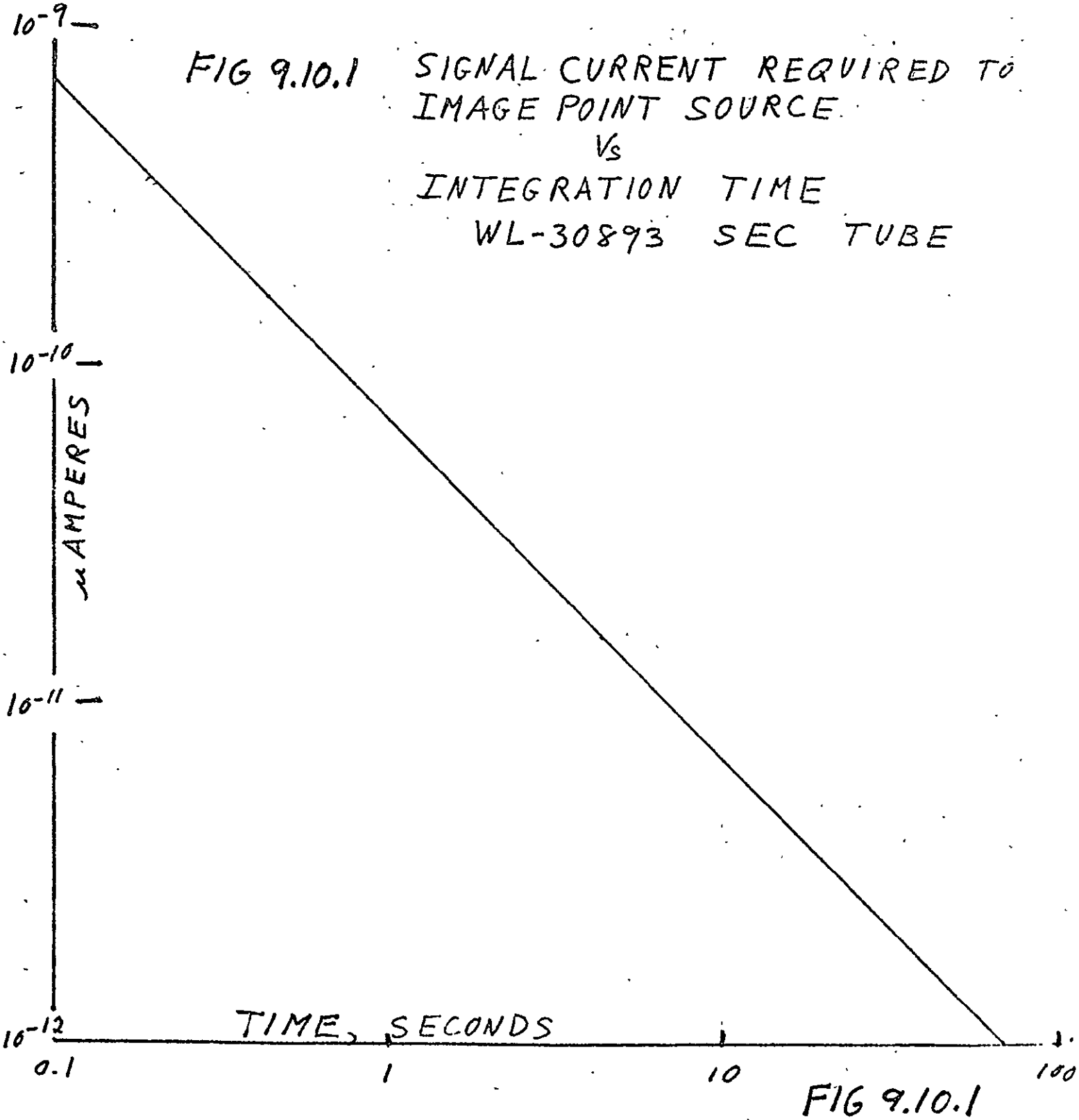

FIG 9.10.1

FIG 9.10.2 RECIPROCAL RELATIONSHIP BETWEEN SIGNAL CURRENT AND THE SQUARE ROOT OF THE INTEGRATION TIME REQUIRED TO MAINTAIN 400 TV LINES/PICTURE HEIGHT LIMITING RESOLUTION 7967 IMAGE ORTHICON TUBE

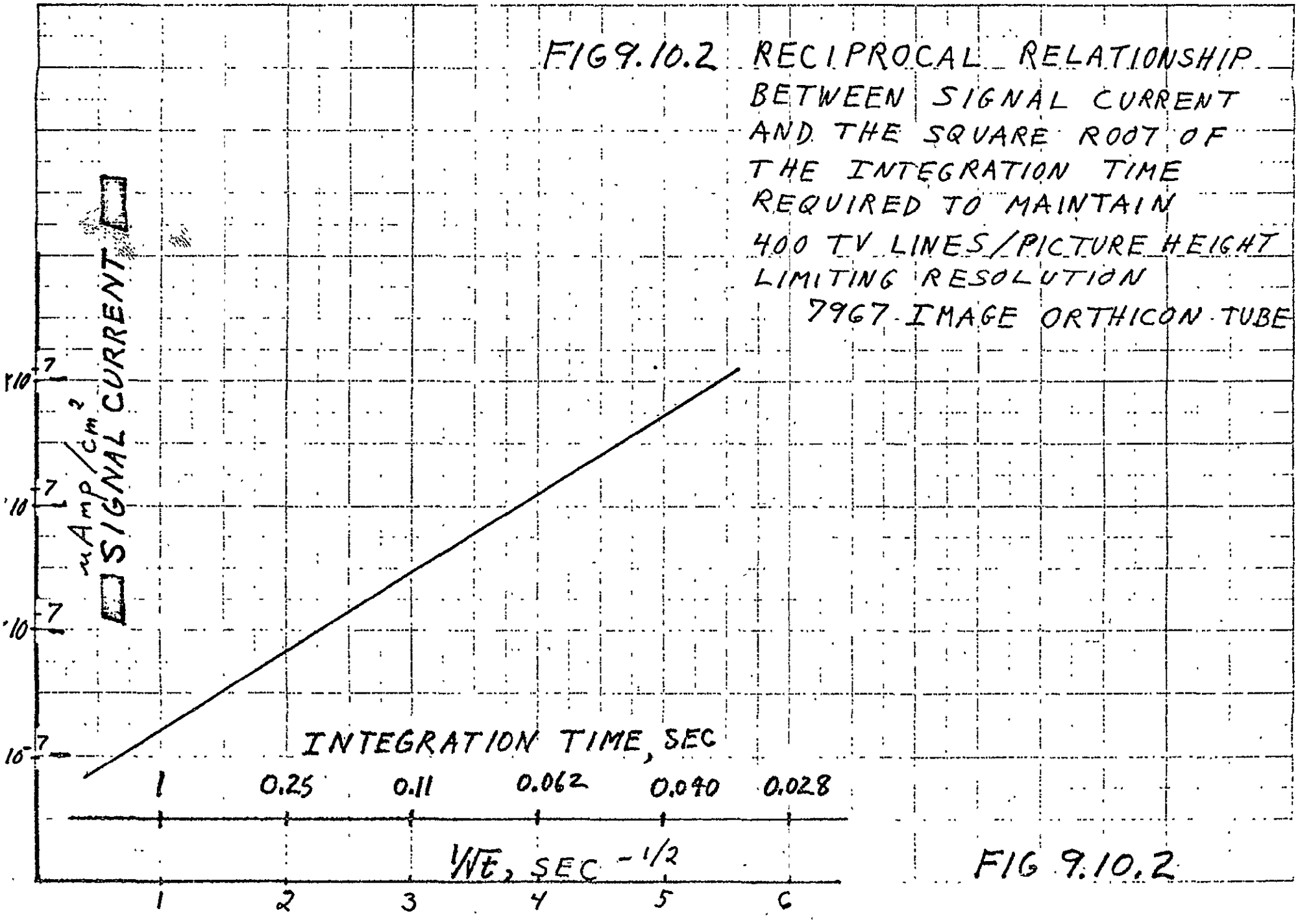

FIG 9.10.2

from General Electric data for a 7967 image orthicon tube covers integration periods from 1/30 sec to 2 sec. The lack of reciprocity probably derives from the inability of the beam to completely discharge the target in a single scan. In addition to the poor reciprocity, the image orthicon is limited by lateral target leakage which (depending on the target processing and the temperature) becomes significant when the integration time exceeds 2 seconds. In some cases integration times of as much as 32 sec can be achieved.

At the moment there is little specific information available concerning the integration properties of EBS (SIT) tubes. Generally, they have lag and beam landing characteristics similar to those of SEC tubes. Consequently, at least for short integration times, (< 2 sec) reciprocity probably holds. At longer times, the integration is limited by lateral leakage across the target and also by dark current within the individual diodes. Currently-available tubes can integrate for approximately one second (private communication from Westinghouse). It seems probable that reciprocal integration for up to 4 seconds will be easily obtainable for the early AMPS missions. However, this is an area that clearly requires further investigation.

10. EXPERIMENT CALCULATION PROCEDURES

10.0 INTRODUCTION

In the design of a particular experiment or in the determination of whether a desired observation is feasible, a complex and interlocking set of factors must be considered. A brief summary of these factors is given by Fig. 9.1. A possible starting point is specification of the wanted information and the available detector characteristics. One then works upward through the blocks of Fig. 9.1 to find the requirements on an electron accelerator or other device used to produce an active experiment. Another approach can begin with a given capability to produce electron beams, ion releases, etc. and then work down through the blocks of Fig. 9.1 to determine the detector characteristics required for successful observation of an experiment. A third approach is to specify both the source device and the detector capabilities and then determine what experiments are feasible. At the moment, this third approach seems most efficient.

10.1 ELECTRON ACCELERATOR EXPERIMENTS

We assume the availability of an electron accelerator capable of producing a 50 kw electron beam with pulse duration at least 1 sec. The recent report by J. M. Sellen, Jr. (1975) considers an accelerator design permitting a maximum current of 2.5 amps and a voltage range from 4 kv to 20 kv. For illustrative purposes it may be useful here to incorporate the somewhat wider range of current and voltage shown in Table 10.1.

TABLE 10.1

Accelerator Voltage (kev)	Current (amp)	Power (kw)	Energy[1] Deposition ($ergs/cm^2 sec$)	Altitude of[2] Penetration (km)	Production[3] N_2^+ ING 4278 (kR)	Production[4] (OI) 5577 (kR)
0.5	10	5	281	190	$281 \times 135 \times 10^{-3} = 37.9$	(4278)x6 = 227
1.0	10	10	562	150	$562 \times 157 \times 10^{-3} = 88.2$	(4278)x5 = 441
4.0	2.5	10	562	114	$562 \times 190 \times 10^{-3} = 107$	(4278)x2.5 = 267
10	2.5	25	1404	100	$1404 \times 203 \times 10^{-3} = 285$	(4278)x$\sim$2 = 570
20	2.5	50	2809	93	$2809 \times 210 \times 10^{-3} = 590$	(4278)x$\sim$1.5 = 885
40	1.25	50	2809	85	$2809 \times 210^{-3} = 590$	(4278)x$\sim$1.3 = 767

[1] Assume deposition in an area of radius 75 meters = 1.78×10^8 cm^2

[2] From Fig. 10.1.

[3] From Fig. 9.10.

[4] From Fig. 10.2 (Fig. 4 of Rees and Luckey) For voltages 20 and 40 kev values are extrapolated and therefore less certain; all values derived from extrapolation to 10 kR 4278 of curves on graph of Rees and Luckey.

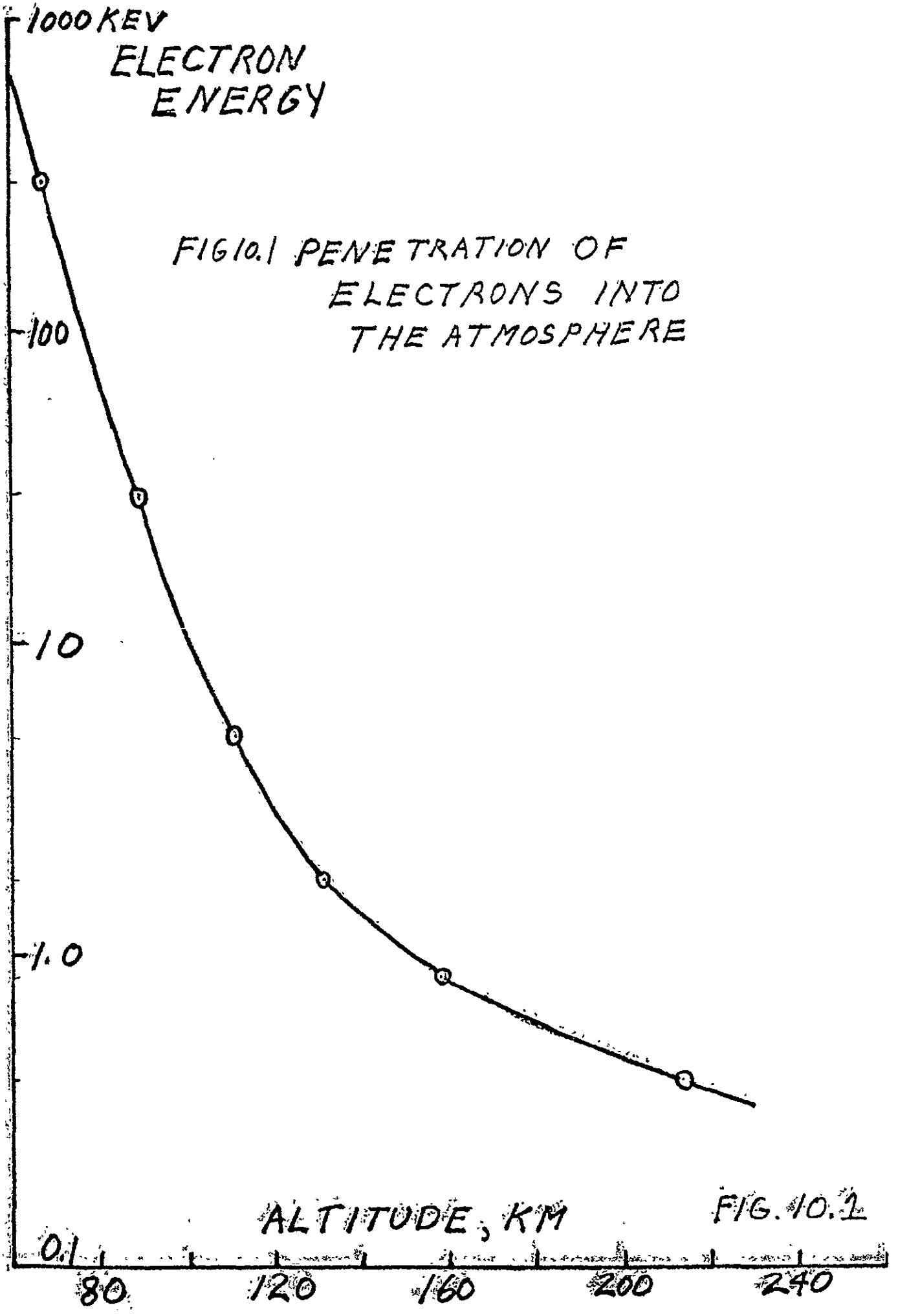

FIG 10.1 PENETRATION OF ELECTRONS INTO THE ATMOSPHERE

FIG. 10.1

10.1.1 Production of Detectable Light with Electron Beams

In Table 10.1 the energy depositions (assuming no losses in transit between accelerator and atmosphere) are listed for a beam deposition area which is roughly midway between that observed for auroras resulting from the downward injection of 8.7 kev electron beams at Wallops Island (diameter 130 $\pm$ 50 m) and the upward ejection to the conjugate region of a 24 kev beam near Hawaii (diameter 210 $\pm$ 50 m) (Davis et al., 1971; Davis, 1974).

The production of N_2^+ 4278 is derived from Fig. 9.10, where it is seen that the production is dependent upon the electron beam energy. The production of any particular emission depends critically upon atmospheric composition and density, both functions of altitude (See Fig. 10.2).

REES AND LUCKEY:

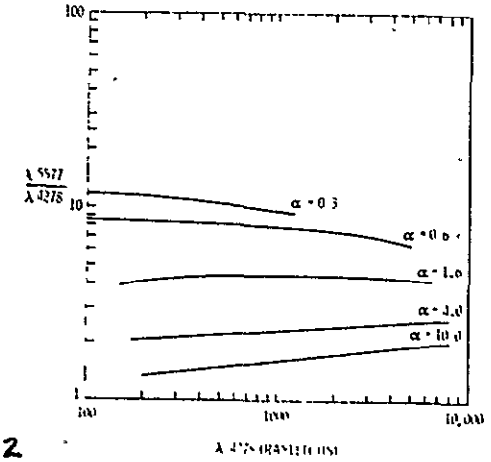

FIG 10.2

Column emission rate ratio 5577/4278 as a function of the absolute emission rate of 4278 Å for electron fluxes of different characteristic energies α.

An example is shown in the last column of Table 10.1 where the ratios of 5577/4278 and the production of 5577 both are given.

For a given electron beam voltage and current, the detailed calculation of all the resulting emissions of interest for an active experiment is somewhat involved. To avoid that problem here, we will make use of an "average" aurora as described in Figs. 2.16-2.19 of Volume II of the MAMOS report (Davis, 1973) and summarized in column 3 of Table 10.2. In this summary the adopted value of the 5577/4278 ratio is appropriate for an aurora of characteristic energy $\sim$ 4 kev. The wavelength range covered by Table 10.2 is the visible band only, in particular, that portion of the band to which an S-20 photocathode is sensitive. From the fifth column in Table 10.2, the detector photocathode current resulting from each emission can be obtained by multiplying the entry by $1/f^2$ (f = lens focal ratio) and taking into account the transmission of the detector optics.

Let us now assume that the aurora produced by the electron beam is to be observed with the Delft Rayxar lens with 105 mm focal length, focal ratio f/0.75 and T-stop (for visual light) 0.81. The relative transmission versus wavelength characteristic of this lens is shown in Fig. 9.6.1. Internal inconsistencies in the manufacturer's specifications cast some doubt on the accuracy of the ordinate-labeling for absolute transmission shown, but it appears that any error does not exceed 5%. (The T-stop is numerically equal to the focal ratio f divided by the square root of the lens transmittance.) Utilizing the lens transmission shown in the next-to-last column and the focal ratio of the lens, the actual photocathode current for each emission is given in the last column of Table 10.2.

TABLE 10.2

Emission from an "Average" IBC III Aurora (Characteristic Energy $\alpha \sim 4$ kev)

Emission	Wavelength	Emission (100 kR 5577)	S-20 Response μamps/photon sec^{-1}	Photocathode Current ($\mu amp/cm^2$) x $16f^2$ x 10^5)	Lens Transmission %	Photocathode Current $\mu amp/cm^2$ (x 10^5)
N_2^+ 1N	3914	60	3×10^{-14}	180	22	4.3
N_2 2P	~3940	1.5	3.1 ↓	4.6	26	0.13
N_2 2P	~4000	2.5	3.2	8.0	40	0.35
N_2 2P	~4050	2.3	3.2	7.4	41	0.33
N_2 VK	~4060	1.5	3.2	4.8	41	0.22
N_2 VK	~4200	1.5	3.2	4.8	69	0.36
N_2^+ 1N	4278	17	3.2	54.4	75	4.49
N_2^+ 1N	~4600	1.5	2.8	4.2	86	0.40
N_2 1N	4709	4.0	2.7	10.8	86	1.02
O_2^+ 1N	~5250	1.6	1.9	3.0	86	0.28
O_2^+ 1N	5274	4.0	1.8	7.2	86	0.68
O_2^+ 1N	~5560	2.3	1.5	3.4	86	0.32
(OI)	5577	100	1.5	150	86	14.19
O_2^+ 1N	5608	12	1.5	18	86	1.70
N_2 1P	5854	2.5	1.2	3.0	86	0.28
N_2 1P	5906	4.2	1.1	4.6	86	0.43
N_2 1P	~5950	5.0	1.1	5.5	86	0.52
O_2^+ 1N	5999.9	8.0	1.1	8.8	86	0.83
N_2 1P	6069	5.5	1.0	5.5	86	0.52
N_2 1P	6128	3.9	1.0×10^{-14}	3.9	86	0.37
N_2 1P	6168	1.4	9.4×10^{-15}	1.3	86	0.12
(OI)	6300	10	8.4 ↓	8.4	86	0.79
(OI)	6364	10	8.0	8.0	86	0.79

TABLE 10.2 (Cont'd)

Emission	Wavelength	Emission (100 kR 5577)	S-20 Response $\mu amps/photon\ sec^{-1}$	Photocathode Current ($\mu amp/cm^2$) x $16f^2$ x 10^5)	Lens Transmission %	Photocathode Current$_2$ $\mu amp/cm^2$ (x 10^5)
N_2 1P	6389	10	7.7	7.7	86	0.73
O_2^+ 1N	~6400	7.0	7.7×10^{-15}	5.4	86	0.51
N_2 1P	6468	9.0	7.4 ↓	6.7	86	0.63
N_2 1P	6544	15	6.9	10.3	86	0.97
N_2 1P	6623	26	6.4	16.7	86	1.58
N_2 1P	6704	40	5.7	22.8	86	2.16
O_2^+ 1N	6735	1.8	5.4	1.0	86	0.09
N_2 1P	6788	25	5.2	13.0	86	1.23
O_2^+ 1N	~6800	4.0	5.0	2.0	86	0.19
N_2^+ M	6822	12	4.8	5.8	86	0.55
N_2 1P	6875	14	4.6	6.4	86	0.60
N_2^+ M	~7030	7.0	3.6	2.5	86	0.24
N_2 1P	~7160	4.0	2.8	1.1	86	0.10
N_2 1P	~7230	4.0	2.5	1.0	86	0.09
N_2 1P	~7270	16	2.3	3.7	86	0.35
N_2 1P	~7380	40	1.8	7.2	86	0.68
N_2 1P	~7500	70	1.4	9.8	86	0.93
N_2 1P	~7600	2.0	1.0	0.2	86	0.02
N_2 1P	~7610	82	1.0	8.2	86	0.78
N_2 1P	~7750	60	6.5×10^{-16}	3.9	86	0.37
N_2^+ M	~7820	35	5.8 ↓	2.0	86	0.19
N_2 1P	~7900	5.0	4.5	0.2	86	0.02
					Total less (OI)	30.66
					Total including 5577	44.85
					Total including	46.4

Several aspects of the final photocathode current values are noteworthy:

1) Even though N_2^+ 1N 3914 is much brighter than N_2^+ 1N 4278, the lens transmission and photocathode response cause these two to produce nearly equal detector response.

2) The relatively strong N_2 1P emissions between 7000 Å and 8000 Å contribute significantly less than the emissions in the range 6000 Å to 7000 Å owing to the decrease in photocathode sensitivity toward the red end of the spectrum.

10.1.2 Other Sources of Light

In planning all optical observations it is important to be aware of extraneous sources of light. Here we consider those which are most likely to be encountered in an AMPS mission. The basic information on light levels is obtained partly from the RCA Electro-Optics Handbook and partly from a report prepared by the Hazeltine Corporation for the Goddard Space Flight Center/NASA in 1963 under Contract NAS 5-3166. The light values have all been converted into the expected photocathode signal current density, an S-20 photocathode and a T1, f/1 lens being assumed. In Table 10.3 the light sources are listed in order of decreasing intensity. Insofar as possible, the match between the distributions of the sources and the spectral response of the S-20 photocathode is taken into account.

TABLE 10.3

Sources of Background Emission

Source	S-20 Photocathode Current μa/cm^2
Sunlit Earth	202
Moonlit Earth	1.0×10^{-3}
Light Scattered from Sun outside FOV	See Section 7
Light Scattered from Sunlit Earth outside FOV	See Section 7
Clouds Illuminated by Night Sky plus Nightglow	1.0×10^{-5}
Nightglow*	6.3×10^{-6}
Starlight	3.2×10^{-6}
Zodiacal Light	1.6×10^{-6}
IBC I aurora (1 kR in 5577)	4.5×10^{-6}

*See Table 10.4

The specific calculations are as follows:

Sunlit Earth - The sun's irradiance is 0.139 watts/cm^2. Assuming a spectrally uniform albedo of 0.5, an S-20 response (11,600 μamp/watt), and an f1 lens, the photocurrent is $j = 0.139\ (0.5)\ (11{,}600)/4 = 202 \mu amp/cm^2$.

Moonlit Earth - From Hazeltine's report, illumination from full moon is 5×10^{-6} times the solar illumination: $j = 5 \times 10^{-6}\ (202) = 1 \times 10^{-3}\ \mu amp/cm^2$.

Clouds Illuminated by Night Sky (including starlight, zodiacal light and airglow) plus directly observed airglow - This is the sum of three quantities, each given in the Hazeltine report for an S-20 photocathode and an f1.5 lens.

nightglow reflected from clouds	0.78×10^{-8} ma/in^2
extra-atmospheric sources reflected from clouds	0.39×10^{-8} ma/in^2
direct nightglow	1.8×10^{-8} ma/in^2
Total	2.97×10^{-8} ma/in^2

$$j = 2.97 \times 10^{-8} \text{ ma/in}^2 \left(\frac{1 \text{ in}}{2.54 \text{ cm}}\right)^2 \left(\frac{f\ 1.5}{f1}\right)^2 \times 1000 \text{ μa/ma}$$
$$= 6.3 \times 10^{-6} \text{ μa/cm}^2$$

Nightglow - $j = 1.8 \times 10^{-8}\left(\frac{1}{2.54}\right)^2 (1.5)^2 \times 1000 = 6.32 \times 10^{-6}$ μa/cm^2 (see also following discussion).

Starlight - The Electro-Optics Handbook gives illuminance from stars as 2.2×10^{-4} lm/m^2. Assuming that the spectral distribution is similar to that of sunlight and that most of the light comes from the myriad of unresolvable weak stars, this can be approximated as an extended source of 2.2×10^{-4} candles/m^2. The photocathode illumination in foot candles is

$$2.2 \times 10^{-4}/4(10.76) = 5.1 \times 10^{-6}$$

From Fig. 9.7.1 it can be seen that the response to sunlight is 11,600/3,200 as great as the response to a tungsten bulb. The response to the tungsten bulb is 0.172 μamp/cm^2/fc.

$$j = 5.1 \times 10^{-6} \ \frac{11,600}{3,200} \ (0.172)$$
$$j = 3.2 \times 10^{-6} \text{ μamp/cm}^2$$

Zodiacal Light - From the Electro-Optics Handbook, zodiacal light is roughly half the value of direct and scattered starlight.

$$j = \tfrac{1}{2}\ (3.2 \times 10^{-6}) = 1.6 \times 10^{-6}\ \mu amp/cm^2$$

IBC I Aurora - Determined by summing photocathode currents appearing in the last column of Table 10.2.

A more detailed indication of expected night airglow emission is presented in Table 10.4 showing the approximate emission of the nightglow continuum as a function of wavelength. The Table is compiled by visually averaging 5-Å resolution spectrometer data obtained at Kitt Peak by Broadfoot and Kendall (1968). When estimating background illumination through relatively wide (>20 Å) filters, the line emissions other than that at 5577 need not be included. Note that the airglow varies from day to day and also as a function of latitude. For example, Shefov (Chamberlain, 1961) obtained values 2 to 5 times those shown in Table 10.4. It is also unclear as to how much starlight is included in the various measurements. Note also the factor of 2 difference between the total emission shown in Table 10.4 and the relevant entry in Table 10.3 obtained from another source.

10.1.3 Contrast Between Artificial Aurora and Background

Using the results presented in Tables 10.2, 10.3 and 10.4, we are in position to calculate scene contrast, an important quantity determining the obtainable observational resolution. Equation 9.4.8 defines the contrast in terms of the apparent emission rates as

TABLE 10.4

Night Airglow Background

Wavelength Range (A)	Emission (R/A)	Emission in Band (R)	Average S-20 Response (μamp/photon sec^{-1})	Photocathode Current x 16f^2 x$_2$10^5 (μamp/cm^2)	Photocathude Current Delft Lens (μamp/cm^2)
3900-4600	0.5	350	3×10^{-14}	1.0	7×10^{-7}
4600-5500	0.75	675	2.2×10^{-14}	1.5	10
5500-6100	0.8*	680	1.2×10^{-14}	0.8	8
6100-6400	1.1	330	8.5×10^{-15}	0.8	3
6400-6800	0.8	320	6.2×10^{-15}	0.2	2
6800-7200	1.5	600	3.8×10^{-15}	0.2	2
7200-7700	2.2	1100	1.5×10^{-15}	0.2	2
7700-8300	5	3000	$\sim 3 \times 10^{-16}$	0.1	1×10^{-7}
8300-9000	8	5600	$< 1 \times 10^{-16}$	< 0.05	-
			Total		3.5×10^{-6}

*Plus 200 R at 5577 from [OI] .

$$\% \text{ Contrast} = \frac{F_{source}}{F_{source} + F_{background}} \times 100$$

Since the emissions from the source and the background are passed through the same optical system and are similarly responded to by the photocathode, the contrast can also be expressed in terms of photocathode current resulting from the wanted source (PC_S) and from the background (PC_B):

$$\% \text{ Contrast} = \frac{PC_S}{PC_S + PC_B} \times 100 \qquad (10.1)$$

10.1.4 Detector Response to Artificial Auroras

By use of Table 10.5 and diagrams such as given in Figs. 9.7.3, 9.7.4 and 9.7.5, the obtainable resolution for a particular source and background combination can be found. The question then is what resolution is necessary to barely detect a source or, more importantly, to permit useful measurements on the source.

Our laboratory testing with a 7967 image orthicon (Fig. 9.7.4) gives an indication of the difference in signal level required to usefully "see" a scene and that required to barely recognize that a scene exists. We define a signal I as that signal required to produce 200 TV line resolution (contrast 100%) on a test pattern. Then it is found that reducing the signal to I/3 leads to the result that the test pattern is still fairly recognizable as a test pattern but that almost no details of the pattern appear. Further reduction to I/25 results in the existence of the test pattern being barely recognized; i.e., this is the level of detection.

TABLE 10.5

Scene Contrast for Various Sources and Backgrounds

Source	Photocathode Current (μamp/cm^2)		Airglow $PC_B=3.5\times10^{-6}$		Airglow +Starlight $PC_B=6.7\times10^{-6}$		Night-Sky Lit Clouds +Airglow $PC_B=1\times10^{-5}$		Moonlit Earth $PC_B=1\times10^{-3}$	
	$\parallel$ to $\vec{B}$	$\perp$ to $\vec{B}$	$\parallel$ to $\vec{B}$	$\perp$ to $\vec{B}$	$\parallel$ to $\vec{B}$	$\perp$ to $\vec{B}$	$\parallel$ to $\vec{B}$	$\perp$ to $\vec{B}$	$\parallel$ to $\vec{B}$	$\perp$ to $\vec{B}$
IBC I Aurora (α=4 kev)	4.6×10^{-6}	6.9×10^{-8}	57%	2.0%	41%	1.0%	32%	0.7%	0.4%	0.0%
IBC II Aurora (α=4 kev)	4.6×10^{-5}	5.9×10^{-7}	93	16	87	9.3	82	6.4	4.4	0.0
IBC III Aurora (α=4 kev)	4.6×10^{-4}	6.9×10^{-6}	99	66	98	51	98	41	32	0.7
IBC IV Aurora (α=4 kev)	4.6×10^{-3}	6.9×10^{-5}	100	95	100	91	100	87	84	6.4
*Artificial Aurora 0.5kv,0.1 amp	6.7×10^{-6}	1.0×10^{-7}	66	3.0	50	1.4	40	1.0	0.6	0.0
*Artificial Aurora 0.5kv,1 amp	6.7×10^{-5}	1.0×10^{-6}	95	22	91	13	87	9.1	6.0	0.0
*Artificial Aurora 0.5kv,10 amp	6.7×10^{-4}	1.0×10^{-5}	99	74	99	60	98	50	40	0.1
*Artificial Aurora 1kv,10 amp	1.5×10^{-3}	2.2×10^{-5}	100	86	100	77	99	69	60	2.1
*Artificial Aurora 4kv,2.5 amp	1.5×10^{-3}	2.2×10^{-5}	100	86	100	77	99	69	60	2.1
*Artificial Aurora 10kv,0.1 amp	1.0×10^{-3}	1.5×10^{-5}	100	81	100	69	99	60	50	1.4
*Artificial Aurora 10kv,2.5 amp	2.4×10^{-1}	3.6×10^{-4}	100	99	100	98	100	97	96	26
*Artificial Aurora 20kv,0.1 amp	2.0×10^{-3}	3.0×10^{-5}	100	90	100	82	99	75	67	2.9
*Artificial Aurora 20kv,2.5 amp	5.0×10^{-2}	7.5×10^{-4}	100	100	100	99	100	99	98	43
*Artificial Aurora 40kv,0.1 amp	4.0×10^{-3}	6.0×10^{-5}	100	94	100	90	100	86	80	5.7
*Artificial Aurora 40kv,1.25 amp	5.0×10^{-2}	7.5×10^{-4}	100	100	100	99	100	99	98	43

*Not including OI emission.

Emperically we find that a resolution of ∿200 TV lines per picture height is the resolution required for useful measurements. Use of Fig. 9.7.4 then dictates that the minimum resolution for detection is ∿100 TV lines.

Having compiled Table 10.5, we immediately recognized that the results contained are not in agreement with our emperical experience with both image orthicon and SIT imagers. We then ran calibration tests which showed that our systems require ∿25 times the photocathode current indicated by the curves in Fig. 9.7.4. Possible reasons for the discrepancy include:

1) A significant error in our calculations,

2) The tested equipment is performing far below specification,

3) There is an industry-wide error in measurement of tube sensitivity.

At this stage we are uncertain of the cause of the discrepancy. The calculations have been checked through and no indication of error found. Equipment tests show that the imager is preamp noise limited rather than tube limited, but it seems impossible to account for the large error in this way.

A real possibility is industry-wide error. That such error is not unreasonable is indicated by the following argument. Testing at low light levels is often performed using tungsten sources. These emit most strongly in the red and infra-red end of the spectrum where the sensitivity of the S-20 is low, so that the major response is near 7500 Å. Neutral-density filters usually are used to reduce the light levels, the Kodak Wratten Filters No. 96 being common examples. Such a filter of neutral density, say, 4 is stated to have a filter factor of 10,000. However,

Kodak data show that the actual filter factor at 7500 Å is only 400, a factor of 25 less than the average over the visible band. This factor of 25 is exactly that needed to explain our apparent discrepancy.

Obviously, more work is required to locate the source of the discrepancy. For now we have no recourse but to believe our emperical results that require a shift of the scales given on the absiccas of Figs. 9.7.3, 9.7.4 and 9.7.5. In the following, the scale marked "ALASKA" rather than the one marked "INDUSTRY" will be used.

Based upon the use of the "ALASKA" scale the allowed ranges of photocathode current from the wanted source and background regions for a satisfactory experiment are given in Table 10.6. The table shows that each of the three detectors considered has about the same upper limit to the allowed maximum photocathode current from the wanted source and the background, but that the SIT coupled to an image intensifier should provide an extra decade at the low-light-level end of the allowed range.

TABLE 10.6

Signal Requirements for a Satisfactory Experiment

Detector	Source Photocathode Current ($\mu amp/cm^2$)	Maximum Background Current ($\mu amp/cm^2$)	Minimum Contrast
40 mm SIT-40 mm II	$2x10^{-7}$ to $1x10^{-4}$	1×10^{-4}	20% desirable 10% limit
40 mm SIT	$2x10^{-6}$ to $1x10^{-4}$	1×10^{-4}	10% desirable 5% limit
7967 IO	$3x10^{-6}$ to $1x10^{-4}$	1×10^{-4}	10% desirable 7% limit

Table 10.6 now can be re-examined to determine which of the sources listed there are in the range allowed for satisfactory observation. One

sees that the IBC I and II auroras can be viewed end-on but the IBC III and IV auroras cannot. (Emperical experience suggests that the IBC III aurora can be effectively viewed parallel to $\vec{B}$ but not the IBC IV.) With the image orthicon or the 40 mm SIT, only the IBC III and IV auroras (of thickness 150 m) can be usefully detected from the side. Similarly, an artificial aurora produced by an electron beam of power $\sim$0.02 kw should be observable end on, but to be usefully observed from the side, the causitive beam should have minimum power $\sim$1 kw. Beams $\geq$20 kw will produce artificial auroras bright enough to permit the use of filters on imagers to investigate the behavior of the brighter individual line emissions.

The preceding paragraph and Table 10.6 apply to the observation of source regions large enough to cover a resolution element equal to the field of view divided by the number of TV lines per picture height, independent of the separation between source and detector. At 200 TV line resolution a lens giving a picture height of 12° (Delft Rayxar, 105 mm). the minimum source size must be $12^{\circ}/200$ = 1 milliradian. Thus, an artificial aurora of diameter 150 m fulfills this requirement for source-detector separations up to 150 km. If the separation is greater, it may not be possible to accurately measure the source diameter, even though the source may still be detectable. Probably the best resolution attainable by an imager likely to be flown on AMPS missions is $\sim$300 TV lines, this resolution being obtained only with bright sources. In this case, a lens giving picture height 12° yields a resolution of 0.7 milliradians.

10.1.5 Procedure for Calculating Feasibility of a Particular AMPS Experiment

The following procedure can be entered at various points; regardless of the entry point, essentially all steps must be considered. With modification, the procedure can be used with ions and other generators of optical emissions.

1. Given an electron beam of known voltage, current and direction, determine the location, shape and volume emission rate of the region where the beam interacts with gases to produce optical emissions.

   1.1 The location of the emitting region will depend upon the location of the gases the beam is to interact with and the configuration of the geomagnetic field in the region extending from electron gun to the final deposition point.

   1.2 The shape of the emitting region will depend upon the distribution of the target gases, the pitch angle of the beam and the scattering that occurs when the beam interacts with the target gas. For distant targets, i.e., the atmosphere, the beam will be cylindrical with a diameter that can be estimated by calculation or use of previous emperical results. For near-Shuttle targets, such as the ambient atmosphere near the vehicle or gas releases from the spacecraft, the shape of the beam will be complex and dependent upon beam focusing, pitch angle and voltage as well as the target gas distribution.

1.3 The volume emission rate of the source region depends primarily upon the composition of the target gas and the degree of quenching of excited states.

2. Having determined the source location, shape and volume emission, consider the view direction and integrate over the line of sight to determine the surface brightness and hence the apparent emission rate which is 4π times the surface brightness seen looking parallel to $\vec{B}$.

3. Determine if the source subtends an angle that is equal to or greater than the angular resolution element of the detector. If so, calculate the number of photons cm^{-2} sec^{-1} entering the detector (Eq. 9.5.1). If the source subtends a smaller angle, correct by using Eq. 9.5.2 or Eq. 9.5.3. Also correct for any extinction or scattering effects between the source region and the detector.

4. Using curves of detector response (such as Fig. 9.7.1) determine the photocathode current ($\mu amp\ cm^{-2}$) resulting from the source.

5. Determine the sources of background emission to obtain their apparent emission rate (in rayleighs) and determine the corresponding photocathode current, as in Step 4.

6. From a plot of limiting resolution versus signal above background (Fig. 9.7.4 is an example) determine if the background and signal currents are in the acceptable range of the detector (see Table 10.6).

REFERENCES

Bedinger, J. F., Thermospheric motions measured by chemical releases, Preprint, GCA Technology Division, Bedford, Mass.

Broadfoot, A. L. and K. R. Kendall, The airglow spectrum, 3100-100,00 Å, J. Geophys. Res., 73, 426-428, 1968.

Chamberlain, J. W., Physics of the Aurora and Airglow, Academic Press, N.Y. and London, 1961.

Davis, T. N., Scientific design of a manned aurora and magnetosphere observatory system for the Shuttle program, Vols. I and II, Final Contract Rept. NAS 9-12649, Geophysical Inst., Univ. of Alaska, Fairbanks, 1973.

Davis, T. N., Television observations of artificial aurora and analyses of flight data from NASA payload 12.18 NE, Final Contract Rept. NAS 9-11815, Geophysical Inst., Univ. of Alaska, Fairbanks, 1974.

Davis, T. N., T. J. Hallinan, G. D. Mead, J. M. Mead, M. C. Trichel and W. N. Hess, Artificial aurora experiment: ground-based optical observations, J. Geophys. Res., 76, 6082-6092, 1971.

Deehr, C. S., Particle and auroral observations from the ESRO I/AURORAE satellite, J. Atmo. Terr. Phys., 35, 1979, 1973.

Eather, R. H. and S. B. Mende, Auroral precipitation patterns, J. Geophys. Res., 76, 1754, 1973.

Grün, A. E., Z. Naturforsch., 12A, 89, 1957.

Leinert, C. and D. Klüppelberg, Stray light suppression in optical space experiments, Applied Optics, 13, 556-564, 1974.

Ney, E. P. and W. F. Huch, Optical environment in Gemini space flights. Science, 153, 297-299, 1966.

RCA Electro-Optics Handbook, Section 6-1, RCA Commerical Engineering, Harrison, N.J., 1974.

RCA Photomultiplier Manual, Technical Series PT-61, RCA Electronic Components, Harrison, N.J., 1970.

Rees, M. H., Auroral ionization and excitation by incident energetic electrons, Planet. Space Sci., 11, 1209, 1963.

Rees, M. H. and D. Luckey, Auroral electron energy derived from ratio of spectroscopic emissions, 1. model computations, J. Geophys. Res., 79, 5181-5186, 1974.